

Thermo-Mechanical Performance Evaluation of Pavement Materials in Cold Regions

by

Arian Asefzadeh

A thesis submitted in partial fulfillment of the requirements for the degree of

Doctor of Philosophy

In

GEOTECHNICAL ENGINEERING

Department of Civil and Environmental Engineering

University of Alberta

Abstract

A pavement system is a multi-layer structure that provides ease of ride for commuters by successfully transferring the traffic-induced loadings to the ground. A typical flexible pavement structure is comprised of Hot Mix Asphalt (HMA), the strongest material in terms of strength, overlying the Granular Aggregate Base (GAB) layer placed on top of subgrade soil which is the weakest material. Each pavement material has its own properties and mechanical characteristics, thus, each respond to traffic and environmental loading, differently. Pavement materials in cold regions are exposed to inclement weather conditions including prolonged winter seasons, short thawing periods and long summer days. Therefore, pavements are prone to several damages and distresses in cold regions. Rutting and fatigue failure are the two main distresses which occur due to lack of sufficient stiffness in the HMA and subgrade layers. This research study aims to evaluate the performance of spring load restriction models used by transportation agencies during crucial periods using field environmental and falling weight deflectometer tests data. HMA is highly sensitive to temperature changes which significantly affect its dynamic modulus. Subsequently, because of high temperature variation between cold and warm seasons in cold regions, the HMA layer experiences damages such as thermal cracking and rutting in cold and warm seasons, respectively. Statistical temperature prediction models were developed and successfully calibrated based on the environmental data collected from field. To evaluate the field performance of HMA layer, statistical temperature prediction models were developed and calibrated based on field weather and asphalt temperature data. Implementing triaxial testing, the permanent deformation and resilient modulus of subgrade materials were evaluated and modeled. The effect of using waste recycled material such as bottom ash and tire derived aggregates were evaluated on the strength of the subgrade soil and fatigue life performance of the pavements. This study was fruitful and proved the satisfactory fatigue life performance of pavements constructed on embankments made with tire derived aggregates.

Preface

This dissertation is the original research study completed by the author and presented in the “paper-based” format. I was the principal researcher and responsible for all of the research planning, experimental studies, data analysis and preparation of manuscripts. **Chapter 3** was published as “Asefzadeh, A., Hashemian, L., Hagi, N.T. and Bayat, A., 2016. Evaluation of spring load restrictions and winter weight premium duration prediction methods in cold regions according to field data. Canadian Journal of Civil Engineering, 43(7), pp.667-674”. **Chapter 4** was published as “Asefzadeh, A., Hashemian, L. and Bayat, A., 2017. Development of statistical temperature prediction models for a test road in Edmonton, Alberta, Canada. International Journal of Pavement Research and Technology, 10(5), pp.369-382.”. **Chapter 5** was published as “Asefzadeh, A., Hashemian, L. and Bayat, A., 2017. Characterization of Permanent Deformation Behavior of Silty Sand Subgrade Soil Under Repeated Load Triaxial Tests. Transportation Research Record: Journal of the Transportation Research Board, (2641), pp.103-110”. **Chapter 6** was published as “Asefzadeh, A., Hashemian, L. and Bayat, A., 2018. The Effect of Bottom Ash on Soil Suction and Resilient Modulus of Medium-Plasticity Clay, Transportation Research Record: Journal of the Transportation Research Board (No. 18-05098)”. **Chapter 7** was published as “Asefzadeh, A., Hashemian, L. and Bayat, A., 2018. Fatigue Life Evaluation of Pavement Embankments made with Tire Derived Aggregates. Canadian Journal of Civil Engineering”.

Dedicated to

My Kind and Supporting Parents

&

My Lovely and Beautiful Wife

Acknowledgements

First of all, I would like to express my solemn gratefulness and gratitude to my supervisor, **Dr. Samer Adeeb**, who kindly supported me at the very hardest moments in my life through my Ph.D studies at the University of Alberta. Without his crucial supports and motivations, I would not be able to finish this long journey. I will be in debt to him and his great favors forever. I would like to sincerely appreciate the great helps, supports and kind considerations that I received from **Dr. Robin Everall**, the Associate Dean of the Faculty of Graduate Studies and Research. My sincere thanks goes to **Dr. Brent Epperson** who dedicatedly helped me with his priceless directions and supports. I would like to express my thankfulness to **Ms. Arlene Figley**, the graduate program advisor, who patiently supported me during the very hardest moments in my educational path. I am also grateful to **Dr. Dave Chan** for allocating time to resolve the issues that I faced on my way to pursue my goals. I am grateful to **Ms. Sasha van der Klein**, the president of Graduate Students Association for fully supporting me throughout all the tensions and stresses by generously dedicating her time and efforts.

I would also like to express my deepest love and thanks to my lovely parents and my beautiful wife who have been always supporting me unconditionally. Having them with me, I have always been able to have the courage and resilience to stay positive at the hardest moments and defeat all the barriers in my life.

Table of Contents

Chapter 1- Introduction.....	1
Statement of the Problem.....	2
Research Objectives.....	4
Scope of the Work.....	5
Structure of Dissertation.....	6
Chapter 2- Literature Review.....	8
Different Types of Pavement Structures.....	9
Flexible Pavement.....	9
Rigid Pavement.....	10
Effect of Environmental Loading on Pavement Materials.....	11
Unbound Materials.....	11
Asphalt Materials.....	13
Spring Load Restrictions (SLR).....	14
HMA Temperature Prediction Models.....	16
Effect of Traffic Loading on Pavement Materials.....	16
Rutting.....	17
Fatigue Cracking.....	18
Subgrade Permanent Deformation.....	18
Subgrade Soil Stabilization.....	20
Use of Tire Derived Aggregates in Road Embankments.....	20
Summary.....	21
Chapter 3- Evaluation of Spring Load Restrictions and Winter Weight Premium Duration Prediction Methods in Cold Regions According to Field Data.....	23
Abstract.....	24
Introduction.....	25
Objectives and Scope of the Work.....	27
SLR Prediction Models.....	28

IRRF Test Road.....	30
Data Analysis.....	32
Ambient Air Temperature.....	32
Calculation of CTI and CFI Based on the Reviewed Methods.....	33
Frost and Thaw Depth in Pavement Layers.....	33
Volumetric Water Content (VWC) Changes throughout the Pavement Structure.....	35
Analysis of the WWP and SLR Application.....	38
Conclusion.....	42
Acknowledgement.....	43
Chapter 4- Development of asphalt temperature prediction models for a test road in Edmonton, Alberta, Canada.....	44
Abstract.....	45
Introduction.....	46
IRRF Test Road Facility.....	51
Development of Models.....	54
Calibration of Park’s Model for the IRRF Test Road.....	65
Validation of Models.....	66
Effect of Temperature on HMA Stiffness.....	68
Conclusion.....	70
Chapter 5- Characterization of Permanent Deformation Behavior of Silty Sand Subgrade Soil under Repeated Load Triaxial Tests.....	72
Abstract.....	73
Introduction.....	73
Literature Review.....	75
Material Characterization.....	78
Discussion of Test Results.....	81
Summary and Conclusion.....	89
Chapter 6- The Effect of Bottom Ash on Soil Suction and Resilient Modulus of Medium Plasticity Clay.....	91
Abstract.....	92
Introduction.....	92

Material and Experimental Procedure.....	94
Compaction Test.....	95
Specimen Preparation.....	96
Resilient Modulus Test.....	97
Matric Suction Measurement.....	98
Data Representation and Discussion.....	100
Resilient Modulus.....	100
Soil Suction.....	104
Conclusion.....	109
Chapter 7- Fatigue Life Evaluation of Pavement Embankments made with Tire Derived Aggregates.....	111
Abstract.....	112
Introduction.....	113
IRRF Test Road.....	115
Falling Weight Deflectometer Testing.....	120
Analysis of Data.....	121
Conclusion.....	128
Acknowledgement.....	129
Chapter 8- Conclusions and Recommendations.....	131
Conclusions.....	132
Recommendations.....	135
References.....	140

Chapter 1- Introduction

Statement of the Problem

A pavement system is a multi-layer structure that provides ease of ride for commuters by successfully transferring the traffic-induced loadings to the ground. A typical flexible pavement structure is comprised of Hot Mix Asphalt (HMA), the strongest material in terms of strength, overlying the Granular Aggregate Base (GAB) layer placed on top of subgrade soil which is the weakest material. Each pavement material has its own properties and mechanical characteristics, thus, each respond to traffic and environmental loading, differently. Over the past few decades pavement design methods have switched from purely empirical approaches to mechanistic-empirical philosophy. In the mechanical part of the design, the causes of pavement distresses and failures are targeted and in the empirical part, the performance of the designed pavement is observed and related to the mechanical inputs through the design procedure. In the Mechanistic-Empirical Pavement Design Guide (MEPDG), environmental and traffic inputs are considered and the ultimate response of the pavement is evaluated in terms of pavement distresses such as fatigue and permanent deformation (rutting) failures. Analyzing the pavement performance in real conditions is the only way in order to evaluate the pavement design approaches.

Pavement materials in cold regions are exposed to inclement weather conditions including prolonged winter seasons, short thawing periods and long summer days. Therefore, pavements are prone to several damages and distresses in cold regions. In the winter, as the ambient air temperature decreases below the freezing point of water, the frost depth penetrates throughout the pavement layers. This leads to the formation of ice lenses, which further causes differential frost heave on the pavement surface. During rapid thawing season, accumulation of excess moisture content within the subgrade layer tends to drastically decrease the respective Resilient Modulus (M_r) of subgrade material. In order to lessen the damages and distresses imposed on

the roads during the crucial short thawing period, it is very important to take measures by setting Spring Load Restrictions (SLR) on roads with problematic subgrade material to prevent heavily-loaded trucks from trafficking on the roads. With the recent changes in global climate patterns, the onset of freezing and thawing seasons does not necessarily follow an expected schedule from year to year. Therefore there is a need to evaluate the performance of current SLR models to assess their applicability in Edmonton area.

While imposing SLR on roads can reduce the pavement damages and distresses during the critical thawing season, rutting and fatigue failure can potentially occur anytime during the service life of roads. Subgrade and HMA materials are more vulnerable to rutting failure while fatigue failure is usually observed within the HMA layer of the pavement. It is well understood that due to viscoelasticity of the HMA material, it is highly sensitive to the variation of ambient temperature values. Therefore, the dynamic modulus of HMA can vary significantly in different seasons. Subsequently, because of significant temperature variation between cold and warm seasons in cold regions, the HMA layer experiences damages such as thermal cracking and rutting in cold and warm seasons, respectively. These temperature-induced fluctuations in the stiffness of HMA would result in subsequent variation in the overall bearing capacity of the pavement structure. Ability to accurately measure/predict the exact temperature within the depth of the HMA layer plays an important role in successfully analyzing the pavement performance.

As stated before, rutting failure can also be observed in subgrade layer. A weak and soft subgrade soil could contribute to almost 40% of the total permanent deformation in the pavement structure; hence, clarifying the permanent deformation mechanism in subgrade soils and developing predictive models can help engineers design more durable pavements with optimal thickness of asphalt concrete layers. Modelling of permanent deformation of pavement

granular and subgrade layers is one of the research topics that has less been studied by researchers in previous years.

Weak subgrade material can be modified or completely replaced by new types of recycled/waste materials in order to improve pavement performance with respect to subgrade permanent deformation and fatigue life of the HMA layer. In this approach, there are two alternatives available due to their abundance in Alberta including Bottom Ash (BA) and Tire Derived Aggregates (TDA). BA is a waste byproduct of coal-fired power plants which are dominating in production of electricity in Alberta. TDA material is made by recycling scrap tires which can be sourced from mining and light weight trucks or passenger cars tires. In Alberta, Canada, more than five million tires reach the end of their life cycle each year, and an increase in this number is expected as the population increases. Simply discarding tires is not a solution because of limited landfill sites. Thus, sustainable use of recycled materials in order to address the engineering problems and decrease the burden on landfills and respective environmental side effects is highly appreciated.

Research Objectives

The main goals of this study was to evaluate the thermo-mechanical performance of different layers within the pavement system. The thermal performance of roads during winter and thawing seasons were evaluated based on collected field data. Temperature prediction modelling for the HMA layer was performed in order to help pavement engineers better estimate the performance of asphalt concrete with respect to seasonal temperature variations. Additionally, the mechanical performance of subgrade soils under dynamic loading in terms of M_r and permanent deformation was studied. Finally, the effect of using recycled material as soil stabilizer or road embankment filler was evaluated based on lab and field testing.

To achieve the objectives, the following tasks were targeted:

- Perform Falling Weight Deflectometer (FWD) at an instrumented test road in Edmonton with the aid of advanced data acquisition system in order to evaluate the actual pavement layers' performance with respect to seasonal effects.
- Characterize the HMA, GAB and subgrade layers' respective moduli at field based on the backcalculation of FWD data.
- Simulate the pavement response to FWD loading based on Multi-Layer Elastic Theory (MLET) for evaluating SLR models' performance.
- Collect and analyze the field ambient weather station data and field temperature data for developing HMA temperature prediction models.
- Evaluation of the performance of SLR models based on actual field conditions for all pavement layers in Edmonton.
- Design, develop and perform several lab triaxial testing on subgrade soils materials under controlled dynamic loading and moisture contents.

Scope of the Work

To achieve the objectives of this study, several lab testing programs were developed and performed in the lab using Universal Testing Machine (UTM-100) and other lab instruments as per respective standard procedures. Field test were performed at Integrated Road Research Facility (IRRF) located in northeast Edmonton. The test road was instrumented with environmental and traffic response sensors. FWD tests were conducted on top of the HMA layer at exact locations where the strain gauges were embedded at the bottom of the HMA layer. The response data along with all the environmental data were collected using dataloggers from Campbell Scientific Canada and transmitted to the university through remote desktop access. MLET simulation of the pavement structure under dynamic FWD loading was

performed using KENLAYER software. All the statistical modeling were performed using Mathematica and Microsoft Excel computer programs.

Structure of Dissertation

This thesis is prepared in an integrated-article format. Each chapter of the thesis presents separate but related studies. All studies presented in chapters 3 to 7 have been published in peer-reviewed scientific journals.

Chapter 1 consists of an introduction to the conducted research and general explanation of the objectives and scope of the work in this research study.

Chapter 2 is a quick review of the surveyed literature on the general background about the topics covered in the subsequent chapters.

Chapter 3 discusses the evaluation of performance three SLR models, which are currently being used by transportation agencies, in successfully determining the date to apply and remove SLR on vulnerable roads.

Chapter 4 presents the development of temperature prediction models for the HMA layer of pavement based on two-year collected field weather and temperature data.

Chapter 5 explains the results of lab triaxial testing on subgrade material under controlled stress and moisture condition to develop permanent deformation prediction models.

Chapter 6 describes the results of the study to take advantage of BA in improving subgrade soil's M_r .

Chapter 7 discusses using TDA material as tire embankment and the effect of using this material on the fatigue life performance of the HMA layer of the pavement as compared to that of a conventional pavement structure.

Chapter 8 is the summary of findings, conclusions, and recommendations for future studies.

Chapter 2- Literature review

Different Types of Pavement Structures

Flexible Pavement

The most common type of pavement structures in Alberta, Canada are flexible pavements which are comprised of different layers. The top layer of flexible pavement is usually a bituminous material surface course in the form of Hot Mix Asphalt (HMA). Depending on the designed thickness of the HMA layer, it can comprise of two sublayers at the bottom and on top which are called binder course and wearing course, respectively. The wearing course which is directly in touch with traffic and environmental loadings, is constructed with dense graded HMA material. This layer provides enough friction and smoothness of ride to the vehicles and commuters, respectively. The wearing course should be impermeable to protect the entire pavement from the ingress of moisture. The binder course which is underlying the wearing course is comprised of larger aggregate particles and less bituminous material for economical purposes. A bed of compacted GAB layer, which might be underlaid by lower quality compacted granular course called sub-base, is placed directly beneath the binder or wearing course. The GAB provides additional support for distributing the traffic load and also enhances the subsurface drainage of water out of the system. The last layer of the pavement which is supporting all the upper layers is subgrade soil. Usually, the top 6 in of the subgrade layer should be compacted at the optimum moisture content to target the required density. Due to economical design purposes, the quality of materials decreases from top to bottom in that the HMA layer has the highest quality in terms of material load bearing capacity and the subgrade is normally the weakest material (Huang 1993, Alberta pavement design manual 1997). Even though the magnitude of traffic-induced stresses diminishes from the surface of the HMA to the top of the subgrade, the subgrade layer plays an important role in the successful operation throughout the life time of flexible pavements.

Rigid Pavement

In the design of rigid pavements, cement concrete or reinforced concrete slabs are used. The bearing capacity of the rigid pavements dominantly relies on the high flexural strength of the top concrete slabs. Therefore, unlike flexible pavements in which the bearing capacity and permanent deformation of subgrades is a crucial parameter in the operation of roads, rigid pavement structures can withstand locally generated subgrade failures without having the performance of the entire section affected. The weakness in bearing capacity of subgrade soil under dynamic traffic loading can be reflected upon the pavement structure in the form of rutting failure of the entire section stemming from the permanent deformation of this layer (Huang 1993). Figure 2-1 schematically depicts the cross section of flexible and rigid pavements. Table 2-1 briefly compares the rigid and flexible pavement structures.

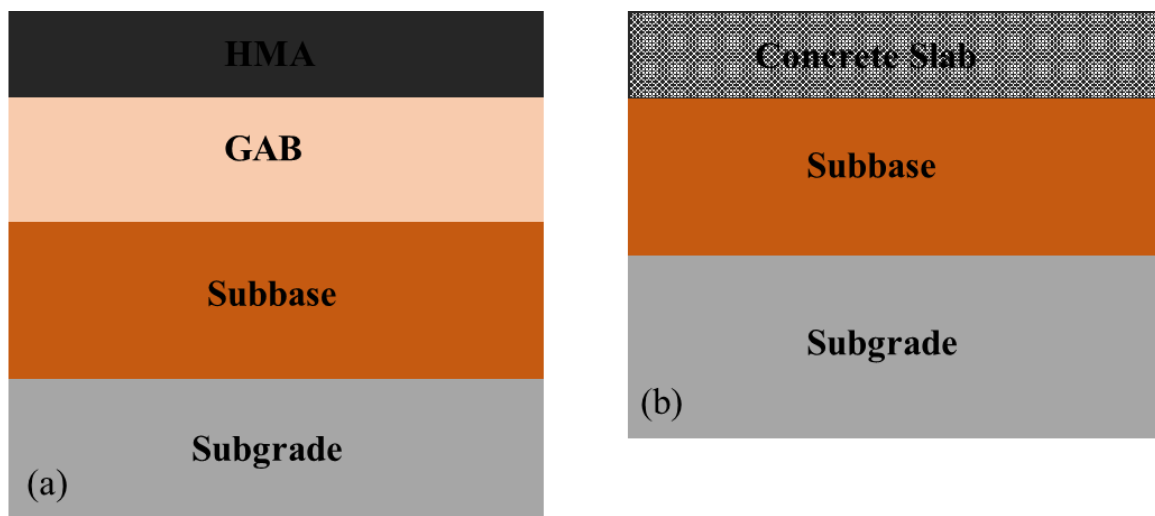


Figure 2-1- Schematic cross section of (a) flexible pavement and (b) rigid pavement

Table 2-1- Comparison between Flexible and rigid pavements (Design R. 2018)

Flexible	Rigid
Design life of 10- 20 years	Design life of more than 30 years
Lower construction costs	Higher construction costs
Higher maintenance costs	Lower maintenance cost
Low flexural strength	High flexural strength
Suitable for high temperature variations	Not good for high temperature variation
Subgrade performance is critical	Local subgrade failures can be withstood

Effect of Environmental Loading on Pavement Materials

Pavement system is a composite structure made out of different materials each of which behave differently in response to environmental loadings. Among all climatic factors, temperature and moisture are the most critical parameters having a noticeable impact on the performance of flexible pavement structures. Unbound granular materials are mostly affected by moisture content fluctuations within the pavement, while bituminous materials such as HMA are highly vulnerable to temperature variations because of their respective viscoelastic properties. In the succeeding sections, the effect of moisture and temperature on pavement materials will be discussed further.

Unbound Materials

In cold regions, with seasonal freeze-thaw during the winter and thawing periods, internal moisture content of the pavement can vary significantly. With the onset of freezing conditions, the freezing front ingresses down through the ground as the heat balance in the system is disturbed by lack of heat supply on the surface of the pavement. Accordingly, pore water starts to freeze and with the formation of ice lenses and ice-bonding, more water tends to be sucked up and form more ice lenses (Konard and Morgenstern 1980). This frozen state within the

unbound materials in the pavement leads to temporary increase in the stiffness of the pavement granular layers. Thus, the load bearing capacity of the pavement increases respectively (Janoo 2002, Janoo and Cortez 2002). Figure 2-2 schematically shows the variation in the stiffness of the pavement unbound granular layers with respect to temperature in cold regions. The frozen condition will temporarily help the pavement structure withstand heavier traffic loading. With the beginning of spring season, thawing process starts which leads to accumulation of excess pore water within the subgrade layer. Due to this event, the M_r of the subgrade significantly drops down and thus, the load-bearing capacity of the entire pavement structure is reduced (AASHTO 1961). This period of time is very critical for the pavement since it can undergo non-reversible distresses and damages under the traffic-induced loading. After the sudden decrease in the stiffness of subgrade, as the excess moisture content drains out of the system over time, the pavement gradually gains back its bearing capacity. Normally, during mid-summer the pavement gets back to its recovered condition in which the moisture content within the layers varies around the pre-frozen condition, and the pavement structure regains its expected load bearing capacity. It is very important to take measures in order to preserve the road with vulnerable subgrade layer from undergoing damages and distresses during the very crucial thawing period.

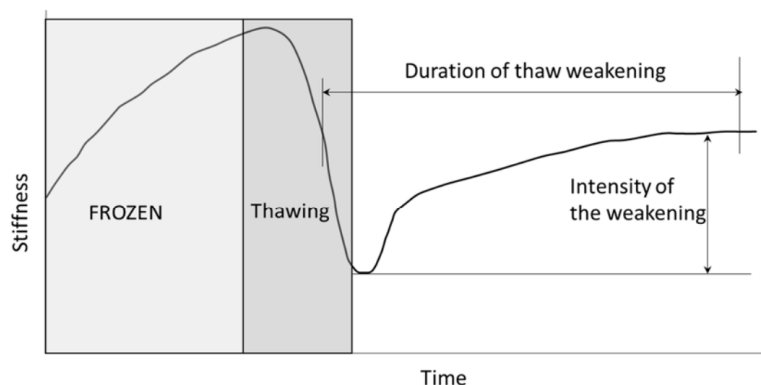


Figure 2-2- Schematic changes in the soil stiffness during the freeze and thaw periods (Doré and Imbs 2002)

M_r was first introduced as an important material property decades ago by (Seed et al. 1962). M_r is defined as the elastic stiffness of subgrade soils under cyclic loading, which is numerically the ratio of the deviatoric stress to resilient or recoverable strains of the material under a constant confining pressure in repeated triaxial load tests. M_r is an important parameter for calculating resilient stresses, strains, and deformations in flexible pavements. Additionally, the thickness of the HMA is chosen based on the M_r values of the unbound material used in the construction of roads. The variations in the M_r values can lead to a vast variation in the chosen HMA thickness. The subgrade stress-strain behavior is reflected in pavement surface deflections and rutting failures (Li and Selig 1994, Burczyk et al. 1994). Therefore, evaluating the M_r for subgrade materials is essential for a successful pavement design, which satisfies the performance expectations and provides ease of ride for commuters. Initially, it was suggested that the RM of soils could be considered a constant value for design of pavements (AASHTO 1993). Later, several studies showed that M_r of subgrade soils depends strongly on the soil structure, stress states and more importantly, moisture content (George 2004, Liang et al. 2008). Variation of M_r in subgrade soils have been reported to be even more than 50 percent as the rainfall changes throughout the year (Ovik et al. 2000). In the literature, there have been several studies trying to develop prediction equation for M_r of subgrade soils based on parameters such as confining stress, bulk stress, deviatoric stress and subgrade soil physical properties. However, few studies aimed to incorporate the effect of moisture variation and respective generation of matric suction in the soil into the M_r prediction models (Liang et al. 2008).

Asphalt Materials

It is well understood that HMA is a viscoelastic material whose mechanical performance, in terms of dynamic modulus, varies significantly with respect to variation of temperature. At low temperatures during winter season, the HMA behaves mostly as a brittle material while visco-

elastic behavior dominates at higher temperatures in the warmer seasons (Pirmohammad and Kiani 2016). The HMA dynamic modulus can vary from 1 GPa to more than 30 GPa due to temperature variations in warm and cold seasons, respectively (Bodin et al. 2016). Characterization of HMA's seasonal variation of temperature plays an important role in design of pavements and in understanding the pavement's seasonal performance with respect to real traffic loading, or in the case of back-calculation of field FWD tests which are conducted to analyze the pavement performance against environmental and traffic loadings.

Spring Load Restrictions (SLR)

The province of Alberta is well-known for its inclement weather conditions in terms of high fluctuations in ambient air temperature between summer and winter seasons. While summer temperatures can go as high as 40 °C, the temperature can drop to -50 °C during the winter period (Watson and Rajapakse 2000). Thus, pavement structures experience severe temperature variation during their service life. As stated above, pavement experiences the lowest bearing capacity during the thawing period due to accumulation of excess moisture content within the top of the subgrade soil. Thus, it is highly vulnerable to truck trafficking-induced distresses and damages. Decreasing the maximum truck axle load or even closing roads to heavy traffic during the thaw-weakening season is a common practice for many North American authorities. It is well-documented that the application of SLR is of utmost importance in increasing the durability of roads (Baiz et al. 2008; Miller et al. 2012, Chapin et al. 2009).

By setting seasonal weight programs, trucks are not allowed to pass on problematic roads at their maximum capacity. Even though applying SLR increases a road's life expectancy, trucking industries struggle with the imposed restrictions. Enforcing detours and (or) restricting a truck's maximum payload usually requires a greater number of trips, which leads to an

inevitable increase in fuel consumption. Thus, to accommodate economic needs and minimize the expenses evoked by the SLR policies, it is important to precisely estimate and enforce the SLR-on period to address the particular conditions of vulnerable roads (Chapin et al. 2012).

One of the first primitive methods to apply and remove SLR was to use predetermined fixed dates based on experience. This method is indeed not accurate since climate does not follow the same pattern each year. The other method is based on visual observation of the field condition and engineering judgement. A problem with method is that by the time that some signs of thawed condition, such as seeping of moisture out of the surface cracks or rapid deterioration of shoulders, are observed the pavement has already experienced some levels of damage. Many researchers and/or transportation agencies developed SLR models based on climatic data and FWD field tests (Ovik et al. 2000).

On the other hand, as applying SLR may cause economic hardship to trucking industries, transportation authorities apply Winter Weight Premium (WWP) on roads during their fully frozen condition in order to take advantage of road's temporary gain in bearing capacity. In this regard, the trucks are allowed to pass on the roads with more than their regular maximum allowed payload without making significant damages to the pavement structure. Each transportation agency has its own policies with respect to percent increase in maximum allowable payload during WWP-on period (Bradley et al. 2012).

With recent changes in global climate patterns, the onsets of freezing and thawing seasons do not necessarily follow an expected schedule from year to year. Prolonged fall seasons, shorter and warmer winter seasons, and an early thawing are some of the recently observed irregularities in Canada's climate patterns (Bradley et al. 2012). These changes demonstrate an immediate need to re-examine the validity of current seasonal weight programs, which include the imposition of WWP and SLR on low-volume roads. Since pavement gains more strength

as the frost depth penetrates through its layers during successive cold days, authorities apply WWP during the early winter to allow an increase in trucks' loading capacities to alleviate the impacts of SLR-on periods on trucking industries (Miller et al. 2012).

HMA Temperature Prediction Models

In the literature, many research studies have tried to predict the temperature distribution along the HMA layer by taking different approaches such as analytical and theoretical, numerical and finite element, and statistical and probabilistic methods (Islam and Tarefdar 2015). Previous studies have considered several climatic and environmental parameters such as air temperature, solar radiation, wind speed, relative air humidity, heat convection, and heat diffusion in the development of prediction equations (Islam and Tarefdar 2015, Alavi et al. 2014, Khadrawi and Al-Shyyab 2012). All of the developed prediction equations have their own strengths and weaknesses. In some cases, the developed equations are too complicated and require the availability of numerous variables in order to predict the pavement temperatures. For example, a numerical temperature prediction model developed by (Han et al. 2011) involved several parameters such as absorption coefficient, emissivity coefficient, downwelling long-wave radiation of heat flux, heat convection by wind, etc., which are not easy to measure for routine engineering practices. Therefore, these models are not practical for routine use in practice. The statistical methods, while efficient at developing simpler prediction equations, sometimes under-predict the pavement's high temperatures, and over-predict the pavement's low temperatures (Islam and Tarefdar 2015).

Effect of Traffic Loading on Pavement Materials

The pavement performance is dominantly influenced by traffic loading in terms of loading magnitude, configuration of loading patterns and the number of loading repetitions by heavy vehicles such as trucks and trailers (Huang 1993). The damages imposed upon the pavement

per pass of vehicles axles is defined based on the AASHTO 1993 definition, standard 80 kN single axle load. Therefore, pavement structures are designed in order to withstand certain number of standard axle load repetitions during their service life. There are several types of distresses developed in the pavement during its operation period. Fatigue cracking on the HMA surface, surface deformation (rutting), disintegration in the HMA mixture such as (potholes, raveling, etc.) and thermal cracking are the most common types of failures observed in flexible pavements.

Rutting

Rutting is reflected upon the surface of the pavement as depression in the wheelpath of the vehicles. . All pavement layers potentially contribute to the accumulation of rutting, which can lead to discomfort to passengers at initial stages and complete failure of the pavement in the case of severe rut development (Uzan 2004). In a pavement with a well-designed asphalt mixture and well-constructed thickness, rutting occurs largely in the unbound granular base course and subgrade layer because of growing traffic-induced irrecoverable compressive strains. These strains lead to large vertical permanent (plastic) deformations in the pavement system. Subgrade rutting happens because of moisture fluctuation within the subgrade layer during freeze-thaw seasons and in the case of heavy rainfall when the drainage condition of the pavement is not able to satisfy the expectations. Additionally, high repetitive compressive stresses on top of the subgrade can cause permanent deformation within the subgrade layer which leads to rutting failure of the pavement (Puppala et al. 2009, Uzan 2004). HMA rutting occurs because of poor mix design, temperature variation within the HMA layer and presence of plastic fines in the asphalt mixture.

Fatigue Cracking

Fatigue cracking which is also called alligator cracking is the major type of distress observed in flexible pavements. Even though, fatigue cracking can be associated with several factors such as poor drainage at the bottom of the HMA layer, aging of HMA mixture, or temperature variations, repeated traffic loading is deemed to be the main trigger of fatigue cracks initiation at the bottom of the HMA layer in response to high tensile strains generation (Huang 1993). Fatigue cracking can propagate through the entire depth of the HMA layer. This will let water from precipitations ingress through the unbound granular and subgrade layers. As stated before, moisture condition can drastically affect the M_r of subgrade layer, which in turn leads to rutting failure in the form of excessive deformation within the subgrade layer and entire pavement structure. Several research studies suggested that the tensile strain at the bottom of the HMA layer must be set to a limited magnitude in design procedures in order to limit or control formation of fatigue cracking (Priest and Timm 2006).

Subgrade Permanent Deformation

The magnitude of rutting in a pavement depends on factors such as material stiffness, stress history in the materials, traffic load-induced stresses, materials' permanent deformation potential, and environmental factors (Uzan 2004). Because it is the last layer supporting all the overlying layers, how the subgrade soil performs against rutting is important in the design of successful and durable flexible pavements. A weak and soft subgrade soil could contribute to almost 40% of the total rutting in the pavement structure (Pupalla et al. 1999); hence, clarifying the permanent deformation mechanism in subgrade soils and developing predictive models can help engineers design more durable pavements with optimal thickness of asphalt concrete layers (Pupalla 2009). Of all the laboratory methods researchers have suggested in the past few decades for studying and simulating the development of permanent deformation in pavement

materials, the Repeated Load Triaxial (RLT) test, which allows the soil specimen to undergo stress states similar to the field conditions, is considered to be the best practical procedure (Pupalla 2009, Erlingsson and Rahman 2013). Performing an RLT test on soil specimens provides valuable insight into the M_r and permanent deformation behavior of subgrade soil materials. The general consensus is that because the subgrade soil has a higher M_r , its permanent deformation under repetitive loading would be less (Pupalla 2009). However, silty sand and sandy silt soils are two exceptions for which large permanent deformation has been reported in the literature despite their high resilient moduli (Pupalla 2009, Pupalla et al. 1999, Ullditz 1993).

Many researchers used the elasticity theory to estimate the average typical stress state within the pavement subgrade layers based on numerical simulations and field measurements. The KENLAYER software was used for stress analysis of different types of pavements configurations including different HMA thickness values. FWD testing was also performed to support the theoretical analysis. As a result of these studies, the confining pressure ($\sigma_3 = 13.8$ kPa) and the deviatoric stress ($27.6 \text{ kPa} < \sigma_d < 41.4 \text{ kPa}$) appear to be the more common stress levels on top of the subgrade layer (Elliott et al. 1988, George 2004, Mohammad et al. 2007, Ji et al. 2014). Some research recommended use of $\sigma_3 = 13.8$ kPa and $\sigma_d = 41.4$ kPa to find the M_r of subgrade material in pavement design (Ji et al. 2014). However, because of the complexity of in-service traffic loadings, it is inevitable that the subgrade layer will undergo stress levels below or above the typical average ranges used in design. Also, little research has been conducted on the permanent deformation behavior of silty sand soils under different stress state scenarios. This is mainly because the permanent deformation test is not easy to perform, and because it is a destructive test, each test setup requires a new specimen. Also, this test is time-consuming, particularly if it is run at more than 10,000 stress applications.

Subgrade Soil Stabilization

Soft subgrade soils such as clay generally have undesirable engineering characteristics showing high compressibility and low strength and susceptibility to moisture content fluctuations. Therefore, construction of roads on these types of soils is challenging for pavement engineers. One conventional approach in dealing with problematic soft subgrade soil is to completely remove and replace them with higher strength backfill materials such as gravel or crushed rocks. However, this option is not feasible in all construction fields due to the unavailability of substitute material. Thus engineers have tried to use other materials in order to physically and/or chemically stabilize the in-situ subgrade soils (Senol et al. 2006, Ozdemir 2016). Several researchers studied the feasibility of using different materials, such as lime, cement, husk ash, and fly ash as soil stabilizers in clayey soils (Brooks 2009, Alhassan 2008, Sezer et al. 2006, Misra 1998, Ozdemir 2016, Prusinsiki and Battacharja 1999). Bottom ash has also been used in clayey soil stabilization in other studies and yielded an improvement in the stiffness and elasticity of the clay (Modarres and Nosoudy 2015, Rifa'i et al. 2009). It is worth noting that bottom ash contains high amounts of silica–aluminous compounds, and can enhance pozzolanic reactions which are those reactions forming cementitious bonding between soil particles. Therefore, in other studies, clayey soil was stabilized with a mixture of bottom ash and Portland cement (Osinubi 2000, Ahmed et al. 2014). However, mixing clayey soil with pure bottom ash would result merely in mechanical stabilization of the soil, and there is no chemical reaction involved.

Use of Tire Derived Aggregates in Road Embankments

With dwindling natural sources of aggregates and pavement materials, the need for substitute sustainable construction materials is increasing. On the other hand, construction of pavement structures on problematic soils comprised of unsuitable materials is unavoidable at times. TDA

material is one of the recycled materials which has gained interest in recent years as an engineering material. TDA is made by cutting scrap tires sourced from passenger cars, light weight trucks or off-the-road trucks operating in mining and construction industries. The TDA particle size can normally range from 50 to 300 mm. TDA is a lightweight material with high compressibility and significant drainage capability which makes it a suitable material as backfill in earth retain walls, road embankments and drainage layers in engineering problems (Murphy 2007). On the other hand, feasible application of TDA material can potentially alleviate the environmental side effects and hazards involved with stockpiling scrap tires.

Summary

Flexible pavement structure is a complex system comprised of different layers each of which plays an important role in its successful operation. In Canadian climate with severe freezing temperatures, short thawing period and long summer days, all pavement layers are affected by environmental loading. The dynamic modulus of the HMA layer as a viscoelastic material is highly affected by temperature fluctuations. Any unexpected decrease in the stiffness of this layer leads to premature failure of the pavement. On the other hand, short thawing period can lead to accumulation of excess moisture content in underneath layers. Subgrade soil, as the last layer supporting the entire pavement structure, is highly vulnerable to moisture variations. The M_r of this layer can significantly drop as the moisture content increases. On the other hand, its long-term permanent deformation performance under repetitive traffic dynamic loading directly affects the formation of rutting failure in the pavement structure.

The main goals of this study was to evaluate the thermo-mechanical performance of different layers within the pavement system. The thermal performance of roads during winter and thawing seasons were evaluated based on collected field data. Temperature prediction modelling for the HMA layer was performed in order to help pavement engineers better

estimate the performance of asphalt concrete with respect to seasonal temperature variations. Additionally, the mechanical performance of subgrade soils under dynamic loading in terms of M_r and permanent deformation was studied. Finally, the effect of using recycled material as soil stabilizer or road embankment filler was evaluated based on lab and field testing.

Chapter 3- Evaluation of Spring Load Restrictions and Winter Weight Premium Duration Prediction Methods in Cold Regions According to Field Data

A version of this chapter was published as “Asefzadeh, A., Hashemian, L., Haghi, N.T. and Bayat, A., 2016. Evaluation of spring load restrictions and winter weight premium duration prediction methods in cold regions according to field data. Canadian Journal of Civil Engineering, 43(7), pp.667-674”.

Abstract

Road pavements in frost-susceptible regions are challenged by frost-thaw induced damages. Spring load restriction (SLR) is intended to reduce road distresses caused by heavily loaded truck trafficking. Winter weight premiums (WWP) is applied during early freezing season by increasing the maximum allowable axle loads in order to reduce the economic difficulties that trucking industries undergo during thaw season. While there are various timelines for applying and removing SLR, this chapter reviews three of the SLR prediction models along with a WWP computer simulation and verifies the calculations based on each method using two years of monitored field moisture and temperature data from the fully instrumented integrated road research facility (IRRF) test road in Edmonton, Alberta, Canada. The results revealed that two of the methods showed a significantly better performance in determining the start and end dates of SLR as opposed to the other method. Computer simulations obtained the pavement critical depth beyond which traffic loading did not affect the subgrade material in early freezing season, and collected data aided in estimating the start date of WWP application on the test road. The results were in good agreement with the recommendations suggested by authorities.

Key words: spring load restrictions, winter weight premiums, freeze depth, thaw depth, monitored field data

Introduction

Freezing and thawing in cold regions is a prevalent phenomenon that potentially damages roads by affecting the susceptible granular base and subgrade layers. In the winter, as the ambient air temperature decreases below the freezing point of water, the frost depth penetrates throughout the pavement layers. This leads to the formation of ice lenses, which further causes differential frost heave on the pavement surface. The heave tends to be more pronounced in roads where the subgrade soil is typically composed of moisture-susceptible materials (Baiz et al. 2008, Ningyuan et al. 2006, Miller et al. 2012).

As the temperature rises during the late winter and early spring, thawing begins in both top-down (from the nearest ice lenses to the surface) and bottom-up (where the deepest ice lenses formed) directions. As it progresses, the excess water from melted ice lenses accumulates within the layer, while the bottom sublayers remain frozen. In this partially thawed condition, the drainage of excess water out of the system is hindered by the very low permeability of frozen soil. Therefore, the condition of pavement during thawing season more resembles the unconsolidated, undrained condition, which potentially leads to the entire pavement structure suffering a significant interim loss in bearing capacity (Ningyuan et al. 2006, Miller et al. 2012, Miller et al. 2015). For subgrades comprised of fine-grained soils, its permeability is noticeably low, thus requiring a longer time (from a few weeks to even months) for the excess water to dissipate from the system. As a result, the strength of pavement layers will be affected considerably until the end of the post-thawing season, when the moisture levels within the pavement layers return to those of the normal recovered season.

As indicated by Janoo and Shepherd (2000), more than 90% of heavy traffic-induced damages are exerted upon pavement during the thaw-weakening season. A study conducted by Ovik (2000) observed that the stiffness of a base layer in a Minnesota road with more than 150 mm

hot mix asphalt (HMA) thickness decreased by approximately 38% during the thaw season with respect to what was measured during the fall season when the pavement was presumed to be fully recovered. The stiffness of the subgrade was also reported to decrease by 29% compared to that of the fall values. Therefore, the proper imposition of the spring load restriction (SLR) plays a critical role in preventing distresses to the pavement structure during the thaw-weakening period.

Decreasing the maximum truck axle load or even closing roads to heavy traffic during the thaw-weakening season is a common practice for many North American authorities. SLRs are normally applied in order to alleviate the trafficking-induced damages on vulnerable roads. It is well-documented that the application of SLR is of utmost importance in increasing the durability of roads (Baiz et al. 2008, Miller et al. 2012, Chapin et al. 2009).

Over the past 50 years, human activities have triggered influential climate changes by releasing a substantial amount of carbon dioxide into the atmosphere, which has been recognized as the main reason for global warming (Karl 2009). Therefore, with the recent changes in global climate patterns, the onset of freezing and thawing seasons does not necessarily follow an expected schedule from year to year. Prolonged fall seasons, shorter and warmer winter seasons, and an early thawing are some of the recently observed irregularities in Canada's climate patterns (Bradley et al. 2012). These changes demonstrate an immediate need to re-examine the validity of current seasonal weight programs, along with the imposition of winter weight premium (WWP) and SLR on roads. On the other hand, during successive cold days, pavement gains more strength as the frost depth penetrates through its layers. In order to alleviate the impacts of SLR-on periods on trucking industries, authorities apply WWP during the early winter to allow an increase in trucks' loading capacities (Miller et al. 2015).

Even though applying SLR increases a road's life expectancy, trucking industries struggle with the imposed restrictions. Enforcing detours and/or restricting a truck's maximum payload usually requires a greater number of trips, which leads to an inevitable increase in fuel consumption. Thus, to accommodate economic needs and minimize the expenses evoked by the SLR policies, it is important to precisely estimate and enforce the SLR-on period in order to address the particular conditions of vulnerable roads (Chapin et al. 2012).

During the past several years, transportation agencies have applied various methods to define the start and end dates of SLR. With direct methods, such as frost tube monitoring and deflection measurements by performing falling weight deflectometer (FWD) tests, the actual physical condition of the pavement structure is monitored, and the decisions are made based on the evaluation of the current pavement condition. Alternatively, indirect methods usually use weather databases for developing prediction models. Using fixed scheduled dates or visual observations are also still practiced by some of the agencies; however, the credibility of these approaches is highly questionable. For example, by the time the road damage inflicted by heavy traffic load is visually detected, the pavement has already gone through some levels of irreversible distress (C-SHRP 2000).

Despite financial constraints and the lack of instrumented roads in different climate regions, transportation agencies express a growing need for developing SLR research-based duration prediction models. The primary goal of developing different prediction models is to make them simple, yet precise enough to determine the start and end dates for both SLR and WWP (Chapin et al. 2009).

Objectives and Scope of the Work

In this chapter, three reviewed indirect methods were used in order to calculate the SLR and WWP start and end dates for the integrated research road facility (IRRF) test road in Edmonton,

Alberta during the 2013–2014 and 2014–2015 freeze-thaw seasons. The validity of each method was discussed based on air temperature, moisture, and temperature data collected from the test road during the two-year monitoring period. Furthermore, the application date of WWP on the test road was verified based on the simulation of the pavement during cold season utilizing the field data.

SLR Prediction Models

Thawing index (TI) plays an important role in most of the SLR prediction models suggested in the literature. By identifying the days with an average daily temperature (T_{avg}) higher than or equal to a reference temperature (T_r), the cumulative thawing index (CTI) can be defined generally as follows:

$$CTI = \sum(T_{avg} - T_r) \quad (1)$$

where T_r is the average air temperature when the asphalt temperature is fluctuating around 0°C . As days become longer during late winter and early spring, T_r decreases due to the surface of the asphalt layer absorbing a larger amount of solar radiation. This basically means that thawing of pavement layers occurs at lower ambient air temperature during this period. If CTI obtains a negative value, it should reset to zero. Another parameter for determining the start date of WWP is cumulative freezing index (CFI), which is defined as the absolute value of the sum of all days' temperatures falling below 0°C (Mahoney et al. 1986).

Mahoney et al. (1986) suggested empirical equations for determining CTI and CFI by using a fixed T_r value of -1.67°C . Following the start of thawing period, the recommended CTI values of “should-level” and “must-level” thresholds to apply SLR were 15°C and 28°C , respectively, for thick pavements. They suggested the following equation for lifting SLR:

$$CTI = 0.3 CFI \quad (2)$$

The Manitoba department of infrastructure and transportation (MDIT) conducted weekly FWD tests at four pavement test sites during the 2009 SLR-on period and used the FWD deflection measurements, air and pavement temperature data and temperature and/or moisture data through the depth of the test roads in order to develop a prediction model for the SLR (Bradley et al. 2012). Manitoba's method suggests that SLR should be applied when the CTI reached 15°C-days, but no earlier than March 11.

$$CTI = \sum \text{Daily } TI = \sum \left(T_r + \frac{T_{max} + T_{min}}{2} \right) \quad (3)$$

where $T_r = 1.7^\circ\text{C}$ starting March 1 and increasing daily by 0.06°C until May 31; it resets to zero afterwards. T_{max} and T_{min} are the maximum and minimum values of daily temperatures, respectively. If $\frac{T_{max} + T_{min}}{2} < 0$, then the daily TI will change to $T_r + \frac{T_{max} + T_{min}}{4}$ to compensate for the period during which the ambient air temperature temporarily falls below 0°C . SLR should be removed no later than eight weeks after the application date, when the CTI reaches 350°C-days , or May 31, whichever is soonest. The recommended start date of WWP is when the CFI reaches 150°C-days , which corresponds to a frost depth of 75 cm. The recommended removal of WWP is when CTI reaches 1°C-days .

Minnesota department of transportation's method (Mn DOT 2014) is as below:

$$CTI_n = \sum (\text{Daily } TI - 0.5 \times \text{Daily } FI) \quad (4)$$

- When $\left(\frac{T_{max} + T_{min}}{2} - T_r \right) < 0^\circ\text{F}$ and $CTI_{n-1} \leq 0.5 \times \left(32^\circ\text{F} - \frac{T_{max} + T_{min}}{2} \right)$ then daily TI and daily FI should both be assigned 0°F-day .
- When $\left(\frac{T_{max} + T_{min}}{2} - T_r \right) > 0^\circ\text{F}$ then daily TI = $\left(\frac{T_{max} + T_{min}}{2} - T_r \right)$ and daily FI = 0°F-day .

- When $\left(\frac{T_{max}+T_{min}}{2} - T_r\right) < 0^\circ\text{F}$ and $CTI_{n-1} > 0.5 \times \left(32^\circ\text{F} - \frac{T_{max}+T_{min}}{2}\right)$ then daily TI = 0°F -day and daily FI = $\left(32^\circ\text{F} - \frac{T_{max}+T_{min}}{2}\right)$

where CTI_n is a cumulative thawing index calculated over n days ($^\circ\text{F}$ -days); CTI resets to zero on January 1; CTI_{n-1} is a cumulative thawing index for the previous day; T_r is a reference air temperature (32°F for the month of January). It decreases by 1.5°C daily during the first week of February and then by 0.5°C weekly until the end of thawing season.

In this method, the threshold for the SLR start is $CTI = 15^\circ\text{C}$ -days with a forecast of continuous, non-freezing weather conditions. However, it does not provide a definitive suggestion for determining the end date of SLR, even though measured frost depth data, daily air temperature and other considerations are used to provide a better judgement regarding the removal of SLR. As a general recommendation, the upper removal boundary sets eight weeks after the start date of SLR. The WWP application start date occurs when CFI reaches 150°C -days, which is in compliance with the MDIT recommendation. The removal of WWP is not recommended sooner than February 1 unless continuous warm weather conditions could guarantee the progressing thaw within the pavement.

It is worth mentioning that none of the above-mentioned models consider heat transfer in their assumptions. They are empirically developed models aiming at calculating the SLR-on/off dates based on simple environmental parameters.

IRRF Test Road

The IRRF test road facility, which was not yet open to traffic at the time of this study (2013-2015) and recently opened in October 2015, is a new access road to the Edmonton Waste Management Center (EWMC) located in Edmonton, Alberta, Canada. The construction of the IRRF test road started in May 2012 and was finished in August 2013. The test road has two

lanes, each approximately 500 m long. It comprises 25 mm of hot mix asphalt (HMA) including a 90 mm wearing course on top of a 160 mm binder course overlaying a 450 mm well-graded granular base course (GBC) on top of natural subgrade soil, which is mainly composed of clayey sand (SC). Figure 3-1 shows a schematic representation of the IRRF test road cross-section. Different layers throughout the pavement structure are instrumented with thermometers, thermistors and time domain reflectometers (TDRs) to record the temperature data. TDRs were calibrated in the lab using the same subgrade soil from the field to accurately monitor the volumetric water content (VWC) in the subgrade layer (Haghi et al. 2014).

It should be mentioned that, thermistors are usually good for measuring the temperature by direct contact, while thermometers are a better choice in case of measuring temperature in various environments such as air, water, soil, etc.

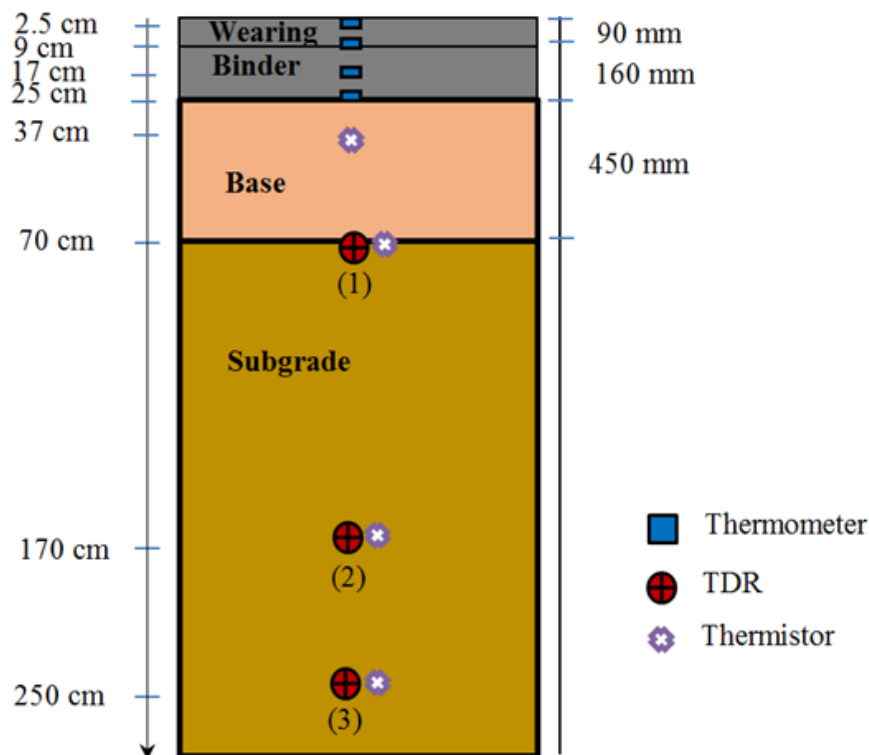


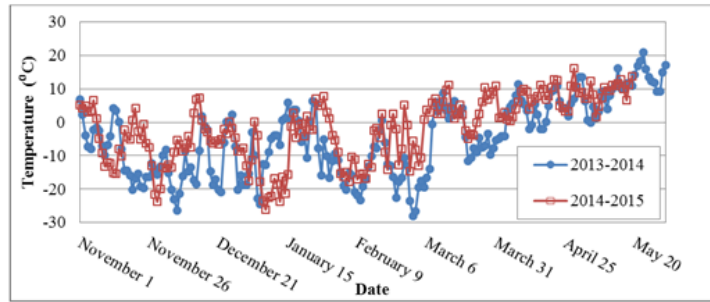
Figure 3-1- Schematic picture of the IRRF test road pavement cross-section

Climate data were collected from the EWMC's closest weather station, located approximately 700 m from the test road. The temperature and moisture data were collected from the sensors connected to a CR-1000 datalogger from Campbell Scientific Canada. The data were then transmitted to the University of Alberta through a remote desktop access. This study has analyzed the retrieved data from November to May during a two-year period of 2013–2014 and 2014–2015 in order to evaluate the validity of the aforementioned methods in accurately predicting the appropriate dates to impose and remove WWP and SLR. It should be mentioned that only TDR-1 was used for VWC data at the top of the subgrade layer. However, the temperature data collected by all of the sensors shown in Figure 3-1 were used in the chapter.

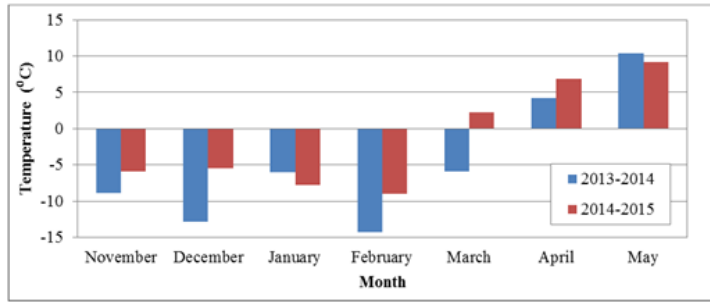
Data Analysis

Ambient Air Temperature

The average daily air temperature and average monthly temperature data during November to May of 2013–2014 and 2014–2015 are presented in Figures 3-2(a) and 2(b). With the exception of January, the winter of 2014 was warmer than the winter of 2013, but the average monthly temperature during March 2015 was approximately 2.2°C in contrast to -6°C during March 2014. This comparison indicates that thawing was likely to occur earlier in the pavement layers in 2015.



(a)



(b)

Figure 3-2- (a) Time history of average daily air temperature (b) Average monthly air temperature during 2013- 2014 and 2014-2015

Calculation of CTI and CFI Based on the Reviewed Methods

Both the CTI and CFI suggested in the three aforementioned methods were calculated using the recorded ambient air temperature data. It is appropriate to note that the T_r used in these calculations was in accordance with the suggested values in each method. However, the future goal is to locally calibrate the models for the test road, and this requires collecting further year-to-year data. Figure 3-3 shows the calculated CTI values over the two-year period. All the calculations were reported in the unit of °C-days for consistency. The only parameter directly influencing the CTI values was the ambient air temperature, and since the winter-spring season of 2014–2015 was warmer, there was a noticeable increase in the CTI values compared to those of the preceding period.

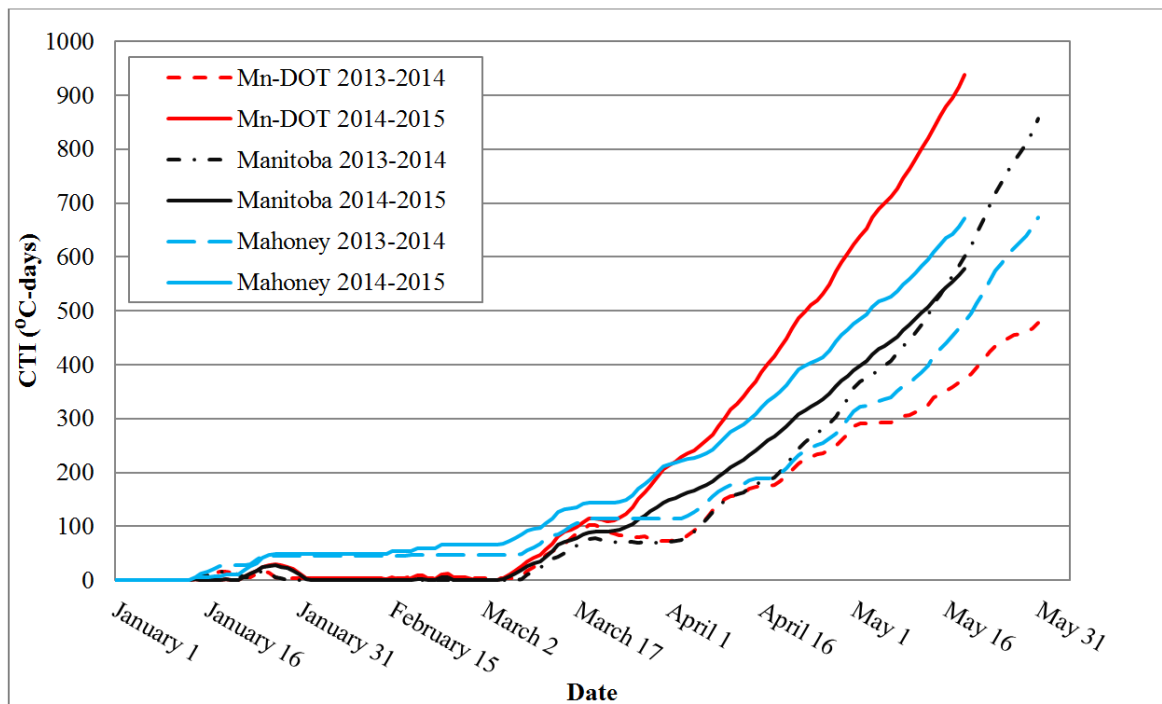


Figure 3-3- Calculated CTI during 2013-2014 and 2014-2015 winter-spring season

Frost and Thaw Depth in the Pavement Layers

Figure 3-4 shows the measured frost and thaw depths throughout the pavement layers. It should be noted that the minimum measurable frost/thaw depth during the 2013–2014 winter-spring season was approximately 37 cm, which was also the depth of the first thermistor placed in the GBC layer. However, the thermometers placed in the HMA layer were wired to the CR-1000 datalogger in August 2014, enabling the researchers to access the temperature data within this layer. Thus, the minimum frost/thaw depth that was measured in the second year was approximately 2.5 cm below the HMA layer surface. Due to technical issues, no data was recorded from November 20, 2014 until January 12, 2015, as seen by the gap in the frost depth data (2014–2015).

It should be mentioned that the frost and thaw depths were calculated based on the vertical temperature profiles generated by collecting the temperatures measured through the depth of the pavement using the embedded sensors. By interpolating between the temperature readings,

and assuming linear variation of temperature, the intersection of the profile with the line $T=0$ °C was found and the frost or thaw depths were calculated.

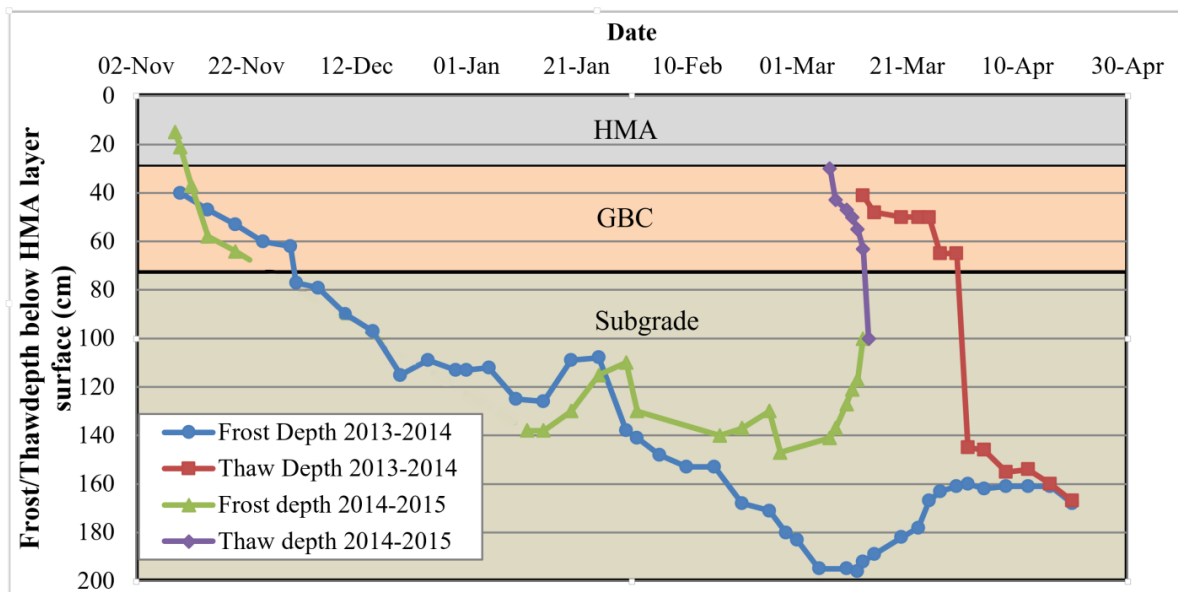


Figure 3-4– Freeze/thaw depths across depth of the pavement structure

The availability of recorded data verified that the frost depth reached the GBC layer on November 10, 2013, two days earlier than the following year, when the same depth within the GBC layer encountered frost on November 12, 2014. Even though the frost depth in the 2014–2015 winter fell below that of the preceding year during mid-January, the subgrade was much less affected by the frost action during the winter of 2014–2015, as the frost depth only reached approximately 150 cm within the layer; however, it was almost 200 cm during the winter of 2013–2014. Furthermore, the maximum frost depth during the second winter was recorded on February 27, 2015, in comparison with that of the first winter, which was recorded on March 12, 2014. Thus, the frost progress period in the winter of 2014–2015 was nearly two weeks shorter than the preceding winter. This fact indicates that a warmer winter would restrict frost depth growth in the pavement layers.

Similarly, a comparison between the two measured thaw depths reveals that thawing started approximately one week earlier in the spring of 2015 compared to the spring of 2014. Moreover, as Figure 3-4 indicates, the thawing duration in 2013–2014 lasted for approximately 37 days starting March 13, 2014, and melted the entire frozen GBC and subgrade layers, whereas in 2015 it finished within one week starting March 7. This could be explained by the difference in average monthly air temperatures in March of both years: 2.2°C in 2015 and -6°C in 2014.

Volumetric Water Content (VWC) Changes throughout the Pavement Structure

The VWC data collected from TDR-1 during the two freeze-thaw seasons are reflected in Figure 3-6. It is worth noting that TDR-1 was selected for the comparison between the two years because this sensor was located at the nearest distance to the pavement surface and thus could be more reflective of the VWC fluctuations due to temperature variation within the upper subgrade layer. On the other hand, as it is depicted in Figure 3-5, the VWC values recorded by TDR-2 and TDR-3 showed less variation and sensitivity to changes in ambient air temperature because of the depth effect which abates sudden changes in temperature at deeper elevations. As recommended by Liu and Shalaby (2013), the highly fluctuating portion of the VWC graph was divided into three steps: (1) Start of rapid VWC increase, (2) Peak of VWC, and (3) End of rapid VWC decrease. Figure 3-6 shows that even though the start of rapid VWC increase occurred on January 13 in both years, the end of rapid VWC decrease in 2015 was observed on February 3, which was almost a week earlier than 2014. A similar one-week time lag was observed when the VWC returned to the recovered levels before the start of the freeze-thaw season. The increase in the VWC during the transition stage in February and March of 2015 can be explained by a noticeably higher ambient air temperature, which accelerated the melting of ice lenses and led to an accumulation of more water within the subgrade layer as opposed to the preceding season. However, the monthly precipitation pattern and groundwater table

fluctuation might also affect the observed difference. At the beginning of the thaw season, the VWC steadily rose up until it reached the recovered level. According to mechanistic-empirical pavement design guide (MEPDG), the recovery period for subgrade soils with $0.1 < (PI)(P200) < 10$ is 120 days. Therefore, for the subgrade soil of the test road with 20% passing through sieve #200 (0.075 mm opening) and plasticity index of 9 the recovery period was deemed to be approximately 120 days (NCHRP 1-37A 2004), suggesting that the dates for recovered VWC levels for the first and second year were June 13, 2014 and June 7, 2015, respectively.

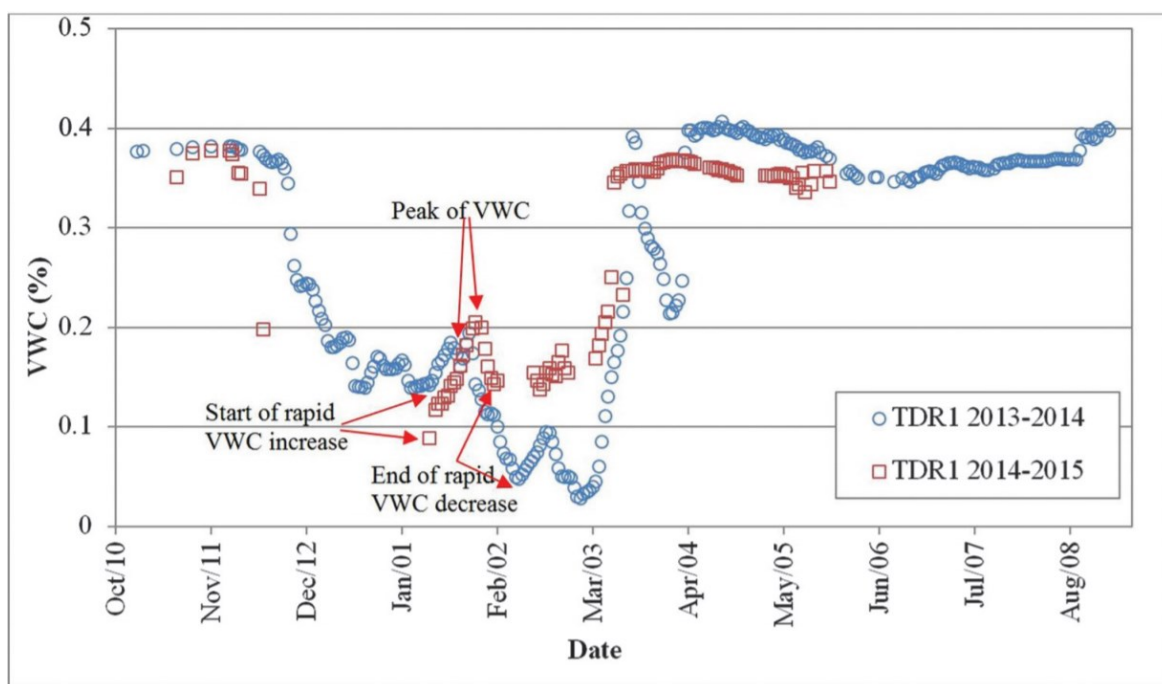


Figure 3-5- VWC recorded by TDR-1 within the subgrade layer

In order to further discuss the moisture variation observed in upper subgrade layer, the VWC measured by TDR-1 was plotted along with temperature time histories in GBC layer and upper subgrade layer measured by the thermistor and TDR-1, respectively (Figure 3-7). It should be mentioned that only data from 2013-2014 was plotted for brevity. It is observed that the trend of VWC changes follows the temperature of GBC and subgrade layers. On the other hand, after mid-March the GBC temperature was obviously higher than that of the subgrade leading to melting of ice in upper GBC sublayers. This would lead to moving of accumulated melt water

downward which supposedly resulted into drastic increase in VWC in upper subgrade during March 12 and March 20, 2014.

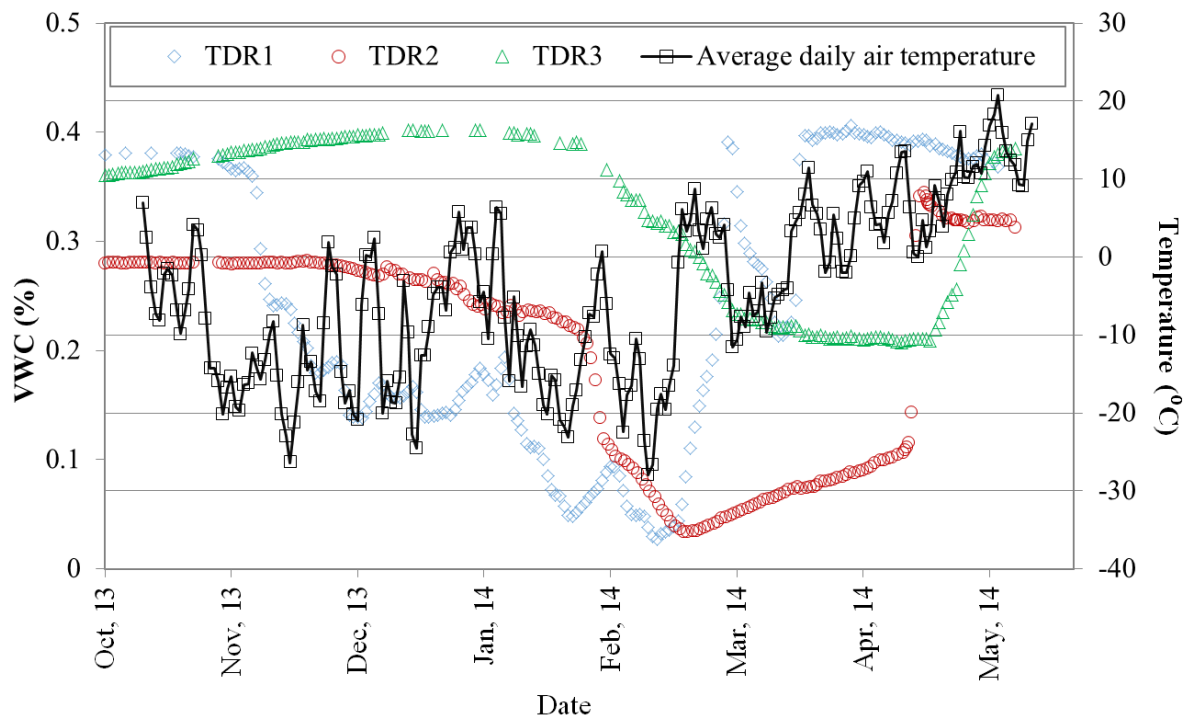


Figure 3-6- Moisture variation through depth of subgrade layer along with average daily temperature in 2013-2014 season

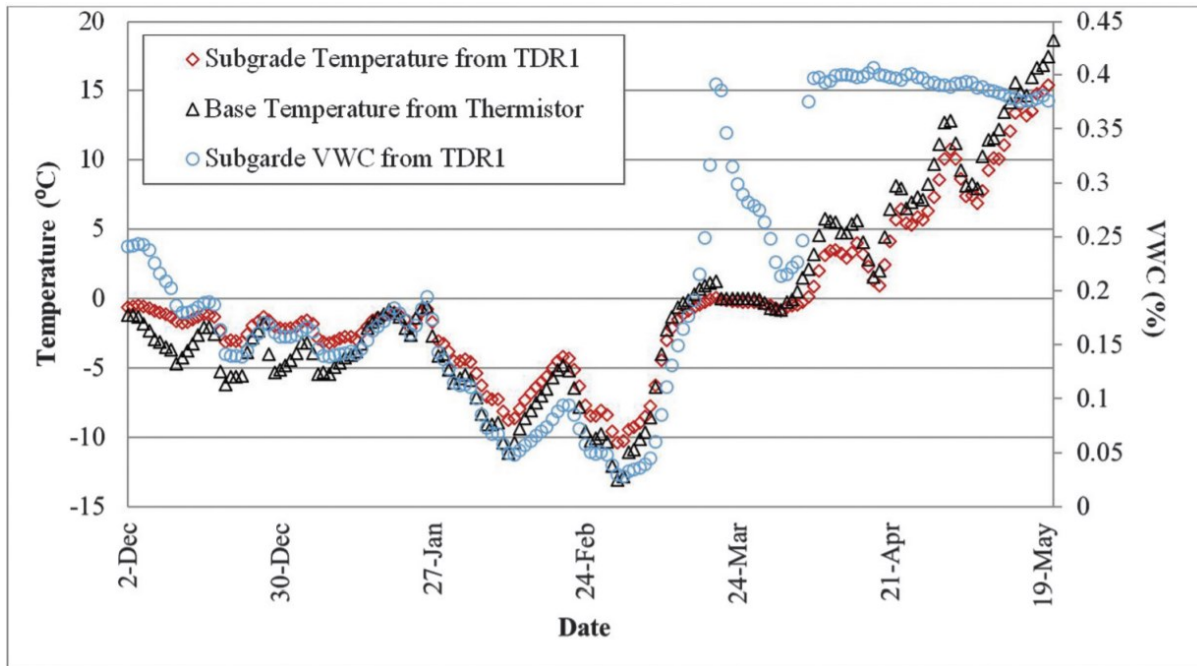


Figure 3-7- Times histories VWC recorded by TDR-1 along with subgrade and GBC temperatures

Moreover, it should be mentioned that the freezing of water in finely graded soil media takes place within a range of temperature and not necessarily at 0 °C. On the other hand equilibrium freezing temperature of water varies in different parts of soil-water system (Williams 1964).

Analysis of the WWP and SLR Application

Finding the critical contact stress depth is essential to determining the start date of WWP application. In this study, the critical depth is defined as the depth through the subgrade layer beyond which the induced vertical pressures caused by traffic loading are insignificant. Al-Qadi et al. (2008) and NCHRP 1-37A (2004) stated that the maximum traffic-induced vertical stress in the subgrade layer becomes insignificant at the depth at which less than 1% of the tire-pavement contact stress is observed. In order to find this depth across the pavement structure of the IRRF test road, the deflection data from a FWD test conducted on the test road on October 17, 2014 were used for the back-calculation of the GBC and subgrade respective

layers' modulus values. The average HMA layer temperature was 11 °C on the test date. The FWD testing completed in October was selected because this was the coldest month prior to November and December, for which the FWD test results were not available. Therefore, it was a rational supposition that the load bearing capacity of the pavement was even higher during November and December because of the colder temperature of the HMA layer.

The corresponding back-calculated modulus values were assigned to subgrade and GBC layers. By rationally assuming that the moduli of GMC and subgrade layers would not significantly change until the start of freezing on November 10, 2013, the coldest average temperature of binder (-1°C) and wearing courses (0°C) found from the corresponding thermometers embedded in each sublayer. To obtain the dynamic modulus of HMA layer, the master curves developed by Shafiee et al. (2015) was used. Therefore, the maximum combined modulus of the entire HMA layer before the start of freezing was found to be 23305 MPa at frequency of 10 Hz. The tire-pavement contact pressure was assumed to be 690 kPa, which is the typical pressure applied on the HMA surface by truck tire. Table 3-1 shows the modulus values that were used as inputs in KENLAYER computer program (Huang 1993) in order to find the critical contact stress depth within the depth of the pavement.

Table 3-1- Back-calculated modulus of pavement layers from FWD test, 17 October 2014

E_{HMA} (MPa)	E_{GBC} (MPa)	$E_{Subgrade}$ (MPa)
23305	200	152

According to the results of stress distribution below the HMA surface, the observed vertical compressive stress was less than 1% of the surface contact pressure at a depth of 105 cm, which was defined as the critical contact stress depth. Table 3-2 shows that how the contact stress distributes within the depth of the pavement. Looking back at Figure 3-4, the frost depth

reached 105 cm below the HMA surface on December 18, 2013, followed by an overall increase in frost depth until March 10, 2014 when thawing process tended to start. It should be noted that there is no data for 2014-2015 season due to datalogger malfunction.

Manitoba’s prediction model for frost depth growth (Soliman et al. 2008) was developed as $FD = c(CFI)^{0.5}T$. This model, along with a linear model, was adopted for the regression analysis on the two-year calculated CTI values. Table 3-3 reflects the results of statistical analysis. It should be mentioned that the statistical analysis was made for those days for which the frost depth was calculated. Thus the sample size for 2013-2014 and 2014-2015 seasons was 37 and 39, respectively. It was concluded that, overall, both prediction models performed well with corresponding high R^2 values and low S_e/S_y ratios. However, the Manitoba model was able to slightly show better statistical performance than the linear model in the second year. It is indisputable that obtaining data in the following years would potentially lead to finding a more reliable statistical model for predicting the freezing depth as a function of CFI addressing the particular conditions in the studied test road. The corresponding CFI value for a freezing depth of 105 cm was discovered to be 515°C-days (on December 18, 2013). However, Bradley et al. (2012) reported a CFI of 150°C-days corresponding to 75 cm of freezing depth as a benchmark for imposing WWP in Manitoba. It should be mentioned that Figure 3-6 shows that a sharp drop in VWC from 0.36 on November 26 to 0.24 on December 1, 2013 occurred at a depth of 70 cm. The same increase in overall pavement strength was indirectly observed in the second year when the VWC decreased drastically from 0.34 on November 17 to 0.20 on November 21, 2014.

Table 3-2- Stress distribution within depth of the pavement under 690 kPa contact stress

Depth (cm)	5	50	80	90	100	105	130
Vertical stress (kPa)	638.2	12.8	8.7	7.9	7.2	6.9	5.5

Table 3-3- Statistical analysis of the frost depth prediction models

Statistical Model	2013-2014			2014-2015		
	R ²	S _e /S _y	Regression Constants	R ²	S _e /S _y	Regression Constants
Linear Model FD = aCFI+b	0.96	0.23	a=0.11 , b=34.84	0.89	0.41	a=0.14 , b=26.56
Manitoba Model FD = c(CFI) ^{0.5}	0.94	0.2	c=4.76	0.96	0.31	c=4.77

In Alberta, WWP starts when the freezing depth reaches 100 cm (Bradley et al. 2012). Thus, the application of WWP would occur on December 15, 2013, which seems to be in acceptable agreement with the date found in this study. However, the author are aware that this conclusion is not generally applicable since it is based merely on the observations from one instrumented test road during the two freeze-thaw seasons. For the current study, the WWP removal date was found to be around February 12, when the CFI started to increase above 0°C-days.

In order to estimate the validity of the start date of SLR as determined by the three methods reviewed in this chapter, it is important to consider the start date of the CTI calculation, as that could have a misleading impact on decision making based on the obtained values. The CTI value depends on the origin date of when the calculations start. As evident in Figure 3-3, the CTI calculation was carried out starting January 1, which led to the CTI values being higher than 15°C-days in mid-January for almost all methods. However, the MDIT method recommends that the SLR should not be applied earlier than March 11. Mahoney et al. (1986) suggested that the CTI should reach specific values following the start of thawing season, which makes it challenging to easily identify the start date of SLR since access to instrumented roads is very occasional.

To address this issue, the author suggest monitoring the weather data to ensure the existence of continuous warm conditions and consider the start date of SLR when the CTI increases at a constant rate. For example, starting March in this study, the CTI kept increasing at the observed

rate of 5–7 °C-days/day. According to what was obtained in this study, the noticeable continual increase in CTI value occurred five and two days ahead of the start of thawing within the pavement in the 2013–2014 and 2014–2015 seasons, respectively. Table 3-4 shows the start and end dates of SLR as suggested by different methods and the start of thawing in each year. It clearly illustrates that the method suggested by Mahoney et al. (1986) was not able to accurately predict the removal date of SLR, since in both years the removal date was determined within or exactly after the end of thaw period while the excess water stemming from melted ice was still in the system. However, looking back at the recovered VWC dates revealed that while MN DOT and Manitoba methods determined the removal dates of SLR more conservatively than the other method, they still seemed not to be precise enough, since the suggested SLR-off dates based on each method fell earlier than the recovered VWC dates.

Table 3-4- The calculated application and removal dates of SLR; pavement thaw and VWC information

	2013-2014		2014-2015	
	SLR-on	SLR-off	SLR-on	SLR-off
Mahoney et al. (1986)	09-Mar	21-Apr	05-Mar	18-Mar
Manitoba (2012)	08-Mar	08-May	05-Mar	28-Apr
Mn DOT (2014)	08-Mar	08-May	05-Mar	05-May
Start of thaw	13-Mar		7-Mar	
End of thaw	20-Apr		14-Mar	
Recovered VWC date	13-Jun		7-Jun	

Conclusion

This chapter utilized the results of two years’ monitored field moisture and temperature measurements in order to evaluate the performance of three prediction models for the application of SLR on the IRRF test road. The WWP application date was also estimated based

on the data collected from the test road during freeze/thaw season 2013–2014. The effect of average monthly temperature on the duration of the thawing process was profound. All three methods discussed in this chapter were very similar in determining the SLR-on date in accordance with the actual thaw condition of the test road. However, the method proposed by Mahoney et al. (1986) was not able to accurately predict the removal date of SLR since the extra moisture accumulated within the pavement layer did not yet completely drain out of the system. On the other hand, the Manitoba's method (Bradley et al. 2012) accurately estimated the removal date of SLR when most of the excess moisture in the pavement sublayers was out of the system.

The regression analysis conducted on the two-year monitored data of CFI and frost depth yielded a linear relationship with high statistics comparable to those of the Manitoba prediction model. Based on the critical contact stress depth of the pavement found via computer simulation, it turned out that the WWP application date found in this study met the recommendations used in Alberta to start WWP.

Even though monitoring the moisture variation in instrumented roads can be a useful measure for evaluating different SLR methods, the development of precise local models would require other promising tests, such as repetitive FWD testing on different roads during the critical period of thawing over the course of several years.

Chapter 4- Development of asphalt temperature prediction models for a test road in Edmonton, Alberta, Canada

A version of this chapter was published as “Asefzadeh, A., Hashemian, L. and Bayat, A., 2017. Development of statistical temperature prediction models for a test road in Edmonton, Alberta, Canada. *International Journal of Pavement Research and Technology*, 10(5), pp.369-382.”

Abstract

This chapter focuses on developing empirical statistical pavement temperature prediction models based on two years of field data collected from an instrumented test road located in Edmonton, Alberta, Canada, from September 2014 to September 2016. Step-wised regression analysis was utilized for developing the regression models based on the most important predictors. The developed models were divided into four categories, including average daily pavement temperature for cold and warm seasons and maximum and minimum daily pavement temperatures at any depth throughout the asphalt layer. One of the models in the literature was adopted and calibrated for the test road to predict instantly the pavement temperature at different depths, which is highly useful for precisely analyzing the results of Falling Weight Deflectometer (FWD) tests. All the models presented in this study showed a significantly high coefficient of correlation. The models were validated using the field data from September to October 2016 and showed satisfactory results.

Introduction

Hot Mix Asphalt (HMA) mixture is a viscoelastic compound whose stiffness and strength is greatly impacted by temperature (Özgan et al. 2013, Özgan 2011, Özgan and Serin 2013). The pavement temperature profile within the HMA layer can be obtained by field measurements through instrumentation of the roads. Even though field-measured temperature can provide the actual pavement temperature at any desired time, this is not a feasible option in all roads because of the costs associated with installing and maintaining the sensors and data collection systems.

Developing theoretical or empirical statistical temperature prediction equations can provide researchers with a cheap and quick alternative in order to obtain an estimation of the actual pavement temperature at any time (Minhoto et al. 2006). Precise prediction of temperature through the HMA layer's depth in different seasons is a very crucial task when it comes to evaluating the pavement performance, calculating its responses to moving traffic, and predicting the long-term stresses that the pavement will experience during its operational period (ARA 2004, Alavi et al. 2014). On the other hand, the predicted HMA temperature records could be used to analyze Falling Weight Deflectometer (FWD) test results for back-calculating the stiffness of the HMA layer (Islam et al. 2015).

In 1957, Barber made one of the first efforts to predict the maximum pavement temperature based on climatic information. A decade later, the Kentucky Department of Highways studied the temperature distribution profile inside the pavement (Southgate 1968). Over the years, many other researchers studied temperature distribution in HMA. Inge et al. (Inge et al. 1995) performed a series of FWD tests at different times of the day on four different pavement test sections with different HMA layer thicknesses in North Carolina over the course of one year. Thermocouples were used to measure the HMA temperature at different depths. In these

experiments, a temperature correction procedure, including using a shift factor, was suggested for temperature prediction. Rumney and Jimenez (Rumney and Jimenez 1971) were able to suggest a predictive method for asphalt temperature estimation based on the collected data in desert areas by measuring pavement surface temperature and solar radiation. Dempsey and Thompson in 1970 implemented heat transfer theories to develop a model for evaluating frost action and temperature profile through multi-layered pavement systems. Minhoto et al. in 2005 used thermodynamics methodology and finite element methods to develop a three-dimensional finite element model. The data used as the input of their model included mean daily values of wind speed and hourly solar radiation and air temperature collected by a weather station. The model was evaluated using field data recorded from an instrumented road in northern Portugal. Islam et al. (2015) developed a series of statistical models to predict minimum, maximum, and average pavement temperature using field-measured data collected from an instrumented road in New Mexico, USA. Park et al. (2016) developed a linear regression model for estimating the pavement's minimum surface temperature from ambient air temperature. They implemented the estimated parameter in another regression-based equation to predict frost penetration depth through pavement. Qin and Hiller (2011) evaluated the effect of ambient air temperature on the distribution of temperature through the depth of rigid pavement slabs. They showed that estimating the actual ambient air temperature, with sinusoidal prediction function as an input in their developed numerical model, yielded satisfactory results.

As mentioned above, many researchers tried to predict the temperature distribution along the HMA layer by taking different approaches such as analytical and theoretical, numerical, and finite element, and statistical and probabilistic methods (Islam et al. 2015). Previous studies have considered several climatic and environmental parameters such as air temperature, solar radiation, wind speed, relative air humidity, heat convection, and heat diffusion in the development of prediction equations (Alavi et al. 2014, Islam et al. 2015, Khadrawi et al. 2012).

All of the developed prediction equations have their own strengths and weaknesses. In some cases, the developed equations are too complicated and require the availability of numerous variables in order to predict the pavement temperatures. Therefore, these models are not practical for routine use in practice. The statistical methods, while efficient at developing simpler prediction equations, sometimes under-predict the pavement's high temperatures, and over-predict the pavement's low temperatures (Islam et al. 2015).

The Long-Term Pavement Performance (LTPP) of the Strategic Highway Research Program (SHRP) started back in 1987. By conducting a Seasonal Monitoring Program (SMP), pavement and air temperatures from different test sites were recorded in order to define the pavement characteristics at the field, to evaluate existing temperature prediction models, and to develop new models to enhance the procedure for binder selection in Superior Performing Asphalt Pavement (SUPERPAVE) (Mohseni 1998). The models were developed to predict the pavement temperature under different scenarios such as low pavement temperature, high pavement temperature, etc. Two of the low pavement temperatures, SHRP and Canadian (C)-SHARP, are presented below as Equation (1) and Equation (2):

$$T_d = T_{\text{air}(\text{min})} + 0.051d - 0.000063d^2 \quad (1)$$

where,

T_d = minimum pavement temperature at depth (°C)

$T_{\text{air}(\text{min})}$ = minimum one-day air temperature (°C)

d = depth (mm)

$$T_{\text{pav}} = 0.859 T_{\text{air}(\text{min})} + (0.002 - 0.007 T_{\text{air}})H + 0.17 \quad (2)$$

where,

T_{pav} = minimum pavement temperature (°C)

T_{air} = minimum one-day air temperature (°C)

H = depth (mm)

It should be mentioned that in SHRP models the minimum pavement surface temperature is assumed to be equal to the minimum air temperature.

The SHRP high pavement temperature prediction equations were developed based on heat transfer modeling studies. In the development of regression equations, air temperature, latitude, solar radiation, and wind speed were used. The regression equations are as below:

$$T_{surf} = T_{air} - 0.00618Lat^2 + 0.2289Lat + 24.4 \quad (3)$$

where,

T_{surf} = high surface temperature of asphalt concrete (°C)

T_{air} = seven-day average maximum air temperature (°C)

Lat = latitude of the section (degrees)

$$T_d = T_{surf} (1 - 0.063d + 0.007d^2 - 0.0004d^3) \quad (4)$$

Equation (4) takes depth in the unit of inches and yields temperature in the unit of Fahrenheit.

Park et al. (2001) developed a regression-based prediction equation for pavement temperature along the depth of the asphalt layer at any time of the day. This model was aimed at better predicting the temperature profile layers' structural properties from FWD testing results. The model has the benefit of simplicity by taking only the pavement surface temperature and time of day as inputs, as shown in Equation (5) below:

$$T_z = T_{surf} + (-0.3451z - 0.0432z^2 + 0.00196z^3) \sin(-6.3252t + 5.0967) \quad (5)$$

where,

T_z = temperature at depth z ($^{\circ}\text{C}$)

T_{surf} = temperature at the surface ($^{\circ}\text{C}$)

z = depth from surface (cm)

t = time of temperature measurement in fraction of day

It is important to mention that the development of the SHRP and LTPP models was aimed at helping select the optimum binder for asphalt concrete mixtures based on the predicted annual maximum and minimum pavement temperatures. Therefore, it is not advised to use these models for daily pavement temperature analysis (Diefenderfer 2002). On the other hand, many statistically developed prediction models are location-dependent and cannot be used in other locations. Therefore, this study focused on developing prediction models for the HMA layer temperature in the Integrated Road Research Facility (IRRF) test road.

Objective

This study aimed at developing statistical models to predict temperature within the depth of the HMA layer of the IRRF's test road for different scenarios such as average daily temperature during the spring and summer seasons, average daily temperature during the fall and winter seasons, minimum daily temperature, and maximum daily temperature. The models were developed using the temperature data collected over two years; the performances of the models were then evaluated using the temperature data collected from September to October 2016. Furthermore, Park's model was adopted and calibrated using the IRRF field data.

IRRF Test Road Facility

The construction of the IRRF test road started in May 2012 and finished in August 2013 as a new access road to the Edmonton Waste Management Centre (EWMC) located in northeast Edmonton, Alberta, Canada, with a latitude of 53.594°. The road was open to traffic in November 2015. The length of the two-lane road is about 500 m and is comprised of 25 cm HMA, including a 9 cm wearing course on top of a 16 cm binder course overlaying a 45 cm well-graded granular aggregate base course. The last layer of the test road is a naturally available clayey sand (SC) acting as the subgrade soil. The IRRF test road was heavily instrumented by different environmental and structural sensors in order to monitor and study the effects that environmental and traffic loads have on the performance of the test road.

The focus of this chapter is only on the temperature data collected by the thermistors embedded within the HMA layer at depths of 2 cm, 9 cm, 17 cm, and 25 cm, the last of which is at the bottom of the HMA layer. Figure 4-1 schematically shows the cross section of the test road and the location of the thermistors embedded within the HMA layer. It should be mentioned that this setting was replicated three times to provide reliability in measuring the data if some of the sensors became faulty or damaged, during either the installation or the operation period. The temperatures through the HMA layer were measured every five minutes and a CR-1000 datalogger from Campbell Scientific Canada collected the data. The obtained data were then transmitted to the University of Alberta through a remote desktop access. This study analyzed the retrieved two-year temperature data from September 2014 to September 2016. All of the climate data were collected from the EWMC's weather station, located approximately 700 m away from the test road. The solar radiation values were measured and collected by a pyranometer installed at the site and connected to the CR-1000 datalogger.

The HMA mix design for the two wearing and binder course sublayers was prepared based on the City of Edmonton’s design and construction standards (City of Edmonton Report 2012). The maximum nominal aggregate size of the GBC in the mix design of the two sublayers was 25 mm and 12.5 mm for the binder course and wearing course, respectively. The particle size distributions of the HMA sublayers are provided in Figure 4-2. The physical properties of HMA mixes are depicted in Table 4-1.

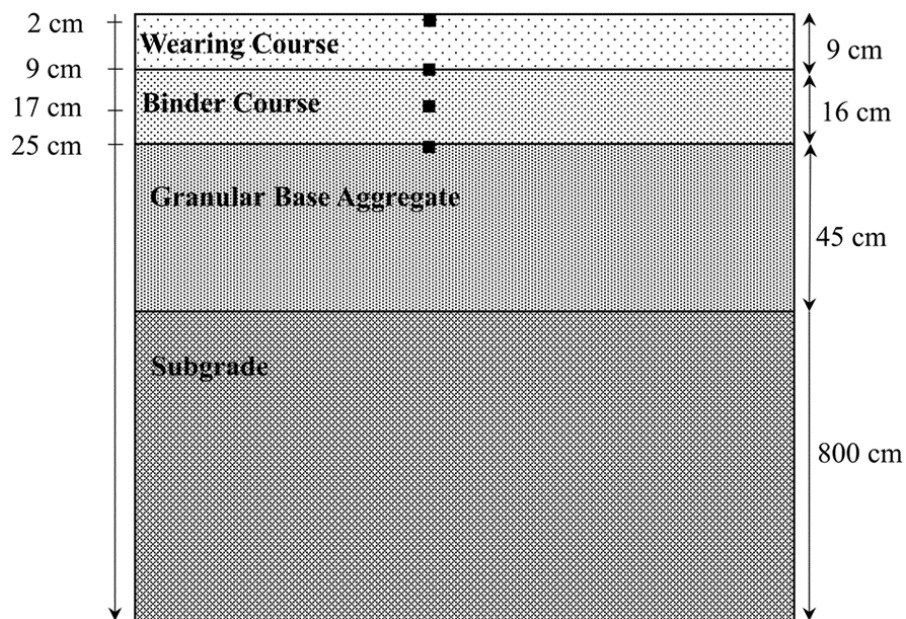


Figure 4-1- Schematic cross section and of IRRF test road location of thermistors

Table 4-1- Physical properties of the HMA mixes used in the test road

Property	Asphalt physical properties	
	Binder course	Wearing course
Maximum aggregate size (mm)	25	12.5
Binder grade	PG 58-28	PG 58-28
Reclaimed Asphalt Pavement (RAP) (%)	20	10
Binder content by weight of mix (%)	4.58	5.3
Void in mineral aggregate (VMA) (%)	13.1	14.3
Void filled with asphalt (VFA) (%)	69.4	74.9
Air voids (%)	4	3.6
Density (kg/m ³)	2,355	2,344
Marshal Stability (kN)	17.7	16.9
Flow (mm)	2.25	2.5
Theoretical film thickness (μm)	6.7	7.1
Tensile strength ratio (TSR) (%)	98	81.6

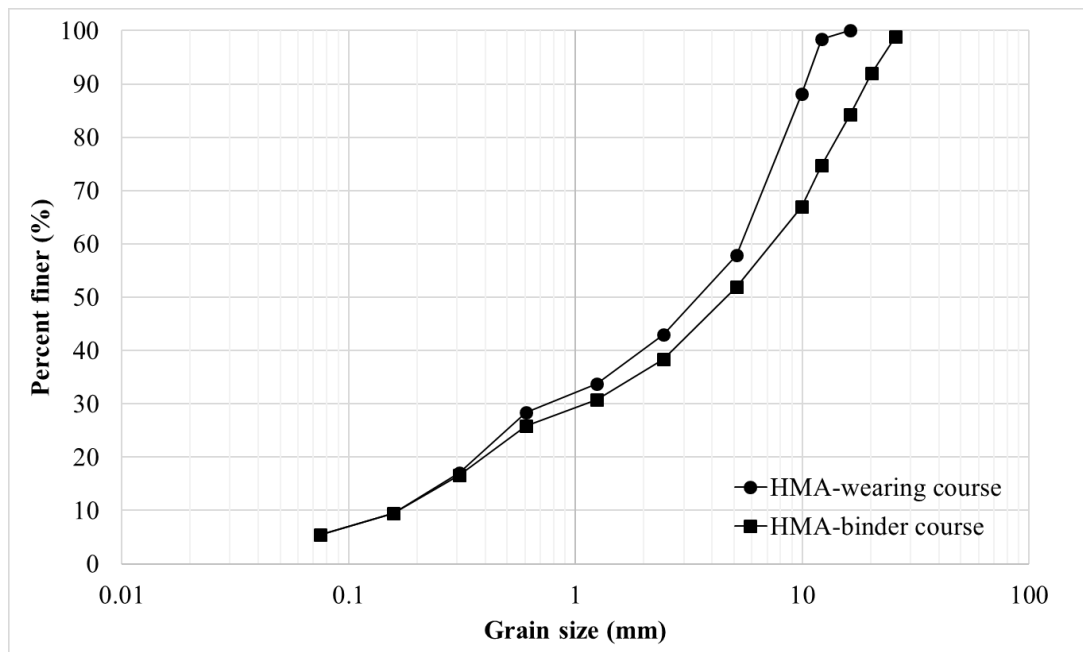


Figure 4-2- Particle size distribution of the HMA layer

Development of Models

For the development of the statistical models, all the environmental data recorded by the weather station, including ambient air temperature, solar radiation, wind speed, and relative air humidity, were considered. Traffic loading and strength and stiffness of the HMA layer was out of the scope of this study. Backward step-wise regression analysis was utilized in order to select the most influential independent variables for the suggested prediction equations. This method includes all of the assumed predictors in the hypothetical prediction model, then it successively removes the variables with the highest P-values one by one until all the remaining predictors satisfy the selected criterion, which is often set as 90% to 95% confidence interval. For 90% confidence interval, no P-value larger than 10% is acceptable, and for 95% confidence interval, no P-value larger than 5% is acceptable. Based on the previous studies conducted on the IRRF's test road (Haghi et al. 2016, Asefzadeh et al. 2016), the warm seasons (spring and summer) and cold season (fall and winter) were defined between the months of April to September and October to March, respectively. It was already observed that the IRRF's pavement structure usually started thawing during mid-March (Asefzadeh et al. 2016); therefore, this month was also considered to be part of the cold season. The average HMA daily temperature prediction equations were then developed for the two pre-defined seasons.

The daily average temperatures of all the data collected from the asphalt thermistors and weather station were calculated. The analyses were conducted at 90% confidence interval. Relative air humidity and wind speed were the first two predictors that were excluded from the correlation equation with P-values of 0.783 and 0.662, respectively, for the warm season. The analysis also yielded a very high P-value of 0.654 for the depth variable during the warm season, indicating that the depth variable also failed to meet the criterion. Therefore, Equation (6) was developed with daily average temperature and solar radiation as the only two effective

predictors with P-values of 0.000 and 0.095, respectively. The P-value for the model's intercept was found at 1.483×10^{-48} ; therefore, it was also included in the model. Since the depth was not included in the prediction model, the predicted values were compared to all the recorded temperature values at depths of 2 cm, 9 cm, 17 cm, and 25 cm, as well as the average of the temperatures measured at four elevations. The highest R^2 , 0.816, was found for the temperature at a depth of 17 cm, while the R^2 for the depths of 2 cm, 9 cm, and 25 cm were found to be 0.785, 0.802, and 0.796, respectively. Additionally, the R^2 was found to be 0.843 as the predicted values were examined against the mean value of four daily average temperatures through the HMA layer's depth. The developed prediction model for average daily temperature of HMA during warm season is as below:

$$T_{\text{daily-average}} = 3.9832 + 1.1288(T_{\text{air}}) + 2.68 \times 10^{-5}(\text{SR}) \quad (6)$$

where,

$T_{\text{daily-average}}$ = daily average temperature of HMA ($^{\circ}\text{C}$)

T_{air} = daily average temperature of air ($^{\circ}\text{C}$)

SR = daily solar radiation (kJ/m^2)

Figure 4-3 depicts the performance of the model for predicting temperature at a depth of 17 cm. It was also found that the mean value of average daily temperatures had a significantly high correlation of $R^2 = 0.996$ with the average temperature at a depth of 17 cm with a regression equation of $T_{\text{mean-daily}} = 0.995T_{17} + 0.128$, indicating that the average daily temperature at this depth could be treated as the mean daily temperature of the entire HMA layer. Table 4-2 depicts the outputs of regression analysis of Equation (6). The very low Significance F value guaranteed that the regression analysis had significant explanatory power. For 95% confidence level the maximum acceptable Significance F is 0.05.

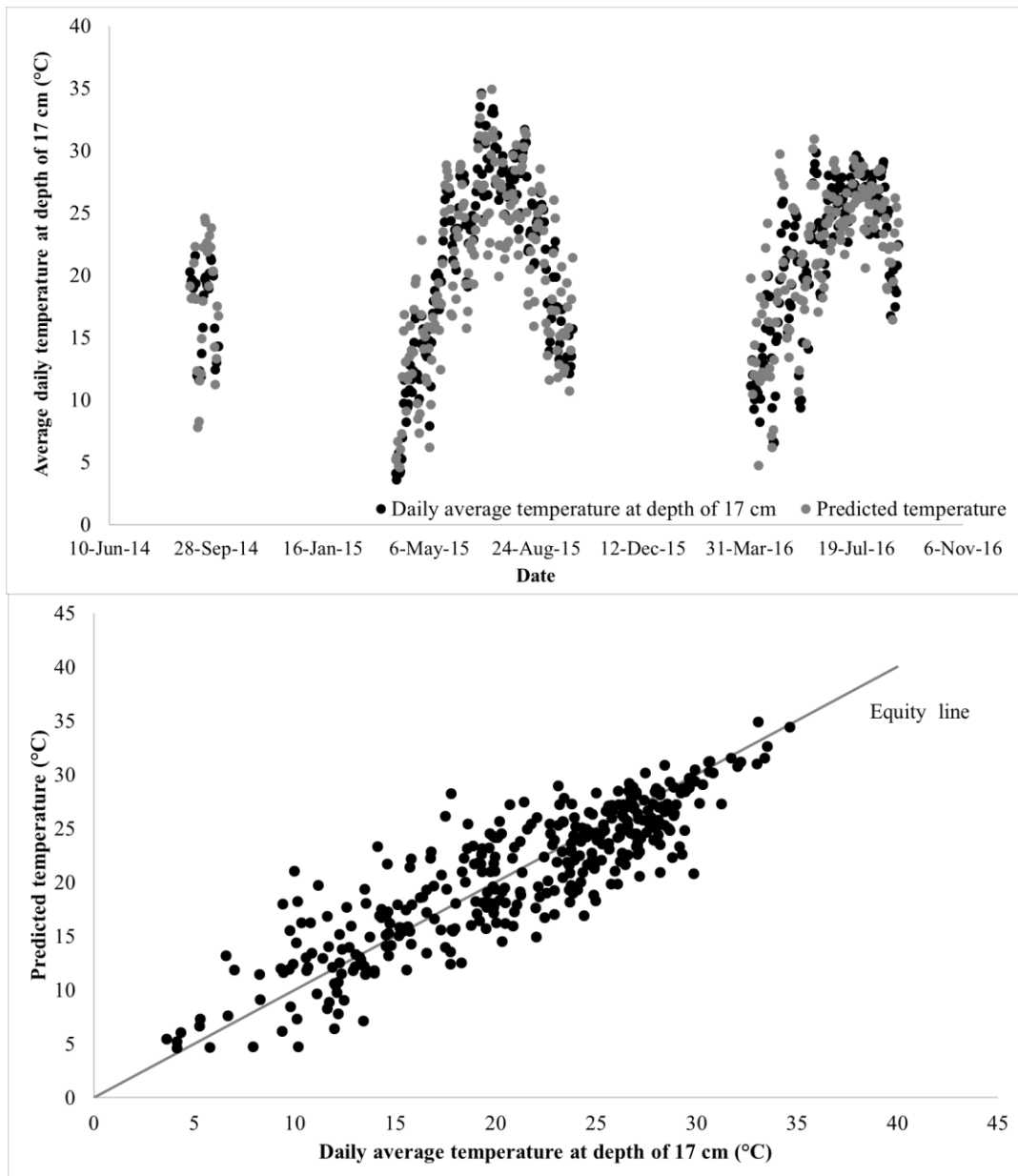


Figure 4-3- Predicted versus measured temperatures at a depth of 17 cm during the warm season

Table 4-2- Multiple regression analysis outputs for Equation (6)

	Degree of freedom	Sum of Squares	Mean of squares	F statistic	Significance F	
Regression	2	82143.8944	41071.9472	3058.1350	0.0000	
Residual	1585	21287.1690	13.4304			
Total	1587	103431.0633				
	Coefficients	Standard error	t statistic	P-value	Lower 90.0%	Upper 90.0%
Intercept	3.9832	0.2628	15.1555	0.0000	3.5506	4.4157
Average daily temperature (°C)	1.1288	0.0178	63.4255	0.0000	1.0995	1.1581
Daily solar radiation (KJ/m²)	2.6790E-05	0.0000	1.6699	0.0951	0.0000	0.0001

Similarly, the same approach was used to develop the prediction model for the daily average HMA temperature during the cold season. In this case, the ANOVA test showed that including the depth parameter in the prediction model had a 90% confidence interval, as the P-value for the depth factor was found to be 0.0737, indicating that it can be accepted as one of the important independent variables. Relative air humidity and wind speed were excluded from the prediction equation with P-values of 0.567 and 0.498, respectively. The R² was found to be significantly high at 0.849. Equation (7) is as below:

$$T_{\text{daily-average}} = -1.7853 + 0.6510(T_{\text{air}}) + 3.37 \times 10^{-4}(\text{SR}) + 2.0326 \times D \quad (7)$$

where,

$T_{\text{daily-average}}$ = daily average temperature of HMA (°C)

T_{air} = daily average temperature of air (°C)

SR = daily solar radiation (KJ/m²)

D = depth (m)

The performance of the model at all four depths was tabulated in Figure 4-4. Table 4-3 depicts the outputs of regression analysis of Equation (7).

Table 4-3- Multiple regression analysis outputs for Equation (7)

	Degree of freedom	Sum of Squares	Mean of squares	F statistic		Significance F
Regression	3	49396.3111	16465.4370	1289.6876		0.0000
Residual	1330	16980.1049	12.7670			
Total	1333	66376.4160				
	Coefficients	Standard error	t statistic	P-value	Lower 90.0%	Upper 90.0%
Intercept	-1.7853	0.2497	-7.1508	0.0000	-2.1963	-1.3744
Average daily temperature (°C)	0.6510	0.0131	49.6012	0.0000	0.6294	0.6726
Daily solar radiation (KJ/m²)	0.0003	3.16047E-05	10.6648	0.0000	0.0003	0.0004
Depth (m)	2.0326	1.1358	1.7896	0.0737	0.1631	3.9021

Figure 4-5(a) shows the average daily temperature profiles through the depth of the HMA layer over the course of the cold and warm seasons. Ten days for each season were selected randomly. A general trend for temperature variation throughout the depth in the cold season was observed, as the temperature increased by depth. This observed trend was dominant for almost all of the bottom three depths; however, during some days, the temperature at 2 cm was warmer than the other three recorded temperatures. This could be attributed to warm ambient air temperature affecting the near-surface HMA temperatures. It can be concluded that Figure 4-4 validates the result of the ANOVA test to include depth in Equation (7) with 90% confidence interval. Figure 4-5(b), conversely, does not reflect a dominant trend between the recorded temperatures and depth during the warm season, as graphing the randomly selected

data would resemble a cone shape. This accredits the ANOVA test result in which depth was excluded from Equation (6).

In order to develop the prediction equations for daily maximum and minimum HMA temperature, all the data collected over the two-year period were considered as the data set. The maximum and minimum HMA and air temperature were found for each day, and stepwise regression analysis was utilized for developing the models. Similar to the previous observations, wind speed and humidity were not found to have a statistically significant impact on the variation of asphalt temperature at different depths and were excluded with P-values of 0.623 and 0.589, respectively. One more statistical predictor was considered in terms of $(T^2 \times SR)^{0.25}$ (Bosscher et al. 1998) in the development of models. For the daily minimum HMA temperature prediction model, the added predictor improved the R^2 from 0.856 to 0.924; however, it made no improvement to the daily maximum HMA temperature, and the R^2 was found to be as high as 0.913 without the new predictor.

The regression prediction equations are as below:

$$T_{\text{daily-minimum}} = -2.8704 + 0.8900 \times T_{\text{air-min}} + 1.26 \times 10^{-4} \times SR + 0.1759 \times (SR \times T_{\text{air-min}}^2)^{0.25} + 15.2324 \times D \quad (8)$$

$$T_{\text{daily-maximum}} = 2.0237 + 0.8709 \times T_{\text{air-max}} + 7.6 \times 10^{-4} \times SR - 16.1886 \times D \quad (9)$$

where,

$T_{\text{daily-minimum}}$ = daily minimum temperature of HMA ($^{\circ}\text{C}$)

$T_{\text{air-min}}$ = daily minimum temperature of air ($^{\circ}\text{C}$)

$T_{\text{air-max}}$ = daily maximum temperature of air ($^{\circ}\text{C}$)

SR = solar radiation (KJ/m^2)

D= depth (m)

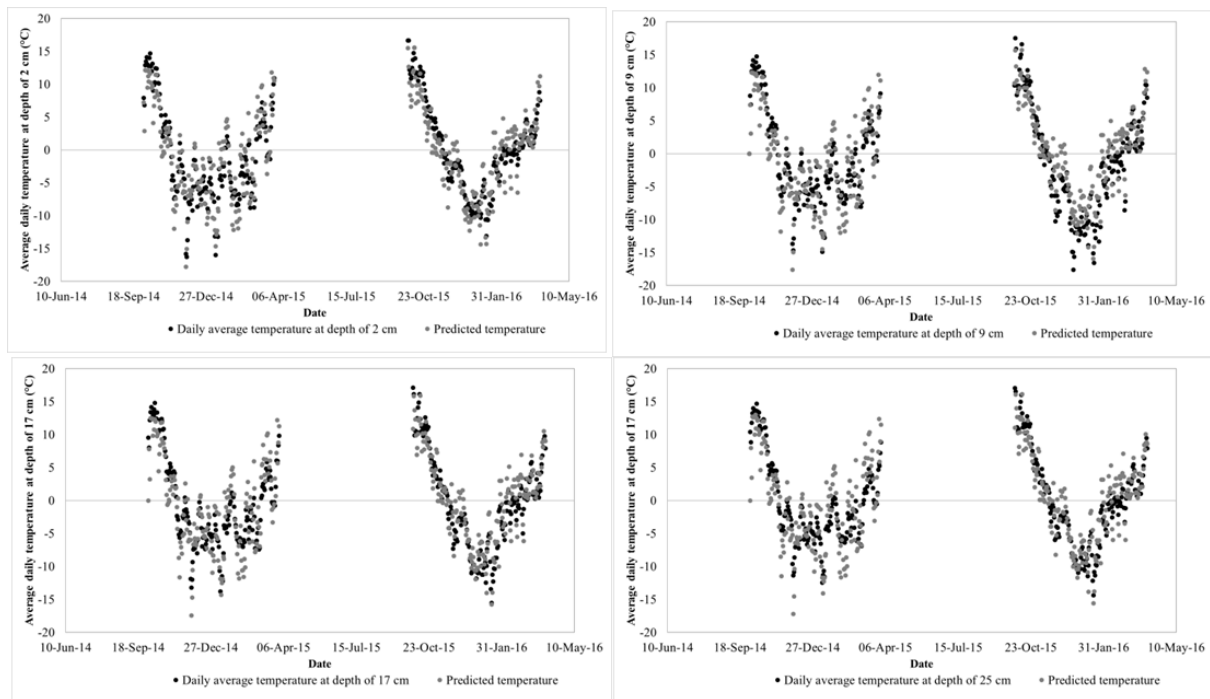


Figure 4-4- Predicted versus calculated average temperatures at four depths during the cold season

The negative and positive signs of the coefficients of depth in Equations (8) and (9) follow the actual diurnal thermal regime within the HMA layer, in which the temperature of the HMA at near-surface elevation is the warmest or coldest when the air temperature fluctuates around its maximum daily value or minimum daily value, respectively. Tables 4-4 and 4-5 depict the results of multiple regression analysis of Equations (8) and (9). The extremely low P-values ensured that the coefficients were acceptable at even higher confidence levels. The performances of Equations (8) and (9) at all depths were tabulated in Figure 4-6 and Figure 4-7, respectively.

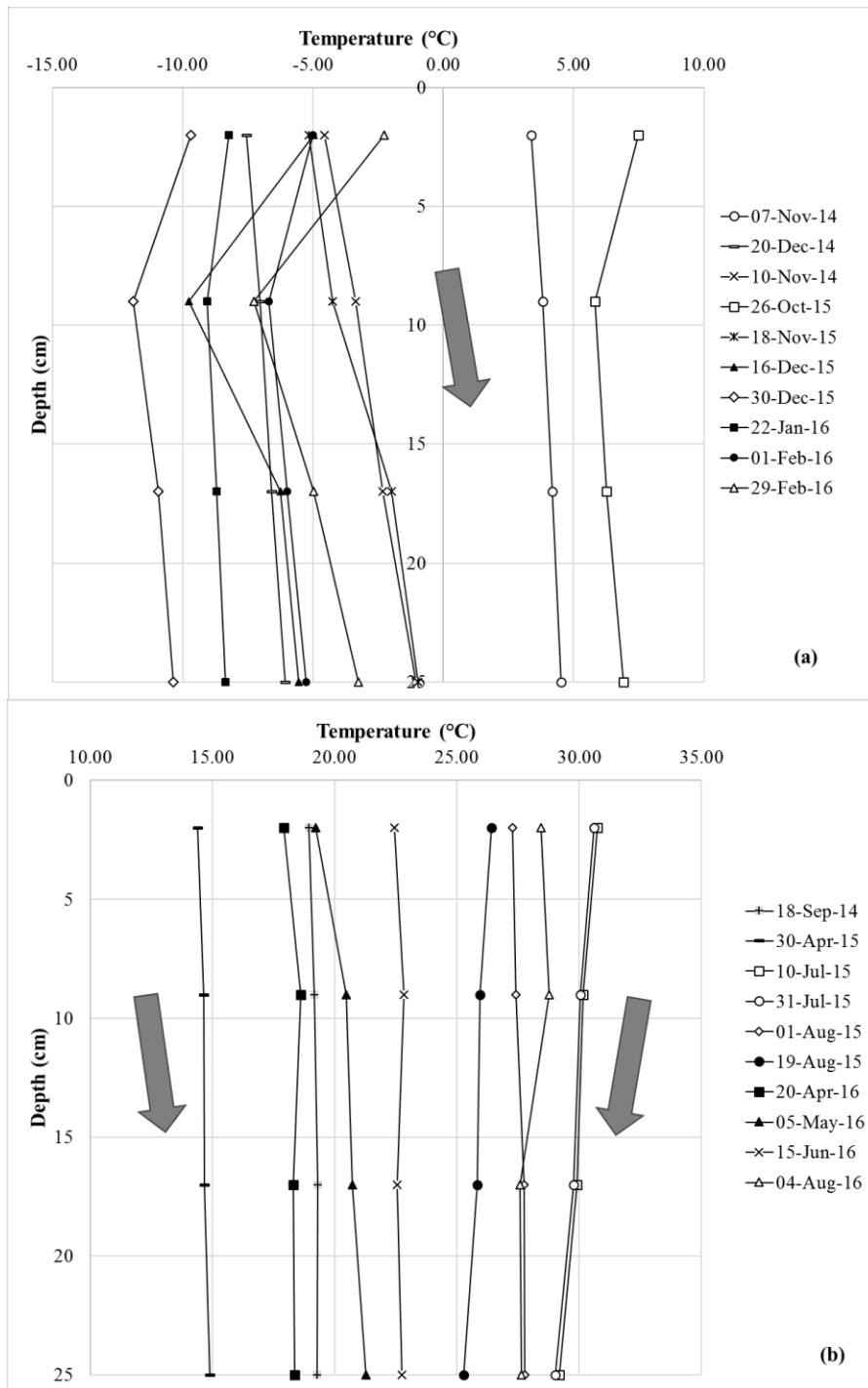


Figure 4-5- Figure 4-5- Daily average temperature profiles through the depth of the HMA layer in the (a) cold season and (b) warm season

Table 4-4- Multiple regression analysis outputs for Equation (8)

	Degree of freedom	Sum of Squares	Mean of squares	F statistic		Significance F
Regression	4	355069.8593	88767.4648	8413.0170		0.0000
Residual	2919	30798.9667	10.5512			
Total	2923	385868.8260				
	Coefficients	Standard error	t statistic	P-value	Lower 95.0%	Upper 95.0%
Intercept	-2.8704	0.1791	-16.0271	0.0000	-3.2216	-2.5192
Min. daily temp.(°C)	0.8900	0.6974	21.8410	0.0000	13.8649	16.5999
Daily solar radiation (KJ/m²)	0.0001	0.0084	106.0976	0.0000	0.8736	0.9065
Depth (m)	15.2324	0.0000	11.1065	0.0000	0.0001	0.0001
(SR.T_{air-min}²)^{0.25}	0.1759	0.0060	29.3677	0.0000	0.1642	0.1876

Table 4-5- Multiple regression analysis outputs for Equation (9)

	Degree of freedom	Sum of Squares	Mean of squares	F statistic		Significance F
Regression	3	594603.6069	198201.2023	11901.0105		0.0000
Residual	2920	48630.1152	16.6541			
Total	2923	643233.7221				
	Coefficients	Standard error	t statistic	P-value	Lower 95.0%	Upper 95.0%
Intercept	2.0237	0.1814	11.1585	0.0000	1.6681	2.3793
Depth (m)	-16.1886	0.8762	-18.4758	0.0000	-17.9067	-14.4706
Max daily temp. (°C)	0.8709	0.0102	85.6515	0.0000	0.8510	0.8909
Daily solar radiation (KJ/m²)	0.0008	0.0000	61.0370	0.0000	0.0007	0.0008
Intercept	2.0237	0.1814	11.1585	0.0000	1.6681	2.3793

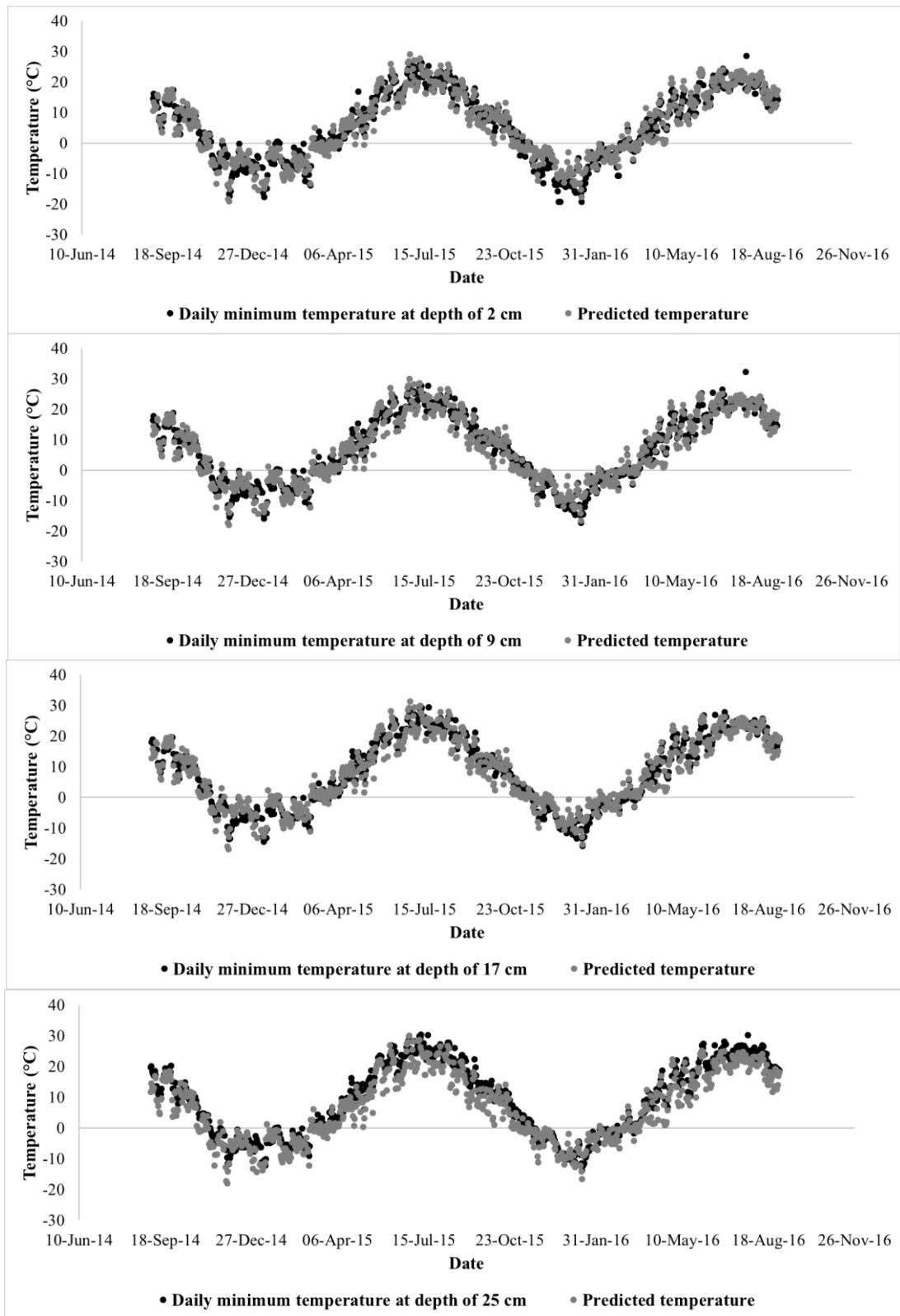


Figure 4-6- Predicted vs. calculated daily minimum temperatures

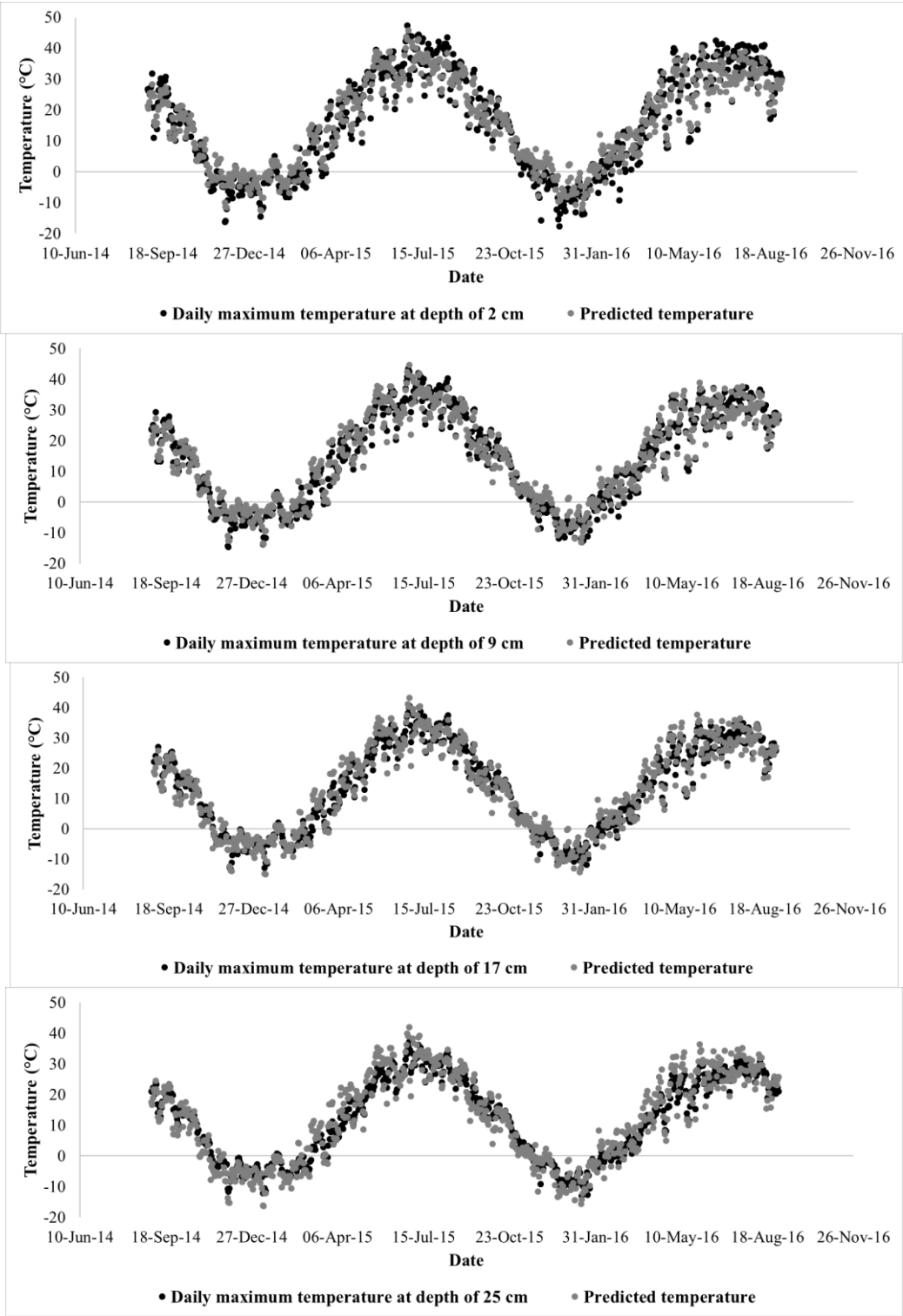


Figure 4-7- Predicted vs. calculated daily maximum temperatures

Calibration of Park's Model for the IRRF Test Road

Park's model, presented in Equation (5), was adopted to fit the two years of field data recorded at five-minute intervals. Mathematica software was utilized for regression analysis and finding the model coefficients. It was found that fitting the model to all the data would result in a moderate correlation between the predicted and measured temperatures in the cold season. Therefore, the data were separated according to cold and warm seasons, as previously defined in this study. It was found that modified forms of Park's model, presented in Equations (10) and (11), highly correlated with the actual data with R^2 , as high as 0.973 for the warm season and 0.931 for cold season. It should be mentioned that the attempt to find the regression coefficients of the original form of the model failed as the software solution did not converge, even with the number of iterations as high as 10,000. It was assumed that the surface temperature was equal to the temperature measured at a depth of 2 cm below the HMA layer. This assumption was examined by using an infrared sensor to compare the available data of measured surface temperatures by infrared sensor in more than 15 field tests on the IRRF test road, at different times of the day, over the course of two years (2014-2016). The regression analysis on the surface temperature and the HMA temperature at the depth of 2 cm below the surface yielded a highly correlated zero-intercept linear relationship between the two variables with slope of 0.978 and R^2 of 0.929 indicating that there was no substantial statistical difference between the two temperatures. Equations (10) and (11) present the adopted Park's model for warm and cold seasons, respectively:

$$T_z = 0.9511T_{\text{surf}} + (0.1462z)\sin(7.5442t + 6.6341) \quad (10)$$

$$T_z = 0.8639T_{\text{surf}} - 0.0385z + (0.1374z)\sin^2(2.2916 - 4.0067t) \quad (11)$$

Figure 4-8 presents the high correlation between the predicted and measured temperatures, for brevity, at depth of 17 cm as a representative of the performance of the models at all four

depths. It should be mentioned that only one twenty-fourth of the total collected data are depicted in the graphs for the sake of the clarity of the figure.

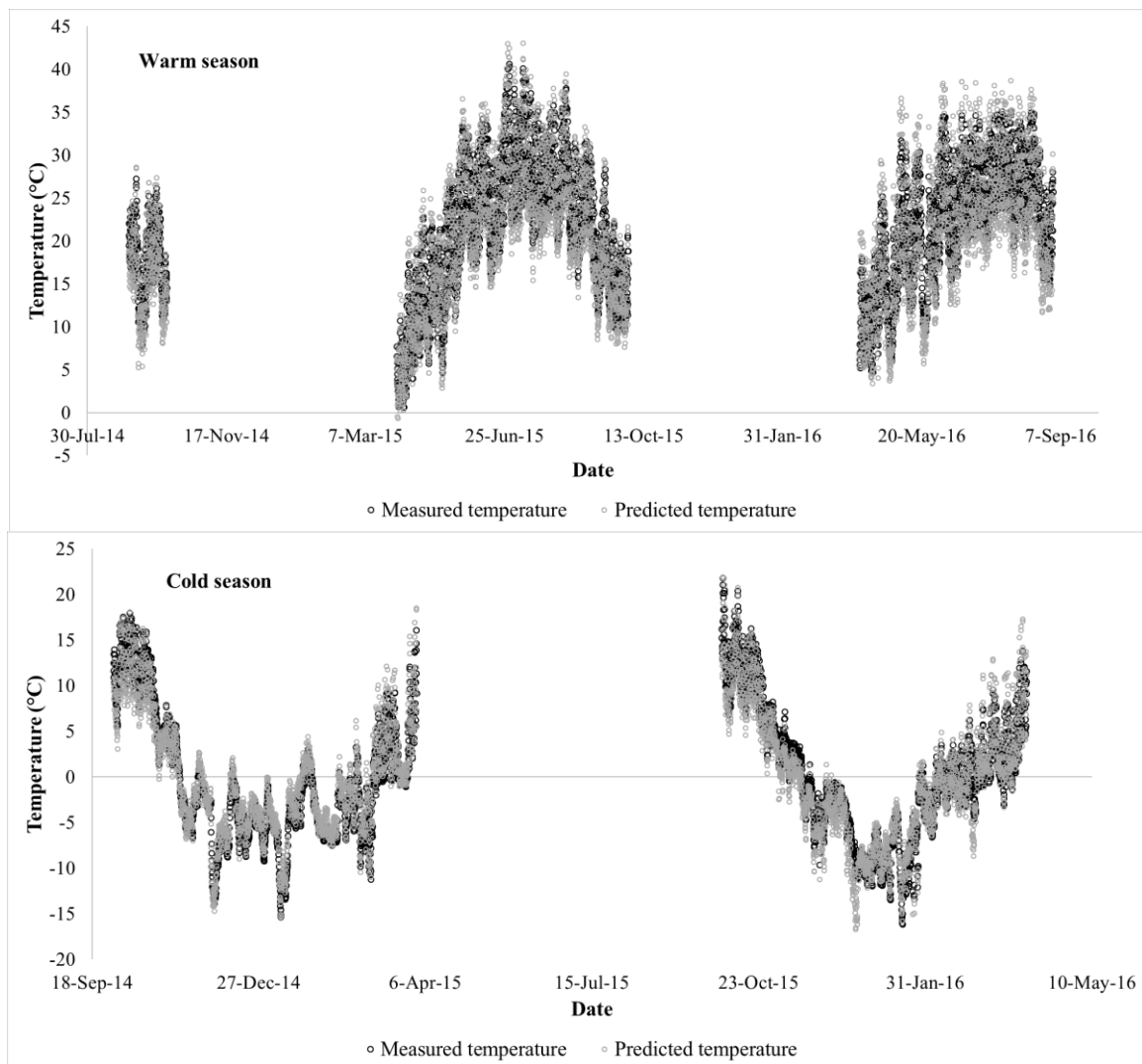


Figure 4-8- Predicted vs. calculated pavement temperatures at depth of 17 cm from adopted Park’s equation during warm and cold seasons

Validation of Models

To evaluate the performance of the developed models in this study, the recorded field data between September 1st and October 31st 2016 were used. It should be mentioned that Equation (6) was the only equation not evaluated because of the difficulty of collecting data in the cold season. Only temperatures recorded at depths of 17 cm and 25 cm were used because the other

thermistors started to malfunction starting in mid-September 2016. Equation (7) showed a satisfactory performance in predicting daily average temperatures at a depth of 17 cm with an R^2 of 0.815, as depicted in Figure 4-9. The R^2 for the predicted values at a depth of 25 cm was found to be 0.806. Figure 4-10 depicts the performance of Equation (8), which precisely predicted the daily minimum temperatures at a depth of 17 cm in the HMA layer with a high R^2 of 0.904. Equations (9), (10), and (11) were also able to predict the measured values with R^2 values of 0.902, 0.912, and 0.921. The high R^2 values of the prediction models in this study shows the success of the developed models in predicting the temperature at the IRRF test road.

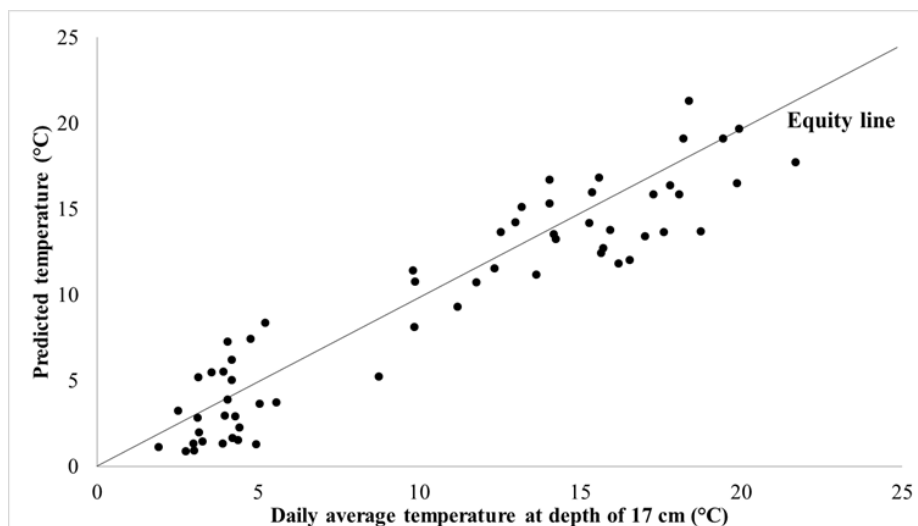


Figure 4-9- Validation of Equation (7) using measured field data

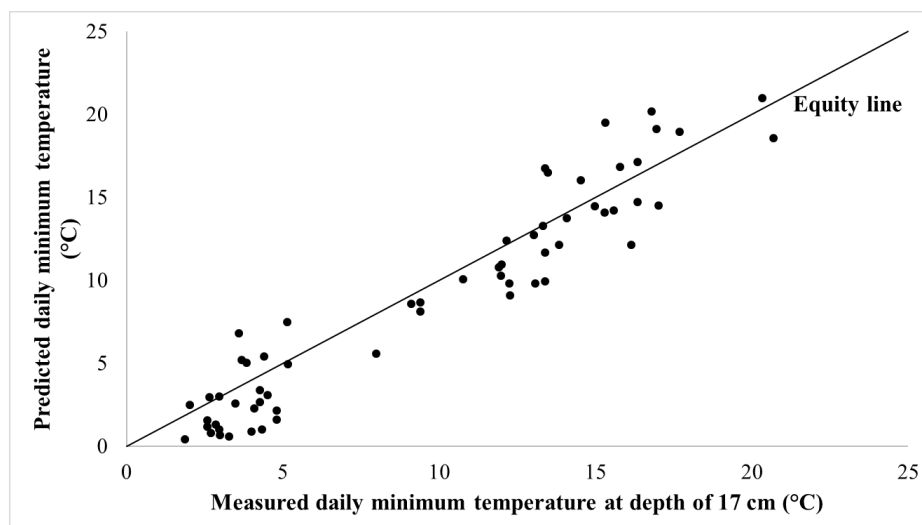


Figure 4-10- Validation of Equation (8) using measured field data

Effect of Temperature on HMA Stiffness

To investigate the effect of temperature on HMA stiffness, dynamic modulus tests were conducted on both HMA layers based on AASHTO TP79 (AASHTO 2009). Cylindrical samples were prepared using a superpave gyratory compactor with 150 mm diameter by 170 mm height from the test road HMA material. Based on AASHTO PP61 (AASHTO 2009), dynamic modulus specimens were prepared by coring the samples to 100 mm diameter and cutting them to a height of 150 mm. The tests were conducted using an UTM-100 machine at temperatures of -10, 4, 20 and 35°C and frequencies of 10, 5, 2, 1, 0.5, 0.2, 0.1 and 0.01 Hz. Figure 4-11 shows the master curves along with the shift factors of both binder and wearing courses of the HMA layer which were developed by Shafiee et al. (2015). They observed that the frequency of the pressure pulse induced by performing the FWD test was approximately the same in different months and remained almost constant (at 33 Hz) within the depth of the pavement structure. Therefore, using the developed master curves and shift factors, the elastic moduli of the HMA layer was calculated for the loading frequency of 33 Hz. To this end, the average of the two temperatures measured within the depth of each sublayer was used for calculating the modulus values in different months, and by taking the weighted mean of the two HMA sublayers' modulus with respect to their corresponding depths, the combined moduli of the HMA layer was calculated. Table 4-6 tabulates the HMA elastic modulus values mid-month over the course of one year as a representative of changes in moduli values of the HMA layer against temperature at a constant loading frequency. The combined moduli value of HMA in July, which recorded the warmest average HMA temperature, decreased by 73% as compared to that of the HMA in January. The average HMA moduli for the warm season and cold season was found to be 12,800 MPa, and 22,400 MPa, respectively, which means that the

average stiffness of the HMA decreased by 43% during the warm season in contrast to the cold season.

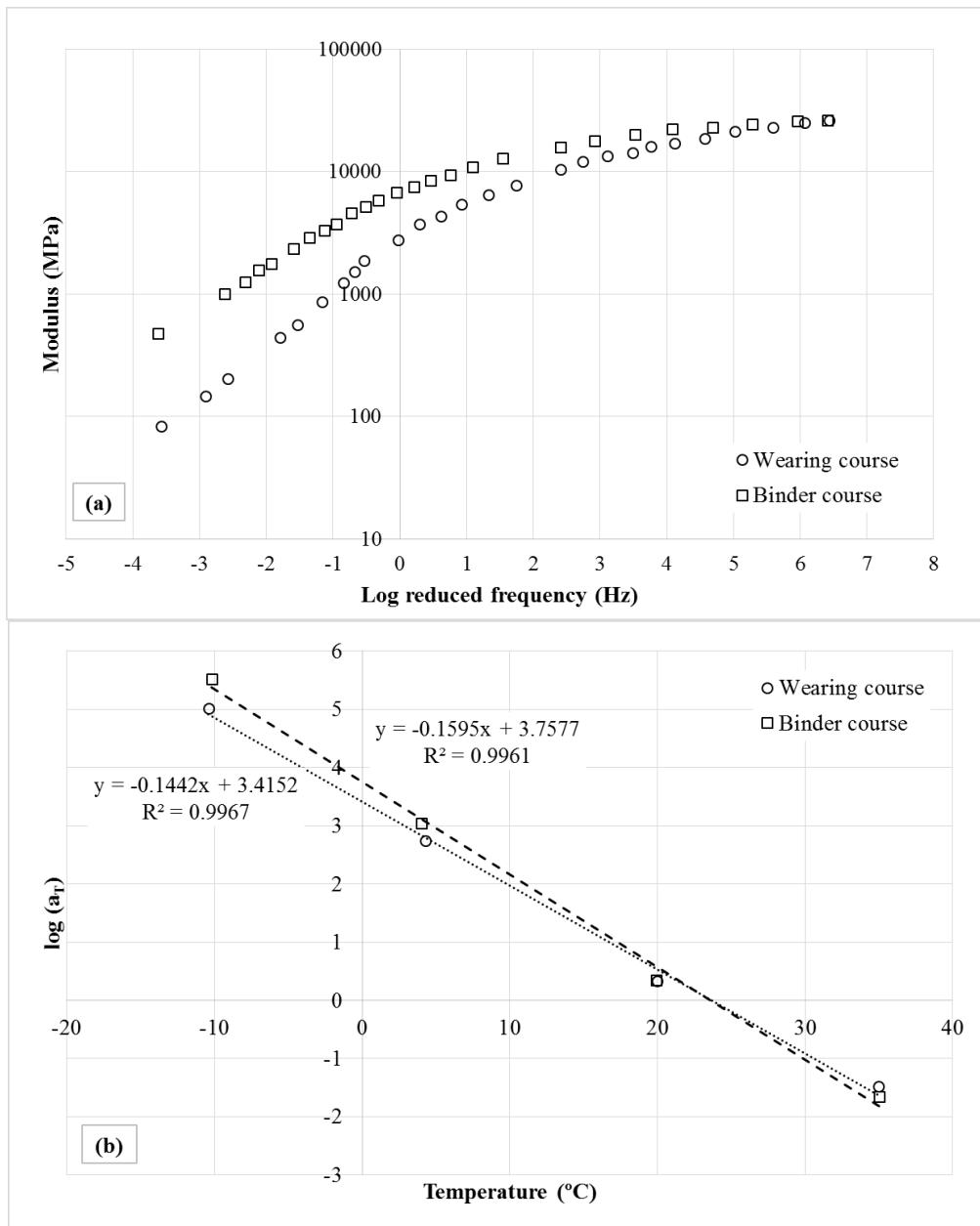


Figure 4-11- Master curve and shift factor for wearing course and binder course (Shafiee et al. 2015)

Table 4-6- Changes of HMA moduli values against temperature at constant loading frequency

Date	Wearing course temp. (°C)	Binder course temp. (°C)	Wearing course moduli (MPa)	Binder course moduli (MPa)	Combined moduli (MPa)
15-Jan-15	-4.4	-4.2	23050	26000	24900
15-Feb-15	-2.5	-2.5	22300	25400	24300
15-Mar-15	4.6	4.2	17800	22250	20650
15-Apr-15	11.7	10.4	13800	20600	18150
15-May-15	20.3	19.7	8850	14400	12400
15-Jun-15	23.5	22.2	7100	13600	11250
15-Jul-15	31.7	30.9	3900	8250	6700
15-Aug-15	20.0	22.7	8900	13600	11900
15-Sep-15	12.3	14.5	13400	18300	16500
15-Oct-15	8.2	10.4	15850	20400	18800
15-Nov-15	0.8	2.1	20250	23000	22000
15-Dec-15	-2.0	-0.4	22100	24600	23700

Conclusion

This study focused on developing empirical statistical models, specifically calibrated for the IRRF's test road, for prediction of daily average temperatures and daily minimum and maximum temperatures within the HMA layer of the pavement. Two years of monitored field data, including environmental data measured by the weather station and temperatures at different depths through the HMA layer measured by thermistors, were used for developing regression models. Step-wise regression analysis was utilized to identify and select the most important variables, which potentially added significant explanatory power to each regression equation. The high R^2 values along with the ANOVA test results indicated the usefulness of models in predicting the measured field data. Another model in the literature developed by Park was adopted and calibrated for prediction of pavement temperature at any depth based on the surface temperature for warm and cold seasons. All models were validated by field data and showed satisfactory results.

The effect of temperature on the stiffness of the HMA was investigated over the course of one year, based on the laboratory developed master curves and shift factors and the measured

asphalt temperatures. The stiffness of the HMA layer in July decreased by 73% compared to that of the HMA layer in January.

Based on the results of this study, it is expected that the models will perform well at predicting the HMA temperatures in roads located at the same latitude and in weather conditions similar to Edmonton, Alberta, Canada; however, verification of the performance of models using field data from other road pavements is recommended.

Chapter 5- Characterization of Permanent Deformation Behavior of Silty Sand Subgrade Soil under Repeated Load Triaxial Tests

A version of this chapter was published “Asefzadeh, A., Hashemian, L. and Bayat, A., 2017. Characterization of Permanent Deformation Behavior of Silty Sand Subgrade Soil Under Repeated Load Triaxial Tests. Transportation Research Record: Journal of the Transportation Research Board, (2641), pp.103-110”

Abstract

The performance of pavement structures is highly dependent on the performance of the subgrade layer as it is the last layer underlying all the other pavement layers. The development of permanent deformation in subgrade material under traffic loads can cause pavement distresses such as fatigue cracking and rutting. This chapter is aimed at evaluating permanent deformation behavior of a silty sand subgrade material in the laboratory at different stress ratios and stress levels. It was found that the shakedown behavior of the material fell within plastic shakedown and plastic creep for stress ratios below 1.0 and stress ratio of 1.5, respectively. A statistical prediction model for permanent deformation was suggested based on the test results.

Key words: Permanent deformation, subgrade soil, plastic strain, prediction model.

Introduction

Pavement systems are subject to repetitive mixed traffic loading. Even though pavement structures are designed to survive under traffic loads, distresses and damages are always expected to occur. One of the most prevalent modes of failure in flexible pavements is rutting damage, which requires extensive pavement maintenance and rehabilitation (Boulbibane and Collins 2015). All the pavement layers can potentially contribute to the accumulation of rutting, which can lead to discomfort to passengers at initial stages and complete failure of pavement in the case of severe rut development (Erlingsson and Rahman 2013). In a pavement with well-designed asphalt mixture and constructed thickness, rutting occurs dominantly in the unbound granular base course and subgrade layer due to growing traffic-induced irrecoverable compressive strains (Uzan 2004, Puppala et al. 2009). This leads to large vertical permanent (plastic) deformations in the pavement system (Puppala et al. 2009). The magnitude of rutting in pavement depends on different factors such as materials' stiffness, stress history in materials, traffic load-induced stresses, materials' permanent deformation potential, environmental

factors, etc. (Uzan 2004). Since it is the last layer supporting all the overlying layers, the performance of subgrade soil against rutting is of utmost importance in designing successful and durable flexible pavements. A weak and soft subgrade soil can potentially contribute to almost 40% of the total rutting in the pavement structure (Puppala et al. 1999); hence, understanding the permanent deformation mechanism in subgrade soils and developing predictive models can benefit engineers in designing more durable pavements with optimal thickness of asphalt concrete layers (Puppala et al. 2009).

Among all the different laboratory methods researchers have suggested over the past few decades to study and simulate the development of permanent deformation in pavement materials, the repeated load triaxial (RLT) test, which allows the soil specimen to undergo stress states similar to the field conditions, is considered to be the best practical procedure (Puppala et al. 2009, Erlingsson and Rahman 2013). Performing an RLT test on soil specimens provides valuable insight into the M_r and permanent deformation behavior of subgrade soil materials. The general consensus is that because the subgrade soil has a higher M_r , its permanent deformation under repetitive loading would be less (Puppala et al. 2009). However, silty sand and sandy silt soils are two exceptions for which large permanent deformation was reported in the literature despite their high resilient moduli (Puppala, et al. 2009, Puppala, et al. 1999, Ulliditz 1993).

Many researchers used the elastic theory in order to estimate the average typical stress state within the pavement subgrade layers. As a result of these studies, the confining pressure ($\sigma_3 = 13.8$ kPa) and deviatoric stress (27.6 kPa $< \sigma_d < 41.4$ kPa) appeared to be the more common stress levels on top of the subgrade layer (Elliott et al. 1988, George 2004, Mohammad et al. 2012, Ji et al. 2014). Some researches recommended using $\sigma_3 = 13.8$ kPa and $\sigma_d = 41.4$ kPa to find the M_r of subgrade material in pavement design (Ji et al. 2014). However, due to the complex nature of in-service traffic loadings, it is inevitable for subgrade layer to undergo

stress levels below or above the typical average ranges used in design. Also, little research has been conducted on the permanent deformation behavior of silty sand soils under different stress state scenarios. This is mainly because the permanent deformation test is not easy to perform, and since it is considered to be a destructive test, each test setup requires a new specimen. It should also be mentioned that this test is very time consuming, particularly if it is run at more than 10,000 stress applications.

Literature Review

Shakedown theory was first implemented in pavement analysis and design as a result of research works conducted by Sharp and Booker (Sharp and Booker 1984, Werkmeister et al. 2001). According to the concept of shakedown theory, what happens to a material under continuous repeated loading is twofold; under low stress levels, the material will eventually show resilient (elastic) behavior and the rate of accumulated deformations with loading cycles gets close to zero. On the other hand, under higher stress levels, the material shows drastic accumulative permanent deformation and fails ultimately. Therefore, it can be concluded that knowing the limiting shakedown loads is of utmost importance to successfully design a pavement structure in which the development of permanent deformations is to be restricted.

Generally, there are three different shakedown behaviors reported for materials under cyclic loading (Werkmeister et al. 2001, Tao et al. 2010). Plastic shakedown is when the material shows some initial accumulated plastic deformations for a limited number of load cycles. As the number of load applications increases, the aforementioned behavior turns into a fully resilient manner in which the rate of plastic deformation tends to zero (Range A). Plastic creep is observed when the material shows continuous development of accumulated plastic deformation with a number of load applications. The rate of plastic deformations decreases during the infinite number of initial loading cycles and stabilizes around a low value (Range

B). Incremental collapse happens when the applied loads are too high. In this case, the plastic strain rate does not decrease at all or decreases very slowly. The accumulated plastic deformation occurs very quickly, which leads to the failure of material (Range C) (Tao et al. 2010, Yang et al. 2008).

A research study conducted by Werkmeister in 2003 suggested a criterion for distinguishing between the three aforementioned shakedown behaviors in unbound granular materials. According to the findings of this research, when the difference in accumulated plastic strains in 3,000 and 5,000 load cycles is less than 45 microstrains, then the material behavior falls in Range A. If the difference is between 45 microstrains and 400 microstrains, then Range B will be dominant. If the difference exceeds 400 microstrains, then Range C is observed. Figure 5-1 schematically depicts the three different ranges of shakedown behavior of material under permanent deformation.

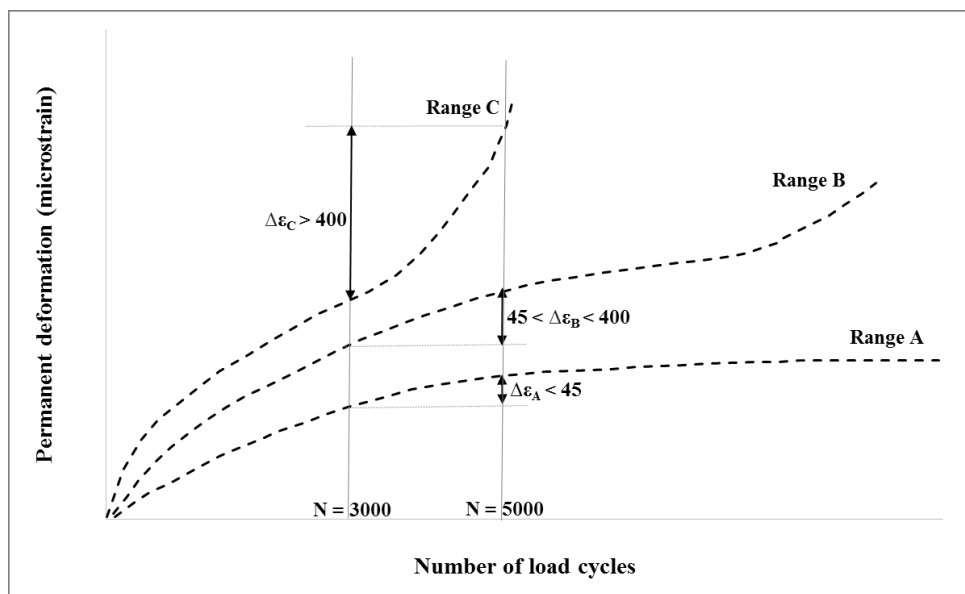


Figure 5-1- Shakedown behavior of material under permanent deformation (Tao et al. 2010, yang et al. 2008)

The literature proposes several different models for estimating permanent strains in pavement materials (Barksdale 1972, Monismith et al. 1975, Majidzadeh et al. 1978, Horny993, Tseng and Lytton1989, Shenton 1974). These methods can be generally categorized in three different

groups depending on their approaches to model the permanent strain. The first group of methods tend to link the permanent deformation merely to the number of loading cycles. These methods do not consider the effects of stress states or other inherent properties of the materials. The second group of models link the permanent deformation of material to the applied stresses. These models do not take into account the relation between number of loading cycles and permanent strain (Werkmeister et al. 2005, Gidel et al. 2001). The third category of models include many parameters such as stress states, number of loading cycles and soil properties for permanent strain predictions.

Among all the models available in the literature, the Tseng-Lytton model (Tseng and Lytton 1989) is approved to be used in the Mechanistic Empirical Pavement Design Guide (MEPDG) (ARA 2004). In the equation the material constants can be found either statistically by fitting parameters to the developed permanent strain at Nth loading cycle or from experimental equations, developed by Tseng and Lytton, to determine the material constants from water content, M_r and bulk stress.

$$\varepsilon_p(N) = \varepsilon_0 \exp(-(\rho/N)^\beta) \quad (1)$$

where

ε_p = permanent strain

$\varepsilon_0, \rho, \beta$ = material constants

N = number of loading cycle

Based on heavy vehicle simulator (HVS) testing, in 2010, Wang et al. developed a new prediction model for permanent deformation of subgrade materials which takes several parameters such as stress state, number of loading cycles, and soil moisture content into

consideration. Inspired by the general nonlinear model implemented in MEPDG for predicting M_r of pavement materials, the new model was developed as follows (Wang et al. 2009):

$$\frac{\varepsilon_p}{\varepsilon_r} = a_1 \left(\frac{\theta}{P_a} \right)^{a_2} \left(\frac{\tau_{oct}}{P_a} + 1 \right)^{a_3} W_c^{a_4} N^b \quad (2)$$

where

θ = bulk stress (kPa)

P_a = atmospheric pressure (101.35 kPa)

τ_{oct} = octahedral shear stress (kPa)

a_i and b = regression constants

W_c = moisture content (%)

N = number of load cycles

It should be mentioned that resilient ε_r was defined as strain imposed in laboratory test to obtain material properties which is not clear enough.

This chapter aims to improve the gap in knowledge that currently exists with regard to the behavior of silty sand soil under different repetitive dynamic loads and plastic strains accumulation in this material. In this study, Wang model was fitted to the current experimental test data and its performance was compared with a prediction model that was developed based on the obtained results from the lab tests.

Material Characterization

The material used in this study was classified as well-graded sand with silt (SW-SM) according to the Unified Soil Classification System (USCS). The soil was found to be non-plastic with less than 5.2% fines and specific gravity (G_s) of 2.565. The maximum dry density and optimum

moisture content of the material were found as 2.13 gr/cm³ and 8.6%, respectively. Conducting a set of direct shear tests in compliance with ASTM D3080 on the soil material, its angle of friction and cohesion was found to be 31 degrees and 40 kPa, respectively. Figure 5-2 shows the gradation of the material.

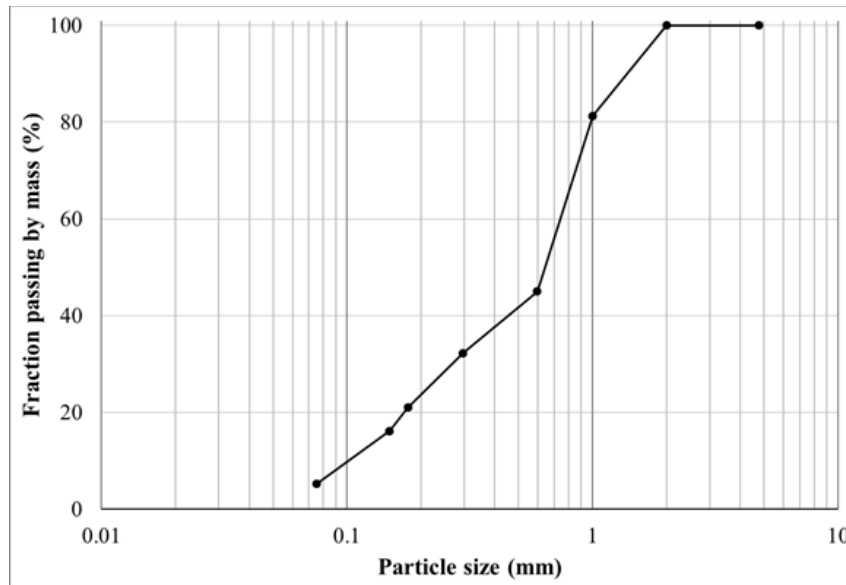


Figure 5-2- Particle size distribution for the well-graded sand with silt

Prior to compaction, the soil material was mixed with water at optimum moisture content. The mixing was made by hand. The moist material was then placed and sealed in plastic bags for two hours to ensure even distribution of moisture within the soil. Soil specimens were then compacted in a brass split mold with 100-mm diameter and 200-mm height at modified compactive effort of 44 blows per layer calculated as per ASTM D1557 based on the five-layer compaction procedure and the volume of the mold. The top of each compacted layer was scarified using a lab claw to ascertain sufficient particle interlocking action in between the five layers.

To conduct all triaxial tests, the IPC Universal Testing Machine (UTM-100) was used. The M_r of the subgrade material was measured in accordance with AASHTO T307-99 which simulates the field stress condition by applying five different deviator stresses on the testing specimen at three different confining pressures. The confining pressures used in the standard were in the

order of 13.8, 27.6 and 41.4 kPa and five different deviator stresses applied on the specimen were 13.8, 27.6, 41.4, 55.2, and 69 kPa, which made overall fifteen different stress states for measuring the M_r of the subgrade material. Figure 3 shows the result of the M_r test on the subgrade material used in this study. The MEPDG nonlinear M_r prediction equation was fitted to the data points, and k_1 , k_2 and k_3 parameters were found as 2.2819, 0.2274 and -7.6726, respectively. Therefore, the M_r equation could be presented as $M_r = 2.2819P_a \left(\frac{\theta_{bulk}}{P_a}\right)^{0.2274} \left(1 + \frac{\tau_{oct}}{P_a}\right)^{-7.6726}$. It should be mentioned that the material showed strain softening behavior with increase in the deviatoric stress. This observation could be attributed to the fact that more 81% of the material passed through sieve No. 18 with mesh

opening size of 1mm. Thus, the behavior of material deviated from granular material with angular particles for which strain hardening behavior against bulk stress is typically expected.

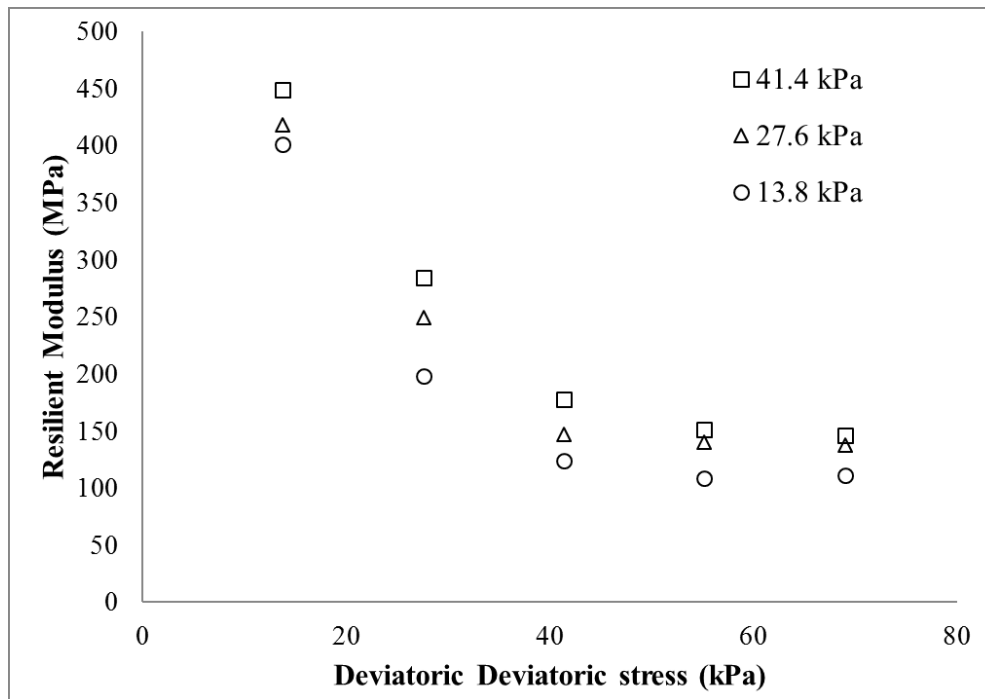


Figure 5-3- Resilient modulus values of the subgrade soil in accordance with AASHTO T307

Testing Procedure

Soil specimens were tested at various stress states as tabulated in Table 5-1. Four different stress ratios (q/p) were considered, in which $q = \sigma_1 - \sigma_3$ is deviator stress, and $p = (\sigma_1 + 2\sigma_3)/3$ is mean stress. At each constant stress ratio, five different deviator stresses and confining pressures were applied on five similar specimens. It is worth noting that the typical stress ratios on top of subgrade fall between 1.0 and 1.5. Two more stress ratios of 0.3 and 0.6 were covered in this study, so the permanent behavior of the subgrade material could be observed within a wide range of stress ratios and stress combinations. Prior to conducting the permanent deformation test, each specimen was put under 500 conditioning cycles at $\sigma_1 = 55.16$ kPa and $\sigma_3 = 13.79$ kPa for settling down and providing sufficient contact between the top of the specimen and the loading plate. Accordingly, 40,000 cycles of repetitive loading at each specified stress state was applied on the conditioned specimen. A haversine-shaped load was

implemented to apply the cyclic deviator stress on specimens with 0.1 s of load duration and a rest period of 0.9 s. The UTM-100 measured vertical deformations developed in the specimens automatically, and no external linear variable differential transducer (LVDT) was used for this purpose.

Table 5-1- Different stress ratios and stress states applied on the specimens

q/p = 0.3						q/p = 0.6					
σ_d (kPa)	5.2	6.9	10.3	13.8	17.2	σ_d (kPa)	11.6	15.5	23.3	31.0	38.8
σ_3 (kPa)	15.5	20.7	31	41.4	51.7	σ_3 (kPa)	15.5	20.7	31	41.4	51.7

q/p = 1						q/p = 1.5					
σ_d (kPa)	23.3	31.0	46.5	62.0	77.5	σ_d (kPa)	46.5	62.0	93.0	124.0	155.0
σ_3 (kPa)	15.5	20.7	31	41.4	51.7	σ_3 (kPa)	15.5	20.7	31	41.4	51.7

Discussion of Test Results

Figure 5-4 shows all the results of the RLT tests conducted on subgrade specimens. It was observed that as the stress ratio (q/p) increased from 0.3 to 1.5, the specimen underwent larger permanent deformations. The range of plastic deformations occurred in samples where $q/p = 0.3$ was between 100–450 microstrains. At $q/p = 0.6$ and $q/p = 1.0$, this range was recorded between 100–1,500 microstrains and 100–2,500 microstrains, respectively. At $q/p = 1.5$, the minimum plastic deformation accumulation in the sample at the lowest stress ratio showed a drastic increase as opposed to the other three stress ratios. The plastic deformations developed in the samples were between 1,200–1,400 microstrains. Figure 5-5 shows the ultimate permanent deformation of the specimen in each test at different mean stress values for all stress ratios. The high coefficients of correlation in linear regression analysis in Figure 5-5 indicate that the permanent deformation of the material linearly increased with p (or similarly, q). A similar observation was reported in (Gidel et al. 2001). In pavement design, the permanent deformation developed in subgrade material is negligible when it is less than 0.08% or 800 microstrains (Abu-Farsakh et al. 2014). At all five stress levels of $q/p = 0.3$, the permanent

deformation of the specimens fell below 500 microstrains which was insignificant. At $q/p = 0.6$, the sample specimens showed significantly larger permanent deformation behavior as the deviator stress increased from 23.3 kPa to 31 kPa and 38.8 kPa. At the last stress level in this stress ratio, the specimen experienced 1471 microstrains which was not negligible. The material showed a drastic increase in permanent deformation at the two highest stress levels at $q/p = 1.0$, similar to what was observed for $q/p = 0.6$. For the first three stress levels, the material did not undergo significant plastic deformations in stress ratios of 0.6 and 1.0. For the last tested stress ratio ($q/p = 1.5$), the material showed significantly large permanent deformation at all five stress levels.

In an attempt to evaluate the shakedown behavior of the subgrade material under different stress scenarios, the aforementioned criteria were used. It turned out that at all different stress levels in stress ratios from 0.3 to 1.0, the material tended to show plastic shakedown (Range A) behavior. This indicates that even at higher stress ratios and bulk stresses, the material experienced larger permanent deformation; however, as the structure of the material experienced the post-compaction deformation phase, it tended to react mostly as an elastic material under further loading cycles. The material only showed plastic creep (Range B) behavior in a stress ratio of 1.5 and for all of the stress levels. It is worth mentioning that the deviator stresses applied upon the specimens under $q/p = 1.5$ were mostly above the normal range of deviator stress levels on top of subgrade layer in the field. Thus, it can be concluded that the subgrade material used in this study showed acceptable performance with regards to the shakedown behavior of unbound materials under cyclic loadings even though it roughly underwent substantial initial deformations. The calculation of strain rates in all cases also tabulated that the subgrade soil did not tend to show significant permanent deformation growth at a higher number of load cycles at $q/p = 1.5$ which was similar to the behavior observed at a low stress ratio of $q/p = 0.3$. However, the amplitude of strain rates was higher in the higher

stress ratio. During the initial 1,000 number of load repetitions, the strain rate was noticeably high at $q/p = 1.5$ (and the highest stress level) among all other tests, followed by a gradual dwindling during the rest of the load repetitions. Figure 5-6 shows sample strain rates at the lowest and highest stress states.

In another study conducted by Gidel et al., a specimen was subjected to 20,000 cycles of repetitive high-stress levels. The same specimen was then put under a lower stress level to see how the permanent deformation development would react to the lower stress level. This study showed that the permanent deformation in a specimen did not change in response to a lower stress state because it had already experienced a plastic strain beyond the maximum strain at the less-damaging stress level (Gidel et al. 2001). This can be translated to the construction time at the field when the subgrade layer is subjected to high stress levels caused by construction machineries such as trucks and roller compactors as compared to the normal stress levels on top of the subgrade level during road operations. If the subgrade level experiences most of its plastic deformation during construction time, it will be less likely to undergo large permanent deformations when the road is open to traffic.

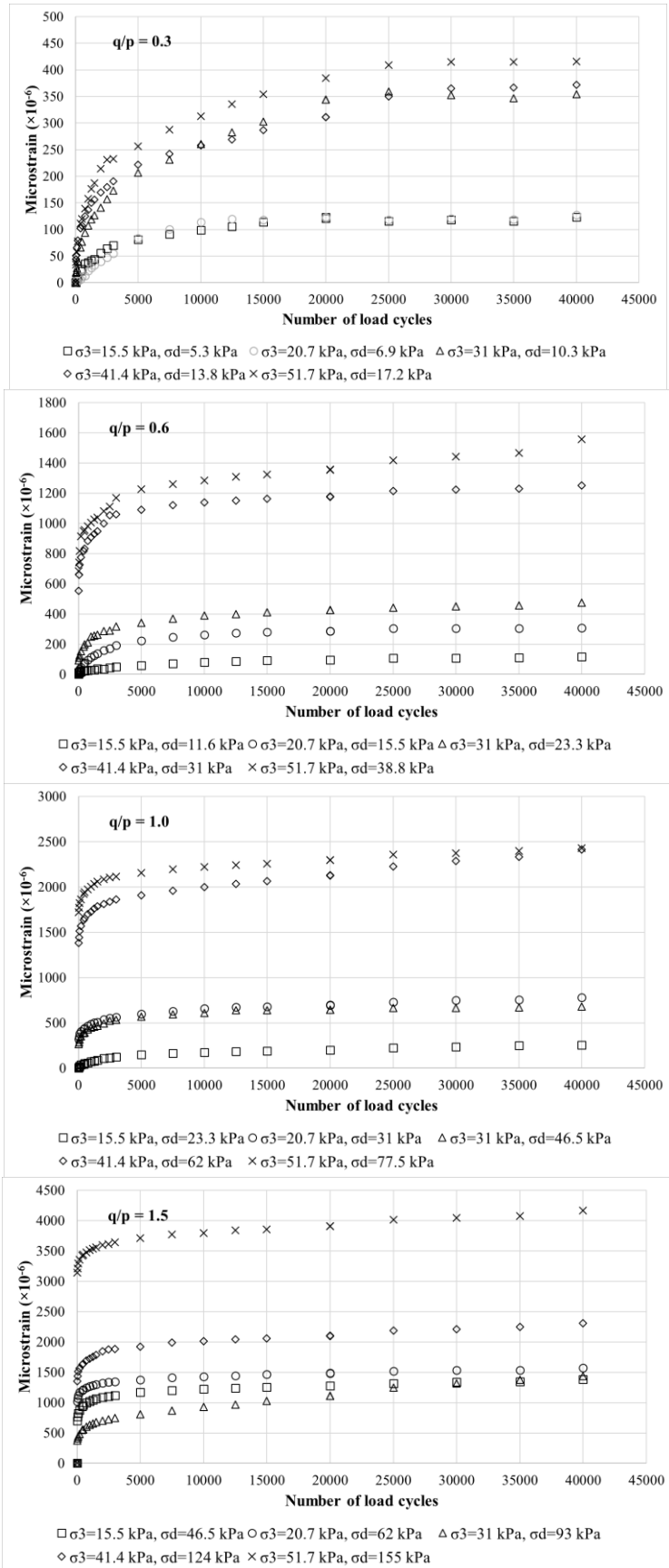


Figure 5-4- Relationships between plastic strain and number of load cycles

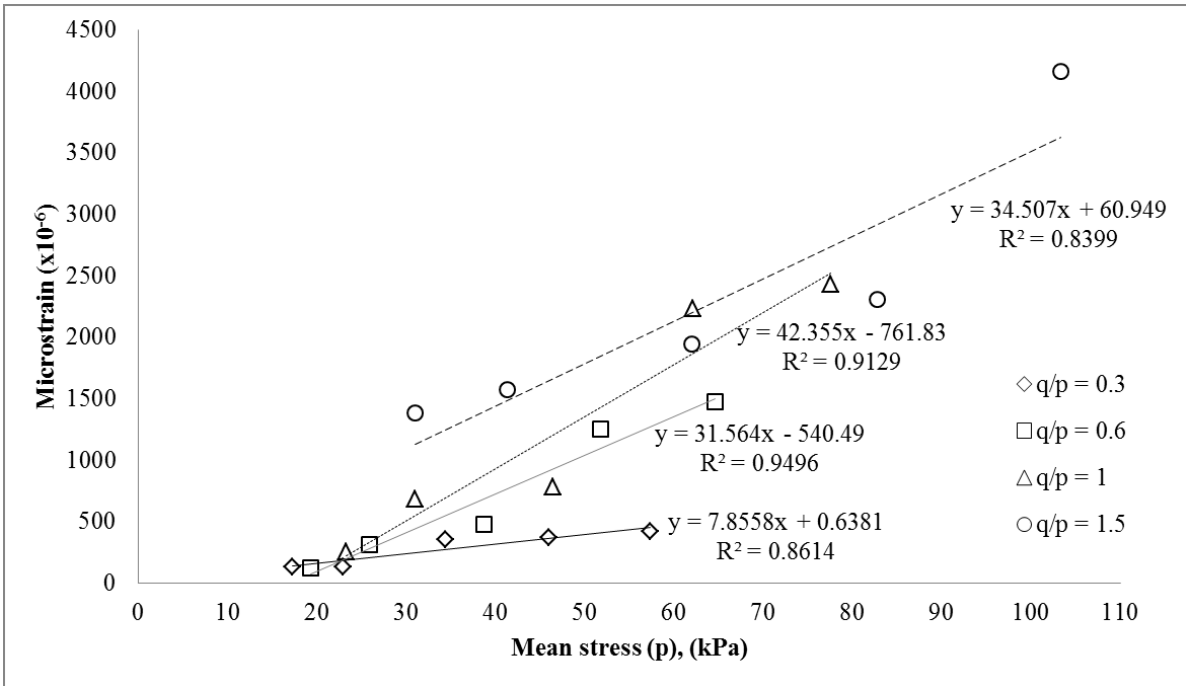


Figure 5-5- Relationships between ultimate plastic strain at the end of load cycles and mean stress

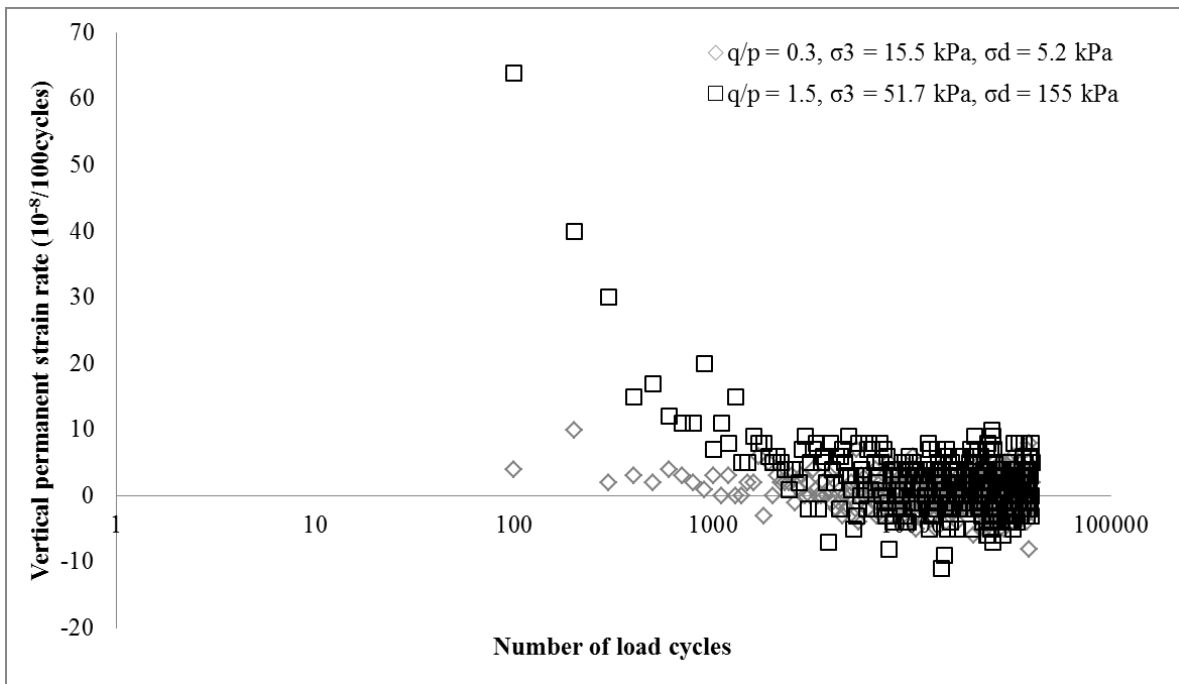


Figure 5-6- Strain rate variation against number of load repetitions at different stress levels

In an attempt to obtain and optimize the parameters in the MEPDG and Wang equations for predicting permanent deformations in the tested specimens, the least squares curve-fitting procedure was implemented using the Wolfram Mathematica V.10.3 computer program. In the first step, the models were fitted on each test individually. As expected, both the MEPDG and Wang models gave satisfying statistical performances in the context of coefficient of determination and S_e/S_y , which is the ratio of standard error of estimate from the prediction model over the standard deviation within the measured data. However, imposing no constraints on Wang model parameters led to irrationality in some cases despite yielding high R^2 and low S_e/S_y values. For example, as the moisture content or deviatoric stress increases, observing lower permanent deformation is not expected as the problem was reflected in negative a_2 or a_4 .

One of the deficiencies in MEPDG is that this model does not take into account the stress states under which the subgrade material undergoes plastic strains. Therefore, obtaining a general prediction model for permanent deformation at different stress conditions is not feasible. The Wang model addressed this issue by considering the stress states; however, as they calibrated the model for two different types of subgrade soil in HVS experiments, the R^2 obtained for the two calibrated models were moderately good. Moreover, no further statistical information regarding the performance of the model was provided (Wang et al. 2009).

In this study, a new prediction model based on the testing approach is presented as follows:

$$\varepsilon_p (\text{microstrain}) = a_1 P_a \left(\frac{\tau_{oct}}{P_a} + 1 \right)^{a_2} \left(\frac{q}{p} \right)^{a_3} N^{a_4} \quad (3)$$

where

τ_{oct} = octahedral shear stress (kPa)

q/p = stress ratio

P_a = atmospheric pressure (101.35 kPa)

N = number of load cycles

a_i = regression parameters

It should be mentioned that this model was only calibrated for the silty sand subgrade compacted at optimum moisture content. In order to include the moisture content in the model as one of the predictors, all of the tests should be re-run above and below the optimum moisture content, which requires a lot of effort and time. Table 5-2 depicts the regression parameters for the calibrated model along with the goodness of the fit statistics. The R^2 for the model fitted on approximately 1,000 data points was 0.907. The Wang model was also calibrated for all the test results using the same sampled data points. The suggested model proved to outperform the Wang model as it was successful in accurately predicting the test results in two tests with R^2 of 0.77 and 0.65 at $q/p = 1.5$ (fifth stress level) and $q/p = 1.0$ (second stress state), respectively. Figure 5-7 depicts the results. In four other cases, the suggested model showed better performance in predicting the plastic strain behavior of tested specimens. However, in ten and six other groups of tests, both models overestimated and underestimated the test results, respectively.

Table 5-2- Calibrated parameters for permanent deformation prediction model

Parameter	Estimate	Standard error	Confidence Interval
a₁	2.489	0.1453	(2.0825,2.6813)
a₂	3.82407	0.1493	(3.600,4.199)
a₃	0.18043	0.0672	(0.049,0.314)
a₄	0.0623	0.0084	(0.0448,0.078)

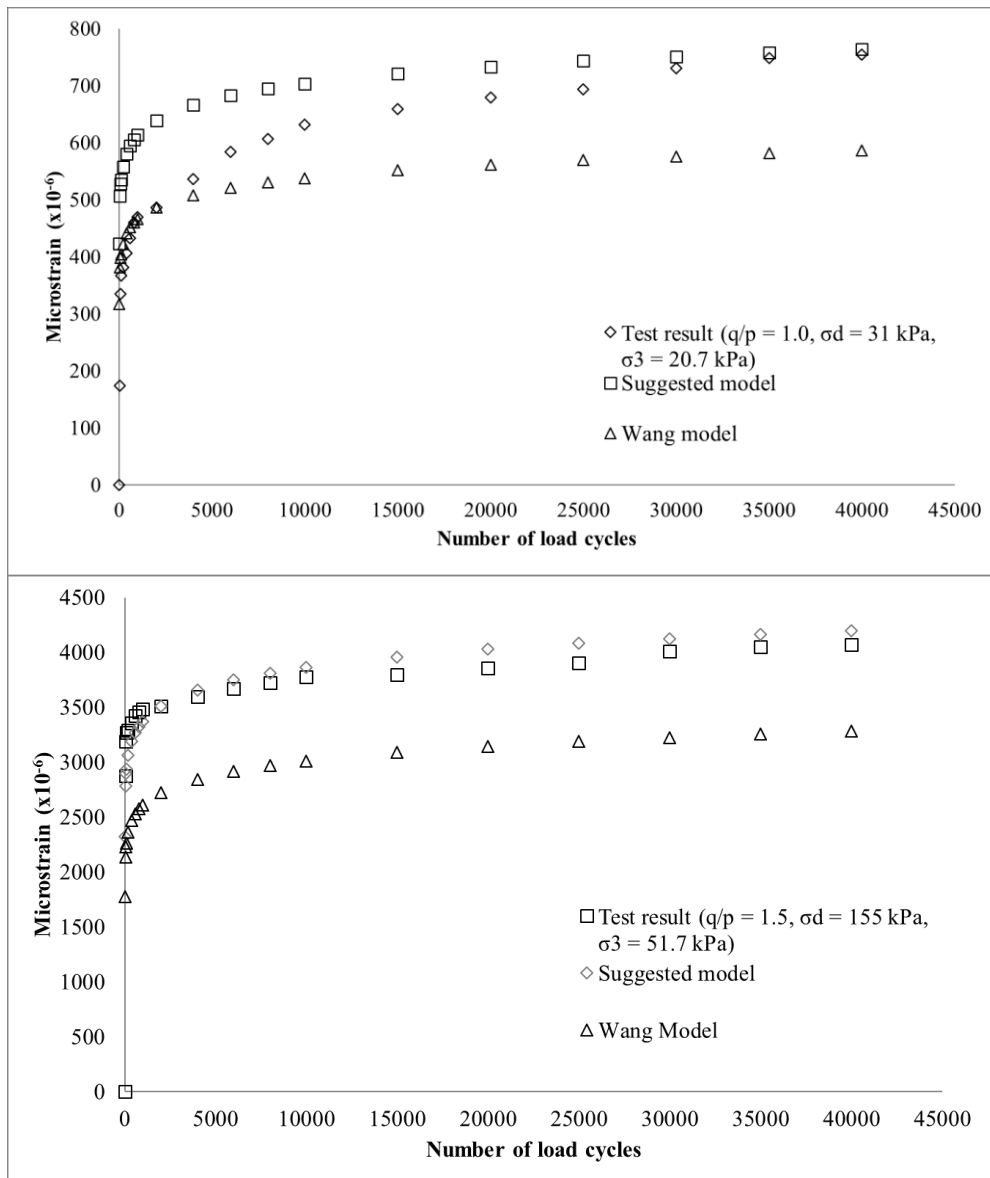


Figure 5-7- Comparisons between test results and the two prediction models

In order to explain the anomaly observed in the performance of the prediction models, it should be noted that the results from the same RLT permanent deformation test on similar sample replicates tend to be highly dispersed (Gidel et al. 2001). Therefore, it is of utmost importance that a reasonable number of replicates would be used to ascertain that the plastic deformation of specimens under each stress state is an accurate representation of material behavior. In the current study, two replicates were used for most of the tests, and a significant dispersion between the two tests was observed. The most important thing, however, is that in order to obtain a stronger prediction model, several inherent parameters of the material (such as soil

type, moisture content, compaction, void ratio, gradation, matric suction, etc.) should be included in the testing program. On the other hand, in order to obtain a sound prediction model addressing the complicated field conditions, the experimental models should incorporate initial high preloading on the subgrade layer during the construction phase, environmental conditions such as moisture variation and freeze/thaw phenomenon, complex traffic loading, etc..

Summary and Conclusion

This chapter aimed at the evaluation of the permanent deformation behavior of a silty sand subgrade material (SW-SM) under different stress ratios and stress levels scenarios. The RLT tests were conducted utilizing the IPC Universal Testing Machine (UTM-100). The shakedown behavior of the material under all different stress levels was evaluated and the strain rate development was found. Based on the test results, a regression prediction model was developed and its performance was evaluated against the Wang model already available in the literature. From the findings of this chapter, the following conclusions were reached:

- As the stress ratio (q/p) increased from 0.3 to 1.5, the specimen showed larger permanent deformations. The specimens did not show significant permanent deformation at $q/p = 0.3$ stress ratio. As the stress ratio increased toward $q/p = 1.5$, the amplitude and frequency of the high permanent deformation cases increased.
- Based on the observations obtained from tests results and the high coefficient of determinations in the regression analysis, it was concluded that the ultimate permanent deformation developed in the samples varied linearly with the mean stress (similarly, deviatoric stress).
- For all stress ratios of 0.3, 0.6 and 1.0, the shakedown behavior of the subgrade material was found to be within Range A or plastic shakedown. Only at a stress ratio of 1.5 did

the shakedown behavior match Range B or plastic creep. It should be mentioned that the stress levels imposed upon the specimens at this stress ratio were mostly above the routine traffic loads on top of the subgrade layer at the field condition.

- The developed prediction model for permanent deformation showed moderately satisfying results; however, in order to obtain a sound prediction model, several inherent characteristics of the material and different field environmental and traffic conditions should be incorporated into the models. The verification of models with actual field test data and fields equipped with multi-depth deflectometers can significantly enhance the accuracy of experimental models.

Chapter 6- The Effect of Bottom Ash on Soil Suction and Resilient Modulus of Medium Plasticity Clay

A version of this chapter was published Asefzadeh, A., Hashemian, L. and Bayat, A., 2018. The Effect of Bottom Ash on Soil Suction and Resilient Modulus of Medium-Plasticity Clay, Transportation Research Record: Journal of the Transportation Research Board (No. 18-05098)”

Abstract

The effect of adding bottom ash to medium plasticity clay as a soil stabilizer was evaluated in this study by performing triaxial M_r tests. Two log-log M_r prediction equations found in the literature (MEPDG and NCHRP 1-28) were selected and calibrated for mixtures of bottom ash and clay at different moisture contents. It was found that, with 25 percent bottom ash in the mixture, the M_r increased between 5 and 23 percent under different stress states. The soil total and matric suctions of the mixtures were indirectly measured using the filter paper method, and the total suction parameter was incorporated in the two log-log prediction models. The nonlinear regression analysis revealed that the average goodness of fit statistics for one of the modified models showed highly satisfactory performance in predicting the M_r values.

Introduction

The subgrade acts as the foundation of the pavement structure and plays a crucial role in supporting the upper layers of pavement and in transferring the repeated traffic-induced loadings onto the ground. The elastic stiffness of subgrade soils to cyclic loading is defined as the M_r , which is numerically the ratio of the deviatoric stress to resilient or recoverable strains of the material under a constant confining pressure in repeated load triaxial tests. M_r is an important parameter for calculating resilient stresses, strains, and deformations in flexible pavements. The subgrade stress-strain behavior is reflected in pavement surface deflections and rutting failures (Li and Selig 1994, Burczyk et al. 1994). Therefore, having knowledge of M_r for subgrade materials is essential for a successful pavement design, which satisfies the performance expectations and provides ease of ride for commuters.

Clay is a fine-grained weak soil, which generally has unsuitable engineering properties including low values of M_r . These properties become worse during wetting due to the ingress of rainfall through the subgrade layer or rising of the groundwater table (Brooks 2009). Studies

showed that the M_r of fine-grained soils drastically decreases as the moisture content increases, which itself leads to the decrease in soil matric suction (Khoury and Zaman 2004, Liang et al. 2008, Sawangsurriya et al. 2009). One of the other environmental parameters, which adversely affects the M_r of clayey subgrade soils, is the freeze-thaw cycle in cold regions. Previous studies found that the M_r of cohesive soils decreases as the freeze-thaw cycle increases (Qi et al. 2006, Wang et al. 2007). As such, using weak soils as a subgrade layer can potentially lead to immature loss of life and unsatisfactory performance of the pavement structure. In road projects where excavating and replacing the local weak soil with stronger material from other borrow pits is not feasible, amelioration of the soil through different additives is considered in order to stabilize the soil, improve its strength and stiffness, and provide a reliable foundation for construction projects, such as road embankments (Solanki et al. 2010, Güllü 2014). Several researchers studied the feasibility of using different materials, such as lime, cement, husk ash, and fly ash as soil stabilizers in clayey soils (Brooks 2009, Alhassan 2008, Sezer et al. 2006, Misra 1998, Jan and Battacharja 1999, Modarres and Nosoudy 2015). Bottom ash has also been used in clayey soil stabilization in other studies and yielded an improvement in the stiffness and elasticity of the clay (Modarres and Nosoudy 2015, Rifai et al. 2009). It is worth noting that bottom ash contains high amounts of silica–aluminous compounds, and can enhance pozzolanic reactions. Therefore, in other studies, clayey soil was stabilized with a mixture of bottom ash and Portland cement (Osinubi 2000, Ahmad et al. 2016). However, mixing clayey soil with pure bottom ash would result merely in mechanical stabilization of the soil, and there is no chemical reaction involved.

Bottom ash is the by-product of coal-fired power generation plants. Generally, around 4–30 percent of coal burned in a furnace turns into ash, and approximately 15–20 percent of the total generated ash collects in the form of bottom ash at the bottom of the furnace (Heidrich et al. 2013, Kayyabal and Bulus 2000). According to the Alberta Utilities Commission, 55 percent

of the electricity generated in the province of Alberta, Canada in 2014 stemmed from 33.8 million tonnes of coal consumption (Quigley 2016). Considering the ratios given above, it can be estimated that roughly 1 million tonnes of bottom ash was generated in 2014 in Alberta. Utilization of bottom ash in construction projects, such as subgrade stabilization in road embankments, can be deemed to be a sustainable alternative to landfilling the waste material in repositories, which can potentially create pollution risks and exothermic hazards to the environment adjacent to the landfill site (Bethanis and Cheeseman 2005, Klein et al. 2001).

The goal of this study is to evaluate the applicability of using bottom ash to improve the M_r of a medium plasticity clay for use as a subgrade material through performing repeated load triaxial tests and obtaining the optimum ratio of soil and bottom ash. The total and matric suctions of soil mixtures at different moisture contents within the dry and wet sides of the optimum moisture content were also measured in order to integrate them into the M_r prediction equations.

Material and Experimental Procedure

In this study, a medium plasticity clay (with a Plasticity Index (PI) of 18) was used, which is vastly found in Edmonton, Alberta, Canada. The bottom ash was sourced from a local coal-fired power plant in Alberta. The gradation of the clay and bottom ash materials is represented in Figure 6-1. The Atterberg limits of the mixtures are tabulated in Table 6-1. Initially, three different nominal bottom ash and clay mixture ratios of 15 percent–85 percent, 25 percent–75 percent, and 35 percent–65 percent were selected based on the total dry weight of the mixture. The gradation on the mixtures was not conducted.

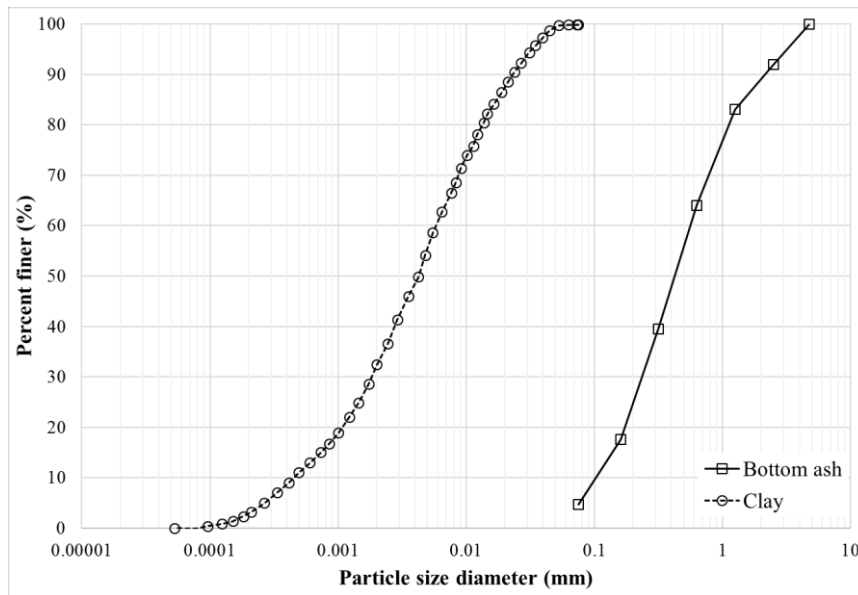


Figure 6-1- Particle size distribution of clay and bottom ash materials

Table 6-1- Atterberg limits of different mixtures (percent)

Mixture	Liquid limit	Plastic limit	Plasticity index
Clay	43	25	18
15% Bot. ash, 85% Clay	45	27	18
25% Bot. ash, 75% Clay	42	26	16
35% Bot. ash, 65% Clay	38	30	8

Compaction Test

To obtain the maximum dry density and the optimum moisture content of the untreated clay and the three mixtures, modified compaction tests as per ASTM D1557 were conducted (AASHTO T307-99 2003). The dry materials were first blended well by hand to achieve uniform mixing. After adding and mixing distilled water with the dry material, the mixture was pulverized through sieve No. 4 to minimize clumpy particles and ensure uniform distribution of moisture. Each mixture was then kept in a sealed plastic bag for at least two hours before compaction. Figure 6-2 depicts the compaction test results for clay, bottom ash, and the three mixtures. The curves in Figure 6-2 are the regression lines. It can be observed that with 15 percent bottom ash added to the clay, the optimum moisture content of the mixture decreased to 13.5 percent as compared to 15.8 percent for the untreated clay. For each increment of

bottom ash in the next two mixtures, the optimum moisture contents increased by 0.5 percent and reached 14 percent and 14.5 percent, respectively. The bottom ash material did not have a conventional compaction curve, and the optimum moisture content was found to be 21 percent.

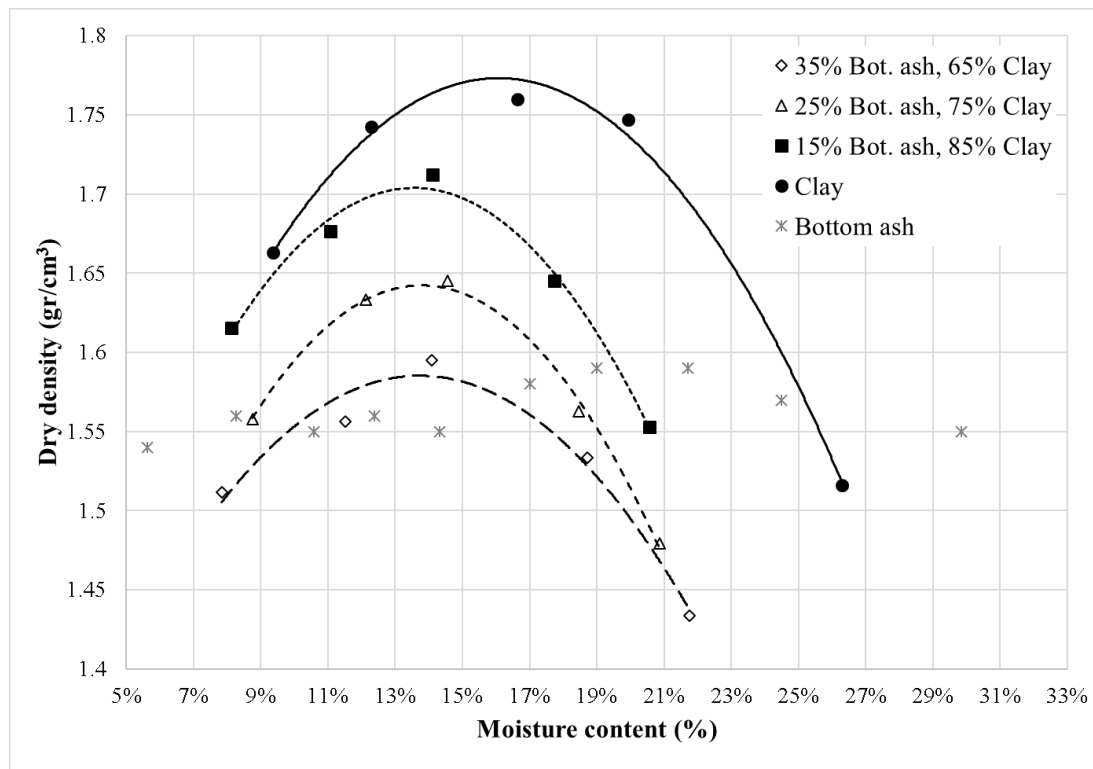


Figure 6-2- Modified compaction test results

Specimen Preparation

To study the effect of moisture variation on M_r , three different moisture contents were considered: optimum-2 percent, optimum, and optimum+2 percent. The specimens for clay and each clay-bottom ash mixture were then mixed with a respective amount of water, pulverized through sieve No. 4, and placed and sealed in plastic bags for at least two hours before compacting. A brass split mold with a diameter of 100 mm and a height of 200 mm was used. To negate the effect of varying dry densities, all the specimens were made at the maximum dry density, corresponding to each mixture's compaction curve. To this end, the exact amount of moist material was calculated based on the compaction data, and the compactive effort was

modified for five layers through a trial procedure to achieve maximum dry density at three predetermined moisture contents. The top of each compacted layer was scarified with a lab claw to ensure sufficient interlocking action between layers. To stay on the conservative side, the specimens were then sealed in plastic bags and placed in a secured enclosure for one day before conducting the M_r tests.

Resilient Modulus Test

The repeated load triaxial tests for measuring the M_r values were conducted using an IPC Universal Testing Machine (UTM-100) in accordance with AASHTO T307-99 standard, which simulates the field stress condition by applying five different deviatoric stresses upon the specimen at three different confining pressures (AASHTO T307-99 2003). The confining pressures used in the test were in the order of 13.8, 27.6, and 41.4 kPa, and deviatoric stresses applied on the specimens were 13.8, 27.6, 41.4, 55.2, and 69 kPa. These confining pressures and deviatoric stresses made overall 15 stress states. Table 6-2 depicts the 15 test sequences and their corresponding bulk and deviatoric stresses. A haversine-shaped load was implemented to apply cyclic deviatoric stresses on specimens with 0.1 s of load duration, and a rest period of 0.9 s. Two External Linear Variable Displacement Transducers (LVDT), with stroke lengths of 5.08 mm, were mounted on the pedestal attached to the axial loading shaft of the triaxial cell in order to measure the vertical resilient deformation of the specimens. Prior to beginning the test, each specimen was put under 500 conditioning cycles at a deviatoric stress of 13.8 kPa, and a confining pressure of 41.4 kPa, to ascertain the settling of the specimen and provide sufficient contact between the top of the specimen and the loading plate. M_r was calculated as the average M_r of the last five cycles at each stress state. Two replicates were used for each mixture under the condition that the M_r values between the two replicates had no more than a 5 percent difference. Otherwise, a third specimen was made and Grubbs' statistical method,

with a 95 percent confidence level (Grubbs 1969), was implemented to ensure that no specimen was an outlier, which means that a measured M_r of a specimen could potentially have a significant deviation from the average value of all three replicates. As per Grubbs' test, three outliers in the untreated clay mixture at optimum moisture content, and mixtures with 15 percent and 25 percent bottom ash contents with a moisture content of optimum-2 percent were rejected. Therefore, 27 specimens were made in total.

Table 6-2- Resilient modulus test sequences

Test sequence	Confining pressure (kPa)	Deviatoric stress (kPa)	Bulk stress (θ), (kPa)	Octahedral stress (τ), (kPa)
1	41.4	13.8	138.0	6.5
2	41.4	27.6	151.8	13.0
3	41.4	41.4	165.6	19.5
4	41.4	55.2	179.4	26.0
5	41.4	69	193.2	32.5
6	27.6	13.8	96.6	6.5
7	27.6	27.6	110.4	13.0
8	27.6	41.4	124.2	19.5
9	27.6	55.2	138.0	26.0
10	27.6	69	151.8	32.5
11	13.8	13.8	55.2	6.5
12	13.8	27.6	69.0	13.0
13	13.8	41.4	82.8	19.5
14	13.8	55.2	96.6	26.0
15	13.8	69	110.4	32.5

Matric Suction Measurement

Total suction in soil is defined as the free potential energy of soil water that can be measured in terms of the vapor pressure of the soil water, or the relative humidity of the soil (Fredlund and Rahardjo 1993, Leong et al. 2003). Total suction is comprised of two components: the matric suction and the osmotic suction. Matric suction refers to the capillary phenomenon stemming from liquid surface tension generated in the soil-water media. It is defined as the difference between the pore gas pressure (surrounding gas pressure in the voids, which are partially filled with water) and pore water pressure. Osmotic suction refers to a decrease in

relative humidity of soil because of the presence of dissolved salts in the soil water (Fredlund and Rahardjo 1993, Leong et al. 2003).

Filter paper test is one of the most referred testing methods in the literature, which is capable of accurately measuring the soil matric and total suctions for engineering practices. If the filter paper's moisture reaches an equilibrium with the vapor flow, it will indirectly measure the total suction of the soil. Matric suction can be measured when the filter paper's absorbed moisture is brought to equilibrium through liquid flow and direct contact with the soil (Bulut et al. 2001). In this study, the indirect measurement of the suctions of the soil mixtures was conducted in accordance with ASTM D5298 standard. Soil samples were compacted in a 75 mm split mold to achieve the maximum dry density at respective moisture contents. For each test, two half-samples, with approximate thicknesses of 25 mm, were prepared. The top of the samples were trimmed with a knife to achieve smooth surfaces. Whatman No. 42 ash-free quantitative Type II filter papers, with 55 mm and 70 mm diameters, were used. To measure the matric suction, a 55 mm filter paper was placed between two 70 mm filter papers to protect it from dirt and contaminants. The stacked filter papers were then placed between the two half-soil samples and the two halves were then secured with electrical tape to cover the gap between them and to prevent the filter paper from absorbing vapor moisture (Bulut et al. 2001). Next, the samples were placed in 10 oz clear, wide-mouth jars. To measure the total suction, O-rings were placed on top of the samples and two 55 mm filter papers were placed on the O-rings without making any contact with the surface of the soil. The jars' lids were closed and secured by electrical tape. The jars were then placed in an environmental chamber at 20 ± 0.5 °C for one week. The calibration curve of the filter paper was adopted from the ASTM D5298 standard. The weights of the filter papers were calculated using an analytical scale with a resolution of 10⁻⁴ gr. Figure 6-3 schematically shows the test setup for matric and total suction measurements.

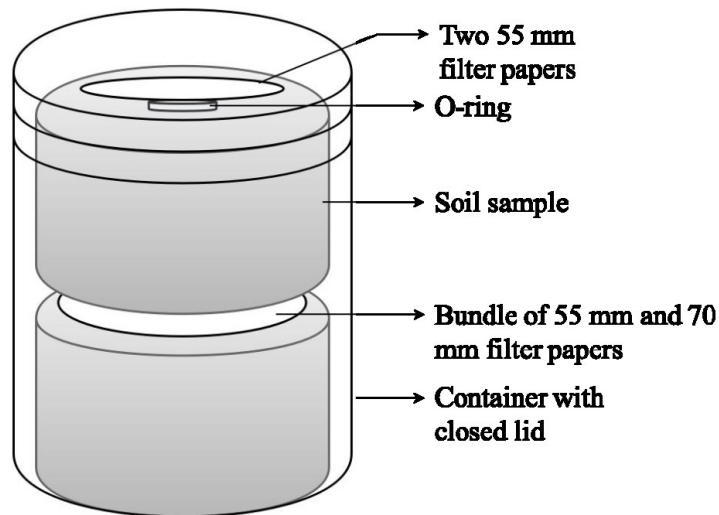


Figure- 6-3- Schematic setup of the filter paper tests as per ASTM D5298

Data Representation and Discussion

Resilient Modulus

Over the course of the past five decades, several M_r constitutive prediction equations, which possess their own merits and demerits, were suggested in the literature (Dunlap 1963, Thompson and Robnett 1976, Moosazadeh and Witczak 1981, Witczak and Uzan 1988). The generalized model, which is a log-log model adopted by the new AASHTO 2002 Mechanistic Empirical Pavement Design Guide (MEPDG), is as follows (ARA 2004):

$$M_r = k_1 P_a \left(\frac{\theta}{P_a} \right)^{k_2} \left(1 + \frac{\tau_{oct}}{P_a} \right)^{k_3} \quad (1)$$

where,

M_r = Resilient modulus (MPa)

k_1, k_2, k_3 = Regression coefficients,

P_a = Reference atmospheric pressure (101.3 kPa),

θ = Bulk stress (sum of three principal stresses: $\sigma_1, \sigma_2, \sigma_3$) (kPa) and,

τ_{oct} = Octahedral shear stress which is defined as $2^{0.5}/3(\sigma_1 - \sigma_3)$ (kPa)

Another log-log M_r prediction model was suggested by NCHRP 1-28 (35) for stabilized soils:

$$M_r = k_1 P_a \left(\frac{\sigma_3}{P_a} \right)^{k_2} \left(\frac{\sigma_d}{P_a} \right)^{k_3} \quad (2)$$

where,

M_r = Resilient modulus (MPa)

k_1, k_2, k_3 = Regression coefficients,

P_a = Reference atmospheric pressure (101.3 kPa),

σ_3 = Confining pressure (kPa) and,

σ_d = Deviatoric stress (kPa)

In this study, Equations (1) and (2) were adopted to calibrate the test results. The average results of two specimens for each mixture are tabulated in Table 6-3. It can be observed, in all mixtures, specimens showed higher M_r on the dry side of the optimum moisture content. The highest increase in M_r , with decrease in the optimum moisture content, was observed in 85 percent clay and 15 percent bottom ash mixtures, with an average of 65 percent, while the smallest increase was recorded for 65 percent clay and 35 percent bottom ash. The untreated clay specimens showed a 24 percent increase in the M_r . Additionally, as the moisture content of the specimens increased by 2 percent, a decrease in the M_r of all mixtures was noted. The mixture with 15 percent bottom ash showed the smallest reduction in M_r by 12 percent, while the clay mixture showed a 23 percent decrease, and both mixtures with 25 percent and 35 percent bottom ash contents yielded a 34 percent decrease. Additionally, all specimens showed reductions in M_r as the deviatoric stress increased. This observation can be attributed to the stress softening behavior of fine-grained soils as opposed to what is normally observed in granular materials where M_r shows a direct relationship with bulk stress.

The effect of adding bottom ash on the M_r of mixtures, compared to that of the untreated clay, is shown in Figure 6-4. For brevity, the results were presented only at optimum moisture contents. Adding bottom ash at 15 percent and 35 percent dry weight ratios drastically decreased the M_r of the mixtures at an average of 27 percent and 22 percent, respectively. Mixing clay with 25 percent bottom ash amended the clay engineering properties, which led to the observation of an average of 15 percent increase in M_r , and an average of 23 percent was the maximum enhancement observed in the second sequence of the test. This observation relates to how the bottom ash is incorporated in the soil particles' structure of the mixture at different ratios. At 25 percent, maximum interlocking of particles between the clay and the bottom ash was achieved, which resulted into a significant increase in the M_r of the mixtures. Adding 15 percent or 35 percent of bottom ash softened the soil mixture, which yielded lower M_r values. It is worth noting that the increase or decrease in M_r of the mixtures at different stress states were found to be variable. This can be attributed to the stress dependency of the material. The same behavior is observed in the M_r of granular materials at different stress states.

Table 6-3- Resilient modulus values of the test mixtures (MPa)

Test sequence	Clay			15% Bot. ash			25% Bot. ash			35% Bot. ash		
	Opt. - 2%	Opt.	Opt. + 2%	Opt. - 2%	Opt.	Opt. + 2%	Opt. - 2%	Opt.	Opt + 2%	Opt. - 2%	Opt.	Opt. + 2%
1	269	213	186	203	101	88	308	237	197	196	150	111
2	123	104	82	121	82	76	187	129	97	111	87	55
3	107	87	65	111	74	69	162	106	70	89	74	41
4	103	83	62	105	70	66	151	99	60	78	69	37
5	99	82	60	102	69	64	144	92	53	73	67	35
6	245	196	173	184	87	73	245	208	164	168	118	114
7	135	103	80	129	73	65	176	121	76	101	75	57
8	104	86	61	105	69	62	156	101	61	84	68	43
9	100	82	57	100	67	61	143	92	55	75	64	37
10	98	81	54	99	67	60	140	88	52	71	64	36
11	218	175	133	178	78	69	226	202	165	158	114	103
12	121	98	79	118	67	57	164	110	77	91	81	53
13	104	86	66	102	65	53	145	102	61	79	69	41
14	100	80	60	97	64	51	135	94	54	70	66	38
15	98	76	58	94	64	53	131	90	51	67	65	36

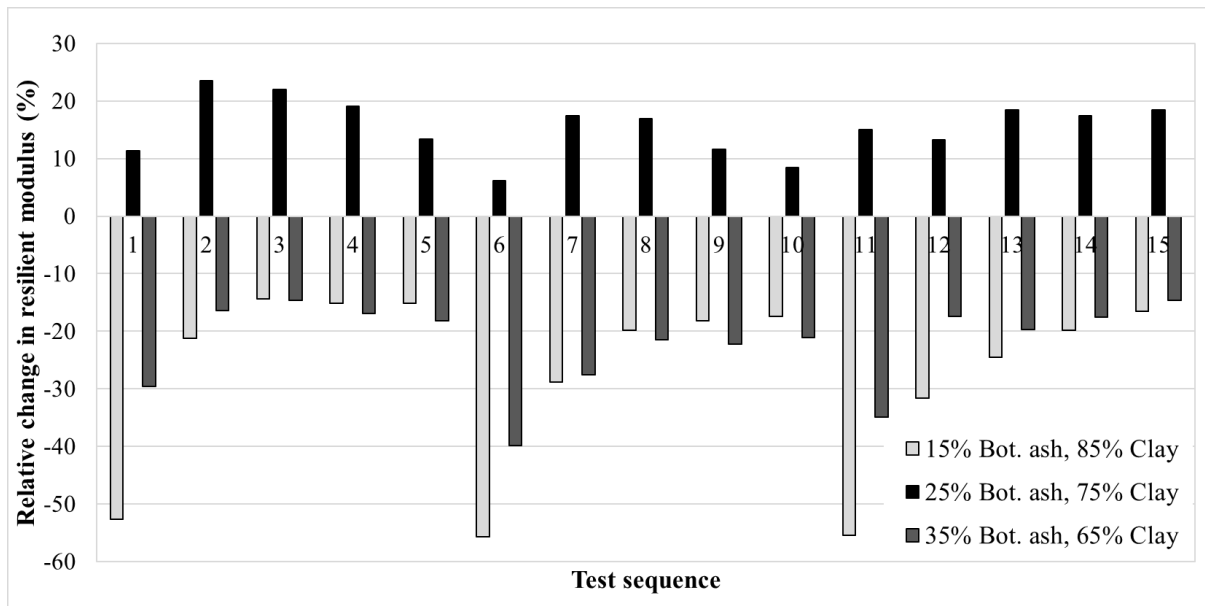


Figure 6-4- Relative change in resilient modulus in different mixtures compared to untreated clay

To calibrate the prediction equations and find the respective regression coefficients for each mixture, a nonlinear curve fitting, using the least squares method in Wolfram Mathematica V.10.3, was implemented. Tables 6-4 and 6-5 show the derived regression coefficient R^2 and S_e/S_y statistic (S_e = standard error of estimate, and S_y = standard deviation within the samples) values for Equations (1) and (2), respectively. Comparing the R^2 and S_e/S_y for the two models revealed that Equation (2) outperforms Equation (1) in predicting M_r values. It was observed that in 8 out of 12 mixtures, the S_e/S_y ratio for Equation (1) was above 0.50, whereas, except for the clay mixture at the moisture content of optimum–2 percent, this ratio for Equation (2) was below 0.50 for the rest of the mixtures. This indicates that the second model has significantly better goodness of fit as opposed to the first model.

Table 6-4- Equation (1) Regression coefficients and statistics for different mixtures

Regression coefficients	Clay			15% Bot. ash			25% Bot. ash			35% Bot. ash		
	Opt. - 2%	Opt.	Opt. + 2%	Opt. - 2%	Opt.	Opt. + 2%	Opt. - 2%	Opt.	Opt + 2%	Opt. - 2%	Opt.	Opt. + 2%
k_1	3.1616	2.4988	2.3576	2.1739	0.9596	0.8466	3.1003	2.7276	2.6699	2.2887	1.5099	1.5541
k_2	0.1520	0.1512	0.2484	0.1066	0.2328	0.3376	0.2526	0.1482	0.1969	0.2167	0.1943	0.0589
k_3	-5.6661	-5.5196	-6.9731	-3.6686	-1.8829	-1.9967	-3.8309	-5.1588	-7.7809	-5.4667	-4.0163	-6.8790
R^2	0.9705	0.9720	0.9690	0.9873	0.9973	0.9978	0.9888	0.9789	0.9736	0.9845	0.9819	0.9770
S_e/S_y	0.9722	0.7611	0.6573	0.5568	0.1495	0.1191	0.7399	0.7507	0.6166	0.5211	0.4462	0.3667

Table 6-5- Equation (1) Regression coefficients and statistics for different mixtures

Regression coefficients	Clay			15% Bot. ash			25% Bot. ash			35% Bot. ash		
	Opt. - 2%	Opt.	Opt. + 2%	Opt. - 2%	Opt.	Opt. + 2%	Opt. - 2%	Opt.	Opt + 2%	Opt. - 2%	Opt.	Opt. + 2%
k_1	0.7184	0.5911	0.4330	0.8228	0.7282	0.7259	1.3600	0.7101	0.3754	0.6083	0.5728	0.2289
k_2	0.1141	0.1146	0.1848	0.0812	0.1525	0.2314	0.1759	0.1080	0.1491	0.1596	0.1316	0.0490
k_3	-0.6686	-0.6534	-0.7765	-0.4504	-0.1898	-0.1739	-0.4287	-0.6105	-0.8592	-0.6205	-0.4704	-0.8022
R^2	0.9887	0.9897	0.9871	0.9959	0.9984	0.9990	0.9951	0.9929	0.9919	0.9960	0.9909	0.9944
S_e/S_y	0.6016	0.4611	0.4168	0.3184	0.1161	0.0800	0.4875	0.4373	0.3425	0.2642	0.3168	0.1817

Soil Suction

Figure 6-5 shows the variation of total, matric, and osmotic suctions in different mixtures at different moisture contents of optimum-2 percent, optimum, and optimum+2 percent. The values of total and matric suctions decreased as the percentage of bottom ash in the mixture increased. This observation was expected as per the fundamentals of soil suction. The osmotic suction in the mixture with 35 percent bottom ash always showed higher values compared to that of the other mixtures. This observation could be attributed to the fact that osmotic suction of soils is a function of ion concentration, and it increases as the concentration of electrolyte increases in the solution (Witteveen et al. 2013). In order to evaluate the effect of total, matric, and osmotic suctions on M_r , linear regression analysis was conducted on all data points for each test sequence. Table 6-6 shows the results of linear regression analysis for three soil suction components corresponding to three moisture contents. It should be mentioned that low R^2 values were not unexpected, since the regression was conducted on all the data. Since the matric suction generally decreases with the increase of the bottom ash in the mixtures, the total suction was considered and incorporated in the M_r prediction models (Rahman and Tarefdar 2015). Table 6-7 shows the R^2 values for linear regression analysis between the total suction, and the M_r for each individual mixture. The overall high average R^2 values refer to a moderately high, and significant, correlation between M_r and the total suction within different mixtures.

Table 6-6- Linear regression coefficients of determination for resilient modulus and soil suction for all mixtures

Test sequence	Total suction	Matric suction	Osmotic suction
1	0.39	0.36	0.21
2	0.26	0.29	0.27
3	0.31	0.36	0.27
4	0.36	0.41	0.30
5	0.39	0.44	0.31
6	0.48	0.46	0.06
7	0.45	0.39	0.22
8	0.36	0.44	0.26
9	0.39	0.45	0.29
10	0.41	0.31	0.30
11	0.35	0.43	0.04
12	0.43	0.42	0.17
13	0.41	0.45	0.20
14	0.43	0.46	0.22
15	0.43	0.45	0.24
Average	0.39	0.41	0.22

Table 6-7- Linear regression coefficients of determination for resilient modulus and total suctions of each mixture at different moisture contents

Test sequence	Clay	15% Bot. ash	25% Bot. ash	35% Bot. ash
1	0.99	0.91	0.93	0.96
2	0.98	0.92	0.94	0.90
3	0.98	0.91	0.92	0.81
4	0.98	0.91	0.89	0.71
5	0.97	0.92	0.89	0.68
6	0.99	0.91	0.80	0.95
7	1.00	0.92	0.88	0.98
8	0.96	0.93	0.90	0.88
9	0.95	0.94	0.90	0.79
10	0.94	0.95	0.90	0.69
11	0.99	0.90	0.74	0.99
12	1.00	0.94	0.92	0.78
13	0.98	0.97	0.85	0.78
14	0.99	0.98	0.84	0.64
15	1.00	0.98	0.84	0.57
Average	0.98	0.93	0.88	0.81

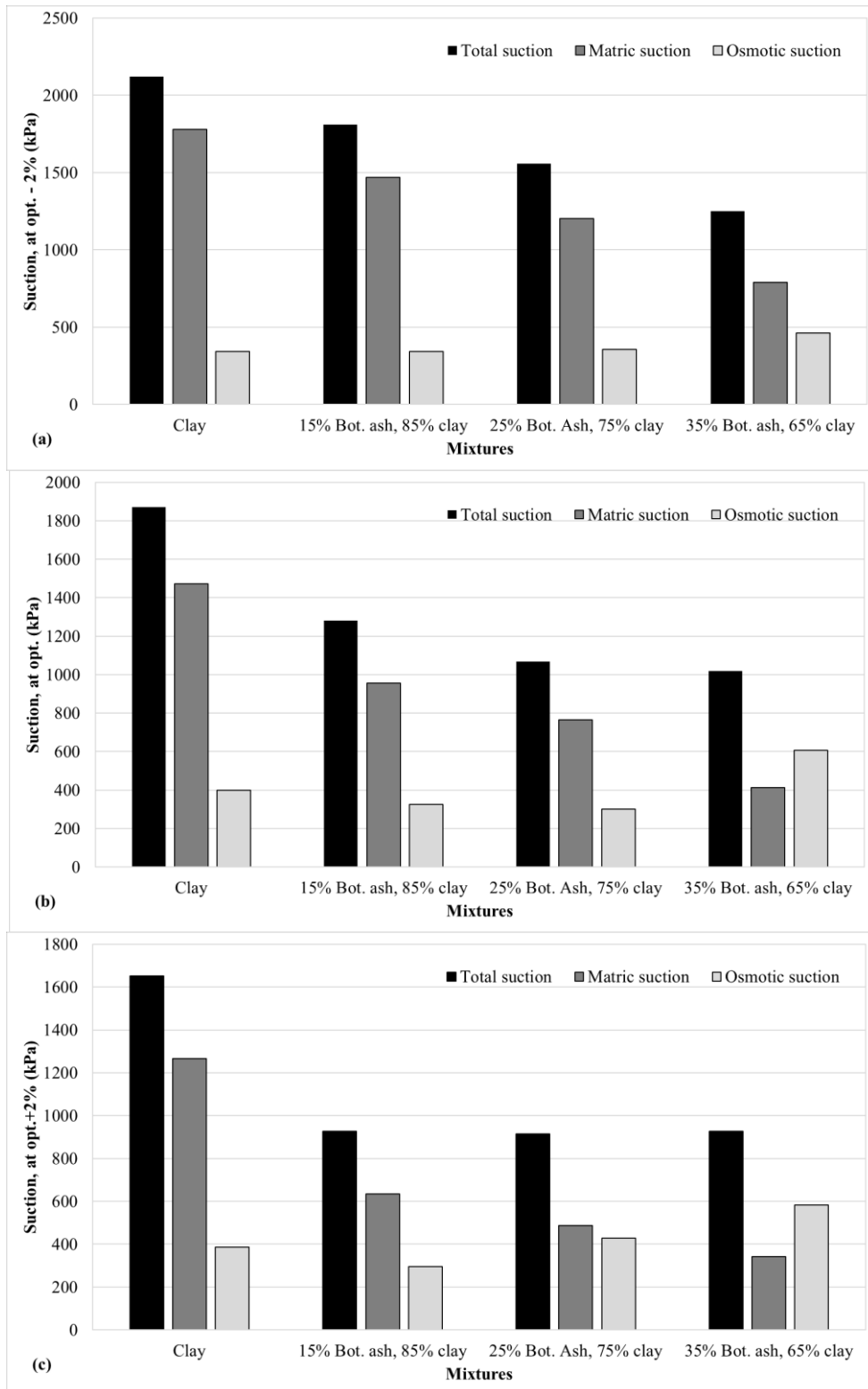


Figure 6- 5- Mixtures Suction Values at Different Moisture Contents (a) Optimum-2 percent, (b) Optimum, (c) Optimum+2 percent

To incorporate total suction into the M_r prediction equations, Equation (1) was modified in the form of Equation (3):

$$M_r = k_1 P_a \left(\frac{\theta}{P_a} \right)^{k_2} \left(\frac{\psi}{P_a} \right)^{k_3} \left(1 + \frac{\tau_{oct}}{P_a} \right)^{k_4} \quad (3)$$

where,

k_i = the regression coefficients,

ψ = the total suction (kPa), and the other parameters are as defined before.

Table 6-8 depicts the calibrated model for the mixtures and its respective statistics. It should be mentioned that all three moisture contents were used in order to calibrate the models. All S_e/S_y ratios found to be lower than 0.50 indicates strong goodness of fits for the model. Additionally, the positive exponent of the total suction term in the equations refers to the direct relationship between M_r and the total suction of soil.

Table 6-8- Equation (3) regression coefficients and statistics for different mixtures

Regression coefficients	Clay	15% Bot. ash	25% Bot. ash	35% Bot. ash
k_1	0.0161	0.0699	0.3848	0.0377
k_2	0.1708	0.1680	0.2160	0.1808
k_3	1.7443	1.1458	0.7777	1.6292
k_4	-5.8727	-2.9463	-4.7817	-5.2476
R^2	0.9696	0.9791	0.9692	0.9746
S_e/S_y	0.4118	0.4071	0.4233	0.3900

Equation (2) was also modified, in the form of Equation (4), incorporating the total suction term as below:

$$M_r = k_1 P_a \left(\frac{\sigma_3}{P_a} \right)^{k_2} \left(\frac{\sigma_d}{P_a} \right)^{k_3} \left(\frac{\psi}{P_a} \right)^{k_4} \quad (4)$$

The regression coefficients of the calibrated model and its statistics are reflected in Table 6-9.

Table 6-9- Equation (4) regression coefficients and statistics for different mixtures

Regression coefficients	Clay	15% Bot. ash	25% Bot. ash	35% Bot. ash
k₁	0.0036	0.0347	0.1253	0.0102
k₂	0.1279	0.1203	0.1551	0.1319
k₃	-0.6851	-0.3463	-0.5497	-0.6077
k₄	1.7421	1.1542	0.7689	1.6235
R²	0.9879	0.9843	0.9798	0.9867
S_e/S_y	0.2603	0.3529	0.3431	0.2822

Comparing Equations (3) and (4) reveals that the latter showed better performance at predicting M_r . Even though the R^2 values are not significantly different between the two models, the S_e/S_y ratio showed a decrease between 5 and 15 percent in Equation (4). Overall, the modified NCHRP model, incorporating the total suction term, outperformed the other models with the smallest average S_e/S_y of 0.30 and an average R^2 of 0.990 within different soil mixtures.

To validate the models, four extra samples from each mixture were made at their respective optimum moisture contents and their M_r values were measured. Figure 6-6 presents the performance of Equation (3) and Equation (4). As expected, Equation (4) outperformed Equation (3) in predicting M_r values with higher R^2 values. It is also worth mentioning that, the over and under predicted values by the models that were evenly distributed within the range of data still indicated a satisfactory performance of the models. This validation showed compelling outcomes to use the developed models to predict M_r of low plasticity clay soil treated with bottom ash.

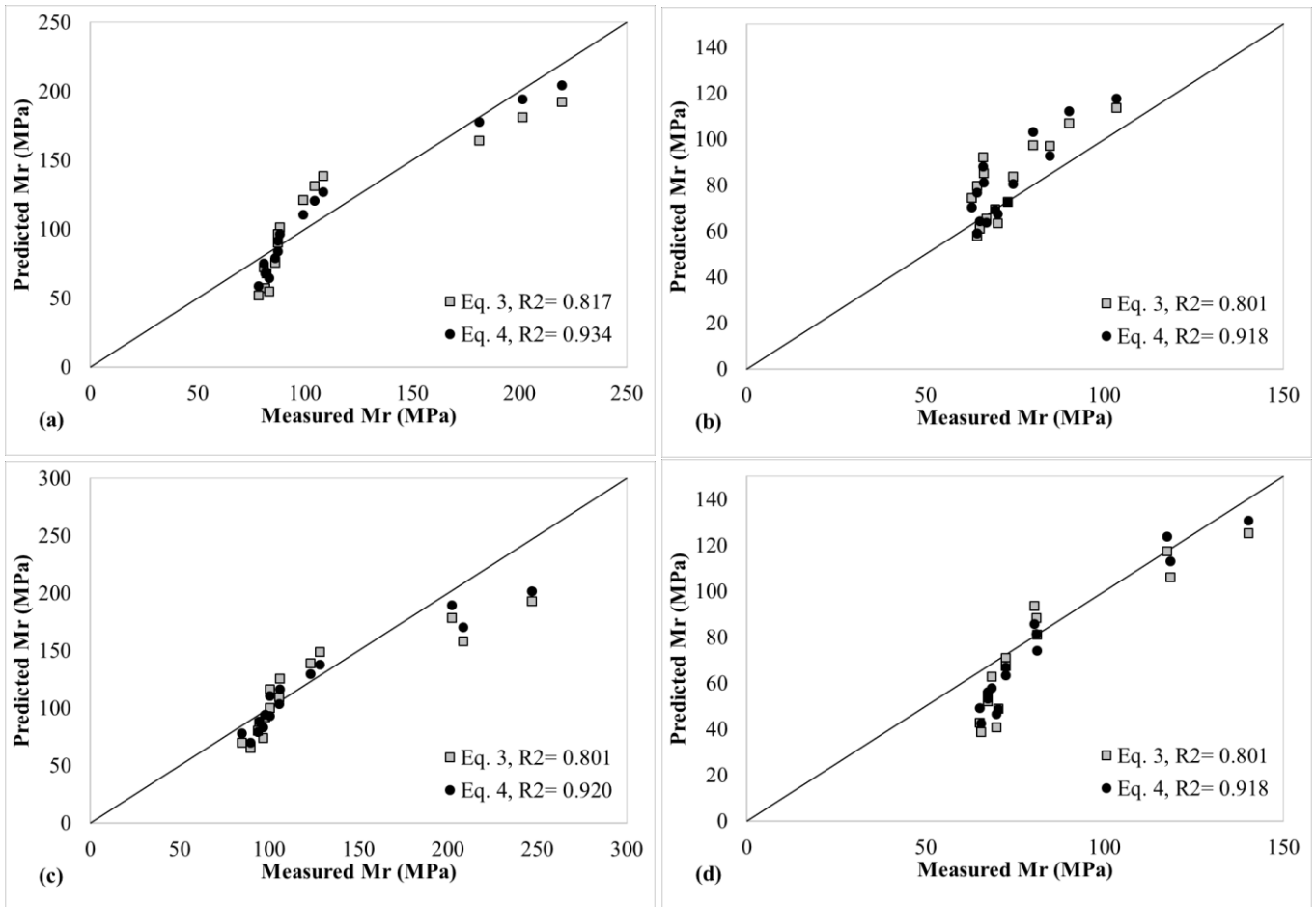


Figure 6-6- Validation of equations 3 and 4 for samples made at optimum moisture contents
 (a) Untreated clay, clay with (b) 15, (c) 25, (d) 35 percent bottom ash

Conclusion

This study was undertaken to evaluate the effect of bottom ash on the M_r of a medium plasticity clay. The clay mixtures were made at 15, 25, and 35 percent bottom ash in M_r specimens. While adding bottom ash at 15 percent and 35 percent of total dry weight of the mixture led to drastic decreases in M_r at optimum-2 percent, optimum, and optimum+2 percent moisture contents, the 25 percent bottom ash significantly increased M_r with a range of 5 to 23 percent among the 15 test sequences. Additionally, two well-referred M_r prediction equations were calibrated for the mixtures. The NCHRP prediction equation showed better statistics compared to the log-log model adopted in MEPDG.

The total and matric suctions at different moisture contents in the mixtures were indirectly measured using the filter paper test. The total suction and matric suction of the mixtures showed a descending trend with the increase of bottom ash in the mixtures. Incorporating the total suctions in the two M_r equations led to a higher R^2 and a lower S_e/S_y ratio. Overall, the modified NCHRP model outperformed the other models with the smallest average S_e/S_y of 0.30 and an average R^2 of 0.990 within different soil mixtures. The two models were validated for one sample from each mixture at their respective optimum moisture content. While the results showed compelling performance of both models, Equation (4) outperformed Equation (3) by showing higher R^2 values.

The author would recommend performing the tests on different soil types within a wider range and more increments of moisture content to better refine the prediction models and enhance their corresponding goodness of fits.

Chapter 7- Fatigue Life Evaluation of Pavement Embankments made with Tire Derived Aggregates

A version of this chapter was published Asefzadeh, A., Hashemian, L. and Bayat, A., 2018. Fatigue Life Evaluation of Pavement Embankments made with Tire Derived Aggregates. Canadian Journal of Civil Engineering

Abstract

Rapid growth of populations and extension of societies leads to the production of waste by-products, which put a burden on landfills. To address this issue, tire derived aggregates (TDA) from scrap tires have been used as road embankments in several projects. Three different test sections using different TDA, and TDA and soil mixtures, were constructed at the Integrated Road Research Facility (IRRF) test road in Edmonton, Alberta, Canada. Based on falling weight deflectometer (FWD) tests in different months, the fatigue life performance of the TDA embankments was evaluated against that of a conventional control section using the measured horizontal strains at the bottom of the asphalt layer and the Asphalt Institute's fatigue model. The results showed satisfactory performance of all three TDA test sections and significantly longer fatigue life as opposed to the fatigue life of the control section. This analysis showed compelling evidence regarding the long-term performance of TDA material as road embankments in construction projects.

Key words: fatigue life, tire derived aggregate, pavement embankment, falling weight deflectometer, strain, dynamic modulus

Introduction

Rapid growth in populations and expansion of societies necessitates the development of industries and construction projects, such as roads and highway networks, to fulfill the ever-increasing demand. With dwindling natural resources, and the creation of large quantities of waste by-products stemming from industrial or construction and demolition activities, sustainable and economical utilization of recycled and waste materials has been of interest to many research studies (Abbas et al. 2009, Huang et al. 2007, Arulrajah et al. 2012, Arulrajah et al. 2014, Meles 2014, Xue et al. 2009). Pavement construction projects are potentially good examples in which large amounts of by-products can be used in lieu of natural materials, such as fresh aggregates. Additionally, agencies involved in this area are also looking forward to alternative materials for which they have to pay less as compared to increasing prices of non-renewable construction materials (Jamshidi et al. 2017).

Disposal of used tires is a problem in many countries, and in Alberta, Canada, more than five million tires reach the end of their life cycle each year, and an increase in this number is expected as the population increases (Meles 2014). Simply discarding tires is not a solution because of depleting limited landfill sites. Additionally, the stockpiles of tires can be fire hazards and create an environmental problem by providing habitat for insidious insects and animals (Eldin and Senouci 1992, Siddique and Naik 2004). Therefore, feasible application of tire derived aggregates (TDA) in construction projects has been examined in literature as an alternative to the stockpiling or landfilling of worn tires. TDA are among the recycled waste materials that have been used as lightweight fill for embankments and retaining walls (Tweedie et al. 1998, Humphrey 2007). The application of TDA as fill material in road construction was first studied in 1992, and then followed by other research (Meles 2014, Eldin and Senouci 1992, Humphrey and Blumenthal 2010, Dickson et al. 2001, Mills and McGinn 2010). Studies

show there were numerous highway construction projects in which TDA were used as the embankment fill. In 2001, a 200 m prototype road section was constructed with approximately 2,500 metric tons of tire shreds to fill the embankment section. The results from a monitoring system showed that the settlement of the embankment was as expected, and no internal heating of the tire shreds was observed (Dickson et al. 2001). Mills and McGinn (2010) used TDA in order to reconstruct an already failed embankment of a four-lane highway in St. Stephen, New Brunswick, Canada. The use of TDA in this project led to the successful construction of the highway, which was completed in 2008. The performance of embankments made from shredded tires, and shredded tires and soil, were compared to conventionally constructed embankments with typical pavement structures in another research study. The results showed that the settlement of the tire-made embankments was controlled using the techniques utilized during the construction (Tandon et al. 2007).

There are different types of pavement distresses imposed upon the pavement structures by repeated traffic loading, one of which is fatigue failure. As previously established, engineering properties of TDA, including compressibility and vertical settlement in the case of road embankments, have already been studied. However, to the best of the author's collective knowledge, the potential effect of TDA road embankments on the long-term performance of the hot mix asphalt (HMA) layer, in terms of fatigue life, has not been targeted in previous research studies. To bridge this gap in knowledge, this chapter aims to evaluate the fatigue life performance of the HMA layer in the pavement structure of the Integrated Research Road Facility (IRRF) test road in Edmonton, Alberta, Canada, based on the data collected from one year of falling weight deflectometer (FWD) tests conducted at the IRRF's test road.

Traffic loading produces horizontal tensile strain (ϵ_t) at the bottom of the HMA layer and vertical compressive strain (ϵ_z) at the top of the subgrade layer, which are deemed to be the main triggers for fatigue failure of the HMA layer, and the rutting of pavement structure,

respectively (Shukla and Das 2008). There are several fatigue models presented in literature in order to define the relationship between HMA moduli and ϵ_t that show the maximum number of allowable load repetitions before resulting in fatigue cracking. Equation (1) was developed by the Asphalt Institute and is one of the most referenced fatigue life models (Huang 1993):

$$N_f = 0.0796 \cdot \epsilon_t^{-3.291} \cdot E^{-0.854} \quad (1)$$

where

N_f = maximum number of allowable load repetitions to produce 20% fatigue cracking

ϵ_t = tensile strain at the bottom of the HMA layer, and

E = dynamic modulus for the HMA layer (psi)

Equation (1) was adopted in this study as a benchmark to evaluate and compare the fatigue life performance of TDA road embankments with that of a conventionally constructed road section at the IRRF's test road.

IRRF Test Road

The construction of the IRRF test road started in May 2012 and finished in October 2013 as a new access road to the Edmonton Waste Management Center (EWMC). The two-lane road is built on a natural subgrade soil, with a length of about 500 m and comprised of 25 cm HMA, including a 9 cm wearing course on top of a 16 cm binder course overlaying a 45 cm well-graded granular aggregate base course. The test road was opened to traffic in November 2015, and has experienced daily traffic loads of roughly 1,000 trucks per lane. The physical properties of HMA mixes are depicted in Table 7-1. It should be mentioned that the Tensile Strength ratio test was conducted as per AASHTO T-283 at Lafarge company's lab. There are three test sections with TDA based embankments, each are 20 m long and made with passenger and light truck tires (PLTT), with a maximum rim diameter of 49.5 cm; off-the-road tires (OTRT),

derived from heavy industrial trucks, with a maximum rim diameter of 99 cm; and a mixture of soil and PLTT at a 50/50 ratio by volume. TDA were selected in accordance with Type B TDA specifications as stated in ASTM D 6270 standard (ASTM D6270-08 2012). Figure 7-1 shows the OTRT and PLTT materials. The subgrade soil profile at the site was comprised of 7 m clayey sand (SC) overlaying poorly graded sand (SP) according to the Unified Soil Classification System (USCS) (ASTM D2487-11 2011). The fourth 20 m test section, adjacent to the PLTT-soil section, called the control section, was a conventionally constructed road embankment overlaying the natural subgrade soil designed to be the touchstone for evaluating the performance of the other three sections. Figure 7-2 depicts the gradation of PLTT, OTRT, and subgrade soil materials. It should be mentioned that we had no control on the gradation of the TDA material as it was sourced from the recycling plants.

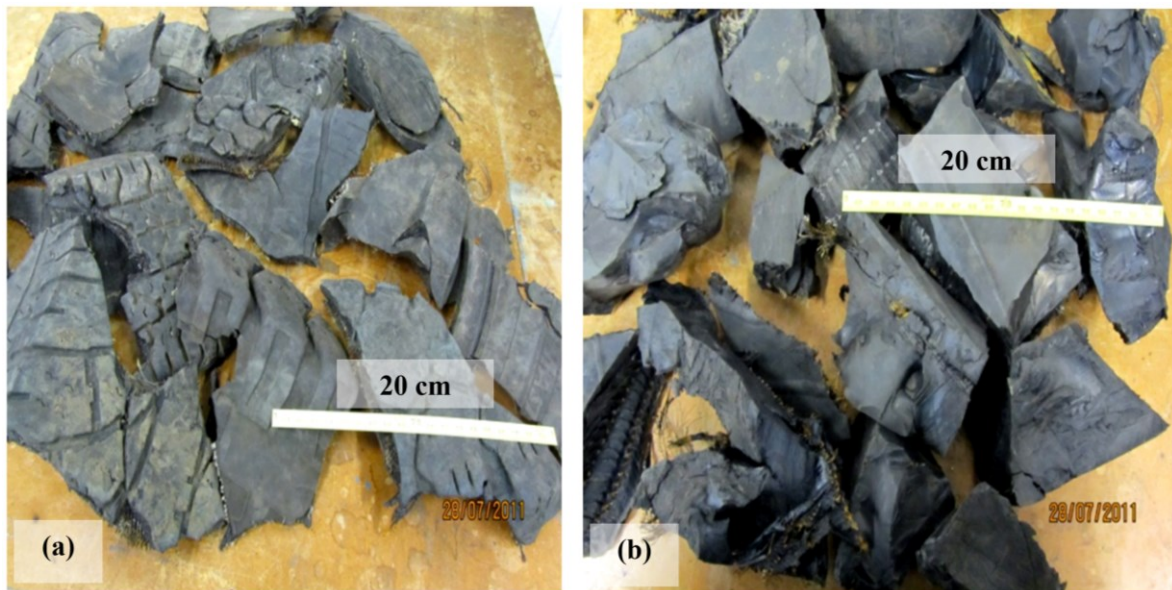


Figure 7-1- TDA materials (a) PLTT and (b) OTRT

Table 7-1- Physical properties of the HMA mixes used in the test road

Property	Asphalt physical properties	
	Binder course	Wearing course
Maximum aggregate size (mm)	25	12.5
Binder grade	PG 58-28	PG 58-28
Reclaimed asphalt pavement (RAP) (%)	20	10
Binder content by weight of mix (%)	4.58	5.3
Void in mineral aggregate (VMA) (%)	13.1	14.3
Void filled with asphalt (VFA) (%)	69.4	74.9
Air voids (%)	4	3.6
Density (kg/m ³)	2,355	2,344
Marshal stability (kN)	17.7	16.9
Flow (mm)	2.25	2.5
Theoretical film thickness (μm)	6.7	7.1
Tensile strength ratio (TSR) (%)	98	81.6

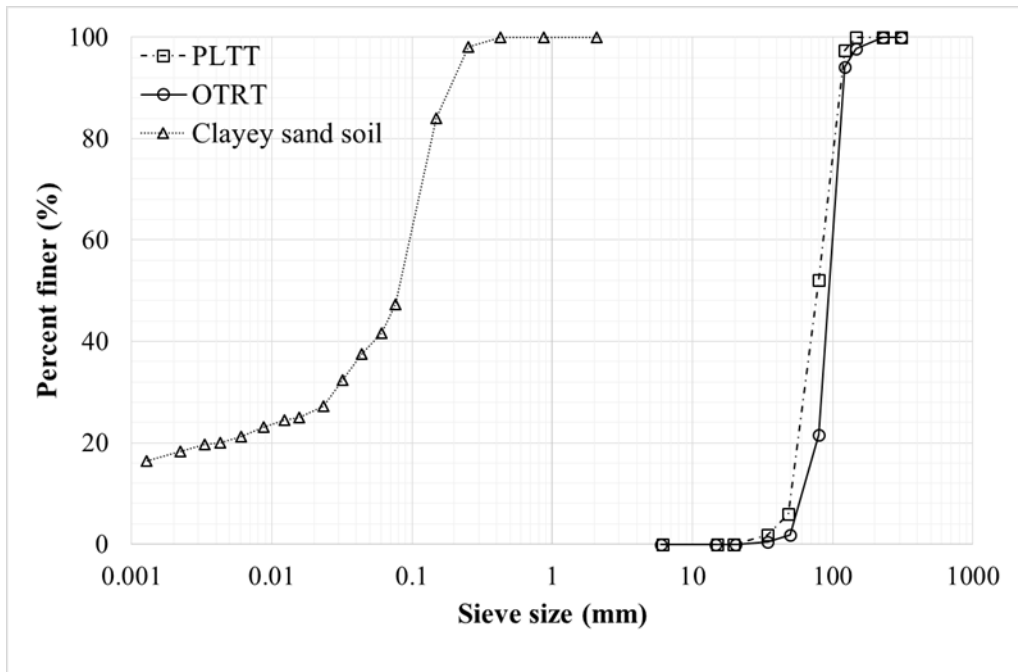


Figure 7-2- The gradation of PLTT, OTRT and subgrade soil materials

To construct the TDA sections, an 8 m deep and 60 m long pit was excavated, with a bottom width of 17 m and top width of 40 m. Upon finishing the excavation, the bottom and side slopes of the excavated pit were covered by geotextile (Geotex 351, Propex), over which the TDA and TDA-soil materials were placed and spread using conventional construction equipment. Each TDA section is comprised of 3 m compacted TDA or TDA-soil underlain by 0.5 m thick compacted soil overlaying another 3 m thick compacted TDA or TDA-soil mixture. The 0.5 m soil layer was used to prevent internal heating of the TDA materials. Geotextile was placed between the layers to stop migration of soil through the TDA voids. Another 1 m thick compacted soil cover was placed on top of the embankment. 45 cm granular aggregate base (GAB) and 25 cm of HMA, comprised of a 16 cm binder course and a 9 cm wearing course, were the next layers of the pavement structure. It should be mentioned that since the TDA were highly compressible during the construction phase, the top soil cap layer ended up being 1.42 m and 1.28 m, and the GAB layer was 53 cm and 52 cm for the PLTT and OTR sections. Further details regarding the construction of the embankments can be found in other research (Meles 2014). The section was also instrumented with thermistors and a settlement plate in order to monitor the heat generated and potential settlements within the TDA layers. Figure 7-3 schematically shows the cross section of the TDA embankments.

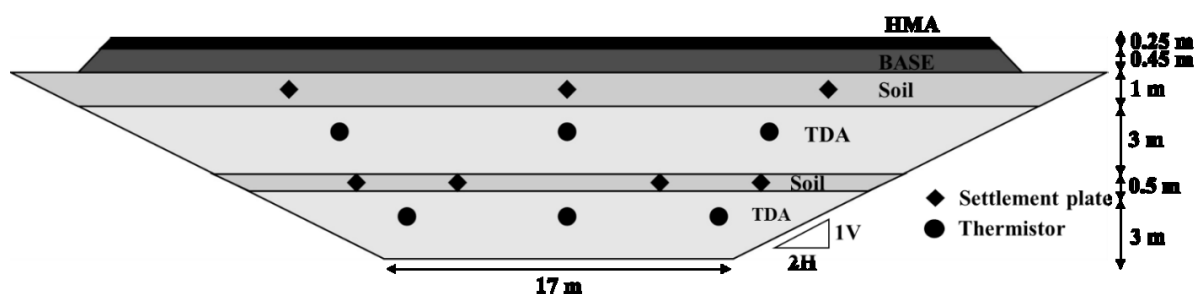


Figure 7-3- Cross section of TDA embankments at IRRF's test road

The HMA layer in the control section was equipped with four thermistors to measure the pavement temperature at depths of 2 cm, 9 cm, 17 cm, and 25 cm elevations. The temperatures through the HMA layer were measured every five minutes, and a CR-1000 datalogger from Campbell Scientific Canada collected the data. To measure the pavement critical responses to traffic-induced loading, three sets of asphalt strain gauges in longitudinal, transverse, and vertical directions were embedded at the bottom of the HMA layer. Figure 7-4 shows the plan of the installed sensors. A high-speed CR9000X datalogger from Campbell Scientific Canada was utilized to collect the data at the baud rate of 500 Hz. All of the obtained data was then transmitted to the University of Alberta through remote desktop access. Figure 7-5 schematically shows the cross section of the control section.

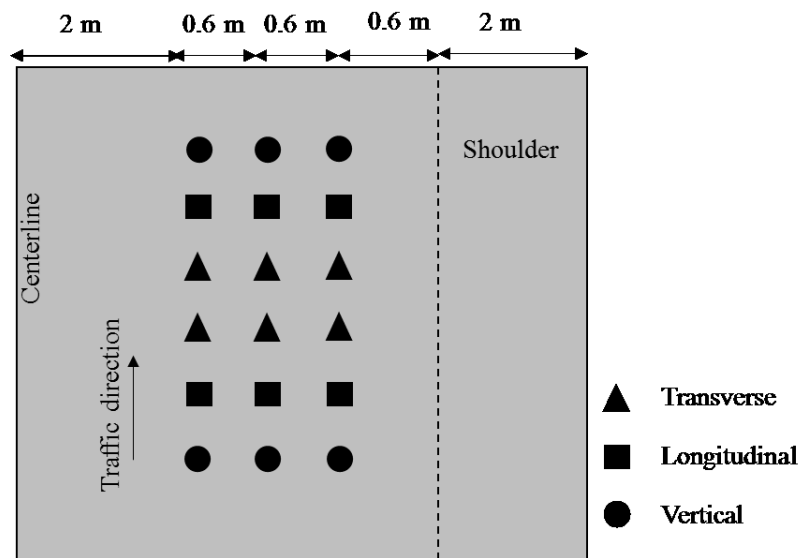


Figure 7-4- Plan view of the embedded sensors at the bottom of the HMA layer in the control section

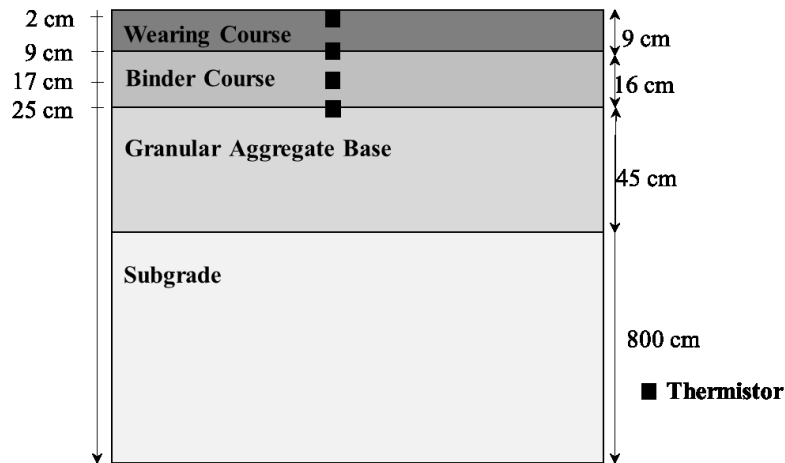


Figure 7-5- Schematic cross section of the IRRF's control section, and the location of asphalt thermistors

Falling Weight Deflectometer Testing

FWD testing is one of the field-testing devices that has obtained extensive acceptance among researchers for long-term evaluation of the structural performance of pavement layers. The FWD test measures the response of a pavement structure to the applied impulse load in terms of deflection measured by geophones at certain radial distances from the center of the loading plate. This test is claimed to simulate realistic pavement responses to actual traffic loading (Mohammad et al. 2003).

A Dynatest 8000 FWD device, with a loading plate diameter of 300 mm, was used. The FWD setup had nine geophones located at radial distances of 0, 200, 300, 450, 600, 900, 1200, 1500, and 1800 mm from the center of the load plate. FWD tests were performed on top of the HMA layer at each point at a tentative force load level of 53 kN, in March–October 2015, to consider different pavement temperatures and seasonality effects on the pavement responses. No tests were conducted in the months of January, February, November, and December because very cold temperatures of the HMA result in its high strength, which in turn leads to inaccurate readings from the geophones and high errors. The average asphalt temperature at the time of the tests was measured using four asphalt thermistors. Additionally, FWD tests were conducted

on top of all three sets of asphalt strain gauges in order to measure accurately the pavement responses underneath the load. All deflections measured by geophones were normalized with respect to the nominal load level to negate the minor load discrepancies during each single test. Table 7-2 shows the average deflections of geophones for all tests, along with the average temperature of the HMA layer at the time of testing. It can be observed that the PLTT section generally showed the smallest deflection bowl with respect to the other three sections. The OTRT section showed the second smallest deformation values measured by the geophones. It is interesting to note that as the TDA were mixed with soil in the PLTT-soil section, the behavior of the deflection bowl became similar to that of the control section. Additionally, the deflections measured by the geophone spaced at 1,800 mm from the center of the loading plate were generally higher in TDA sections compared to the control section. This observation was more pronounced during warmer months whereby the temperature of TDA layers were around 20°C compared to the coldest TDA temperature recorded, which was 5°C.

Table 7-2- Geophones' average normalized deflections and average HMA temperatures at the time of testing

Date	Section	Radial distance of geophones from the center of load plate (mm)										BDI	Average HMA Temperature (°C)
		0	200	300	450	600	900	1200	1500	1800			
March-12-15	PLTT	50.4	43.2	40.1	36.0	31.9	26.7	24.7	22.6	21.6	8.2	3.0	
	OTRT	53.0	42.8	37.7	34.6	29.6	24.5	21.4	20.4	19.4	8.2		
	PLTT+Soil	91.7	83.4	75.2	67.0	57.7	41.2	30.9	25.8	21.6	17.5		
	Control Section	97.9	87.8	79.7	69.7	59.6	44.4	33.3	26.2	22.2	20.2		
April-8-15	PLTT	106.2	95.8	90.6	84.3	80.2	69.8	61.4	57.3	53.1	10.4	12.9	
	OTRT	114.9	103.6	98.4	91.1	83.9	72.5	63.2	57.0	52.8	14.5		
	PLTT+Soil	175.4	160.8	152.4	139.9	125.3	101.3	80.4	63.7	49.1	27.1		
	Control Section	203.7	184.7	171.0	152.0	135.1	106.6	82.3	64.4	50.7	35.9		
May-5-15	PLTT	141.8	123.8	115.8	106.9	97.9	84.9	74.9	67.9	62.9	18.0	16.5	
	OTRT	151.8	133.8	124.8	114.8	105.9	90.9	78.9	70.9	64.9	19.0		
	PLTT+Soil	218.2	192.0	179.0	158.8	139.7	107.6	82.4	63.3	51.3	39.2		
	Control Section	246.3	216.9	195.6	168.2	144.9	108.4	81.1	61.8	47.6	50.7		
June-5-15	PLTT	206.7	175.8	160.8	142.8	125.8	104.9	87.9	79.9	73.9	35.0	28.8	
	OTRT	234.5	188.9	170.3	148.0	129.3	104.2	86.5	78.2	70.7	40.9		
	PLTT+Soil	309.4	259.4	234.0	195.3	161.3	113.2	79.2	61.3	50.0	72.6		
	Control Section	298.1	247.5	225.0	191.3	159.4	114.4	81.6	62.8	49.7	65.6		
July-9-15	PLTT	409.4	257.1	213.5	176.6	145.5	114.5	96.1	88.3	80.5	67.9	36.7	
	OTRT	477.9	302.3	240.9	194.1	159.0	122.9	102.4	94.6	83.9	81.9		
	PLTT+Soil	553.7	380.9	315.1	241.5	184.6	125.7	90.3	72.6	59.9	130.6		
	Control Section	644.7	419.2	361.6	243.4	176.8	122.2	86.4	68.5	57.6	184.8		
August-18-15	PLTT	198.6	165.4	149.2	133.2	118.7	97.1	83.8	73.2	67.1	30.5	25.9	
	OTRT	218.5	187.4	170.3	147.3	124.3	91.7	67.7	51.3	42.0	45.9		
	PLTT+Soil	254.2	215.2	192.1	163.7	131.4	98.4	71.0	52.0	41.4	60.7		
	Control Section	282.8	233.7	207.2	175.0	142.1	106.1	78.8	60.3	49.0	65.1		
September-18-15	PLTT	131.0	113.5	105.2	97.0	88.7	76.3	68.1	61.9	55.7	16.5	17.4	
	OTRT	139.3	122.3	114.4	103.4	95.5	80.6	70.6	63.7	58.7	18.9		
	PLTT+Soil	190.3	169.1	156.0	138.9	121.8	93.6	71.5	54.4	44.3	34.2		
	Control Section	219.3	186.0	170.8	145.6	125.3	93.0	68.7	52.6	41.4	45.5		
October-14-15	PLTT	118.8	106.4	101.2	93.0	85.7	74.4	67.1	58.9	54.8	15.5	10.8	
	OTRT	127.7	115.5	109.5	100.3	92.2	80.1	69.9	64.9	59.8	17.2		
	PLTT+Soil	174.3	157.9	150.8	133.5	119.2	92.7	73.4	58.1	47.9	31.6		
	Control Section	198.6	183.1	163.6	140.9	123.5	92.6	71.0	57.6	45.3	40.1		

Analysis of Data

To calculate the fatigue performance of the HMA layer in the three TDA sections, there was a need to estimate the tensile strains at the bottom of the HMA layer. Equation (2), developed by Park and Kim (2003), was first evaluated using the strain data collected from conducting FWD tests on top of the sensors in the control section. They performed simulation of dynamic FWD loading on the pavement by using ABAQUS. Then they used DataPave in order to survey all the database in LTTP (Long term pavement Performance), and by performing regression analysis, they came up with that equation.

$$\log(\epsilon_i) = 1.078\log(\text{BDI}) + 0.180\log(H_{\text{HMA}}) + 2.772 \quad (2)$$

where

ϵ_t = tensile strain at the bottom of HMA layer (microstrain)

BDI = base damage index defined as the difference in deflection at 300 and 600 mm of the radial distance from the center of the load plate (mm), and

H_{HMA} = thickness of the HMA layer (mm)

This model was able to predict the measured tensile strains at the bottom of the HMA with a significantly high R^2 value of 0.954. It should be mentioned that the average values of longitudinal and transverse strains were taken and used in calculations because of the symmetry. Table 7-3 depicts the measured strains and the average values. Next, the model was calibrated for the test road and the R^2 increased from 0.954 to 0.964. Therefore, the calibrated model in the form of $\log(\epsilon_t) = 0.8806\log(BDI) + 0.9345\log(H_{HMA}) + 0.7475$ was used for all prediction purposes. Figure 7-6 shows the measured predicted values of tensile strains under the 53 kN impact load at the bottom of the HMA layer in the control section in different months for the original and calibrated forms of Equation (2).

Table 7-3- Measured longitudinal and transverse strains (microstrain)

Longitudinal	Transverse	Average
24.60	34.90	29.75
43.50	66.10	54.80
58.20	62.00	60.10
96.90	111.80	104.35
217.10	219.10	218.10
104.60	90.80	97.70
65.00	69.00	67.00
34.20	38.80	36.50

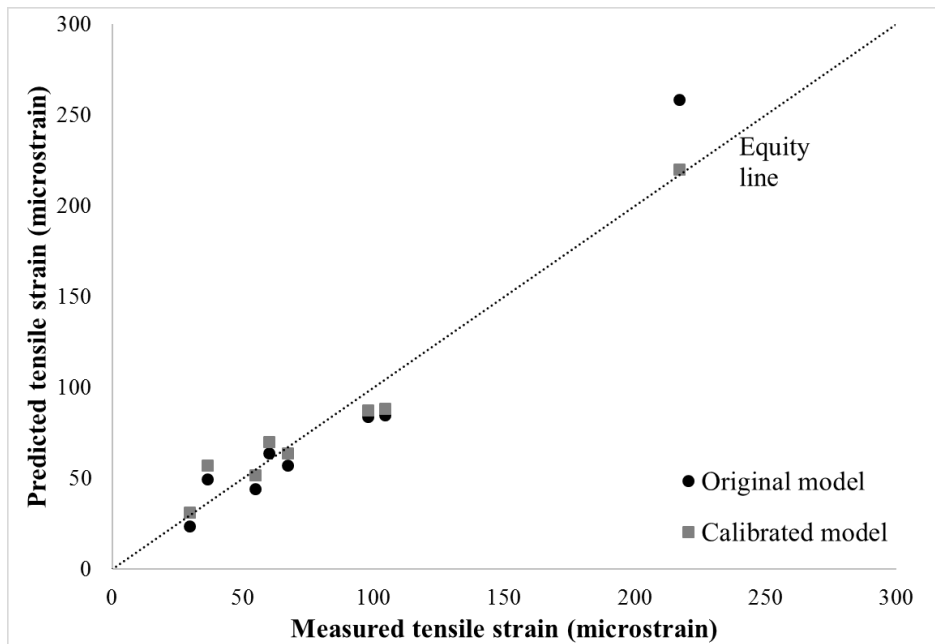


Figure 7-6- Measured and predicted values of tensile strains from FWD tests on the control section

Since all the tire sections were covered by 1 m of subgrade soil, with a reasonable assumption that the temperature profile in the HMA layer in the TDA sections would be likely to be similar to that of in the control section, the same calibrated model was utilized, and the tensile strain at the bottom of the HMA layer in each section was estimated. Figure 7-7 shows the predicted values at the bottom of the HMA layer in the four test sections. With the exception of June, the control section recorded the highest HMA tensile strain among all test sections. On the other hand, except for July and August, the PLTT and OTRT sections showed close tensile strains. This stems from the fact that the embankments of the two sections was made of TDA, and thus it is reflected in the similar responses of the pavement to FWD loading in the PLTT and OTRT sections. All sections showed drastic increase in tensile strains in July where the average HMA temperature was as high as 36.7°C.

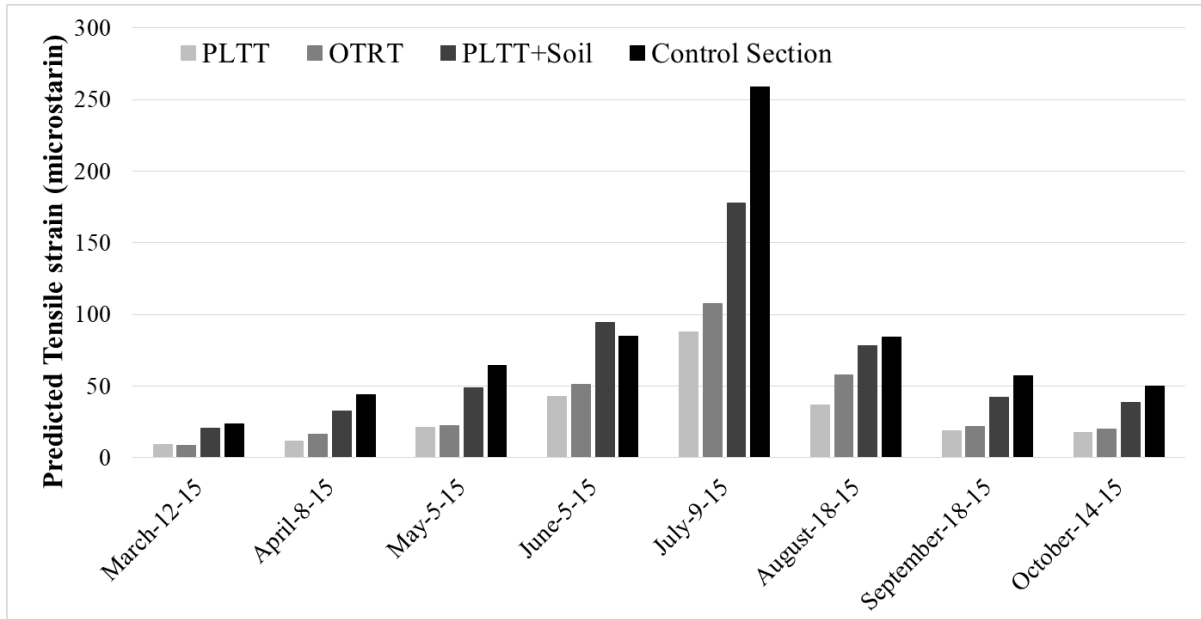


Figure 7-7- Predicted Tensile strain at the bottom of HMA layer in four test sections in different months

In order to calculate the fatigue life of the test sections, the dynamic modulus tests were conducted on both HMA layers based on AASHTO TP79 (AASHTO TP79-09, 2009). Cylindrical samples were prepared using a Superpave gyratory compactor with a 150 mm diameter and 170 mm height from the test road HMA. Based on AASHTO PP61 (AASHTO PP61-09, 2009), dynamic modulus specimens were prepared by coring the samples to a 100 mm diameter and cutting them to a height of 150 mm. The tests were conducted using a UTM-100 machine at temperatures of -10, 4, 20, and 35°C, and frequencies of 10, 5, 2, 1, 0.5, 0.2, 0.1, and 0.01 Hz. Figure 7-8 shows the master curves along with the shift factors of both binder and wearing courses of the HMA layer which were developed in another study (Shafiee et al. 2015). The loading frequency of FWD was reported to be around 33 Hz and almost constant through the depth of the pavement (Shaiffee et al. 2015, Seo et al. 2013). Therefore, using the developed master curves and shift factors, the elastic moduli of the HMA layer was calculated for the loading frequency of 33 Hz. To this end, the average of the two temperatures measured within the depth of each sublayer was used for calculating the modulus values in different months, and by taking the weighted mean of the two HMA sublayers' modulus with respect to

their corresponding depths, the combined modulus of the HMA layer was calculated for each test. Table 7-4 depicts the HMA combined dynamic modulus values, which were derived based on the weighted average method by considering the 9cm and 16 cm thickness values of the wearing and binder courses, respectively, and the 25 cm thickness of the combined layer.

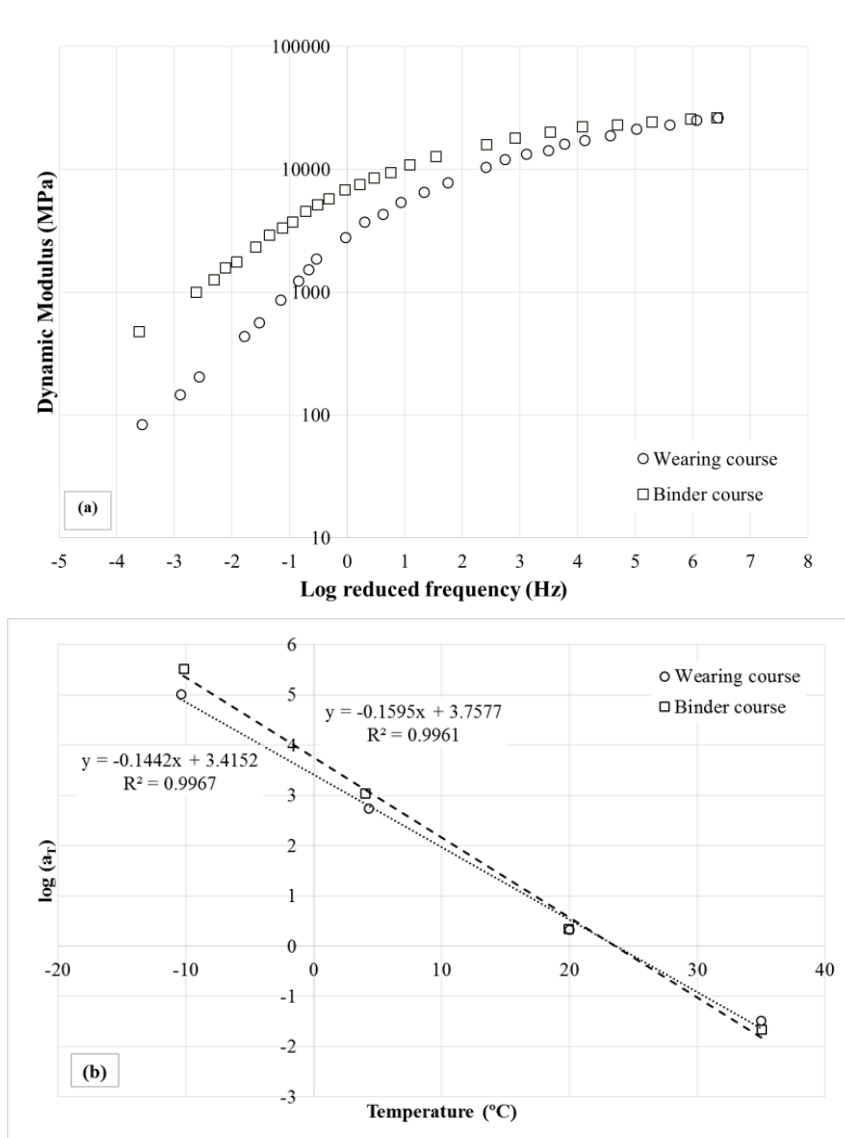


Figure 7-8- Master curve and shift factor for wearing course and binder course (Shafiee et al. 2015)

Table 7-4- Dynamic modulus values derived from the master curve

Date	Wearing course temp. (°C)	Binder course temp. (°C)	Wearing course modulus (MPa)	Binder course modulus (MPa)	Combined modulus (MPa)
12-Mar-15	7.5	2.5	16580	23940	21290
08-Apr-15	15.1	8.7	11770	21930	18270
05-May-15	18.1	15.8	9610	16490	14010
05-Jun-15	32.1	25.1	3580	11090	8390
09-Jul-15	43.8	35.1	650	5750	3910
18-Aug-15	30.8	25.0	3810	11260	8580
18-Sep-15	19.5	15.5	9490	17540	14640
14-Oct-15	9.7	11.9	13520	19520	17360

Equation (1) was utilized to calculate the fatigue life of the four test sections by using the dynamic modulus values and the predicted tensile strains as inputs. Table 7-5 shows the calculated fatigue life values for eight FWD tests. In order to compare the fatigue life performance of TDA embankments with respect to that of the control section, the normalized fatigue life of the test sections was tabulated in Figure 7-9. To this aim, the ratio of each section's fatigue life compared to that of the control section was calculated. Figure 7-10 shows the volumic water content (VWC) on top of the subgrade measured by a time domain reflectometer (TDR) embedded at that depth, and the freeze and thaw depths within the pavement structure in the control section for the 2015–2016 season (Asefzadeh et al. 2015). The gap in the freezing depth curve is because the datalogger temporarily failed to record the data due to a malfunction. Starting mid-March, as the pavement starts to thaw, the moisture content on top of the subgrade drastically increases and it takes until August to drain the excess moisture content at top of the subgrade layer, and the pavement returns to its recovered condition. Therefore, under the premise of similarity of the pavement structures in TDA sections and the control section, the period of August to October, during which the recovered condition prevails and the HMA experiences moderate temperatures, is the most reasonable

period for comparison of fatigue life within the different test sections. It can be observed that all TDA sections excel the control section in terms of fatigue life performance during this period. The average fatigue life of PLTT, OTRT and PLTT-Soil sections was approximately 2, 15 and 27 times more than that of the control section, respectively. The PLTT section generally showed the highest fatigue life in different months. The PLTT-Soil section showed less different fatigue life with respect to that of the control section among the three TDA sections. This can be attributed to the fact that mixing PLTT with soil at 50/50 ratio by volume leads to having the embankment behave more similarly to the conventional embankment. All sections showed a drastic decrease in fatigue life in June, which can be directly attributed to the high temperature of the HMA and low dynamic modulus value of only 3901 MPa, which is more than 70% less than the average modulus value of all months. Based on the findings of this study, the fatigue life performance of the TDA-made embankments were found to be satisfactory. Yet, it is worth mentioning that, the performance of the test sections were only monitored over a period from March to October (see Table 7-2) and the long term performance over a period of 10 years or longer is still unknown.

Table 5- Calculated fatigue life (N_f) of four test sections (allowable load repetitions to produce 20% fatigue cracking)

Test Section	March-12-15	April-8-15	May-5-15	June-5-15	July-9-15	August-18-15	September-18-15	October-14-15
PLTT	9.1E+09	4.5E+09	8.1E+08	1.2E+08	2.2E+07	1.9E+08	1.1E+09	1.0E+09
OTRT	9.4E+09	1.4E+09	6.7E+08	6.8E+07	1.1E+07	4.4E+07	6.5E+08	7.0E+08
PLTT+Soil	6.2E+08	1.5E+08	5.1E+07	8.9E+06	2.1E+06	1.6E+07	7.9E+07	8.1E+07
Control Section	3.8E+08	5.6E+07	2.1E+07	1.3E+07	6.2E+05	1.3E+07	2.9E+07	3.5E+07

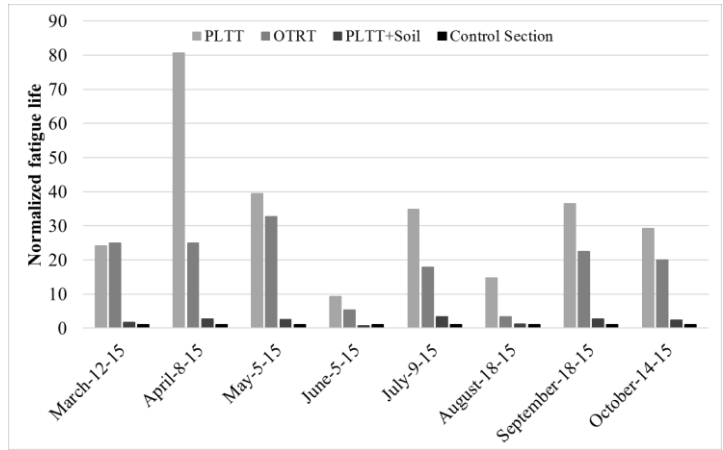
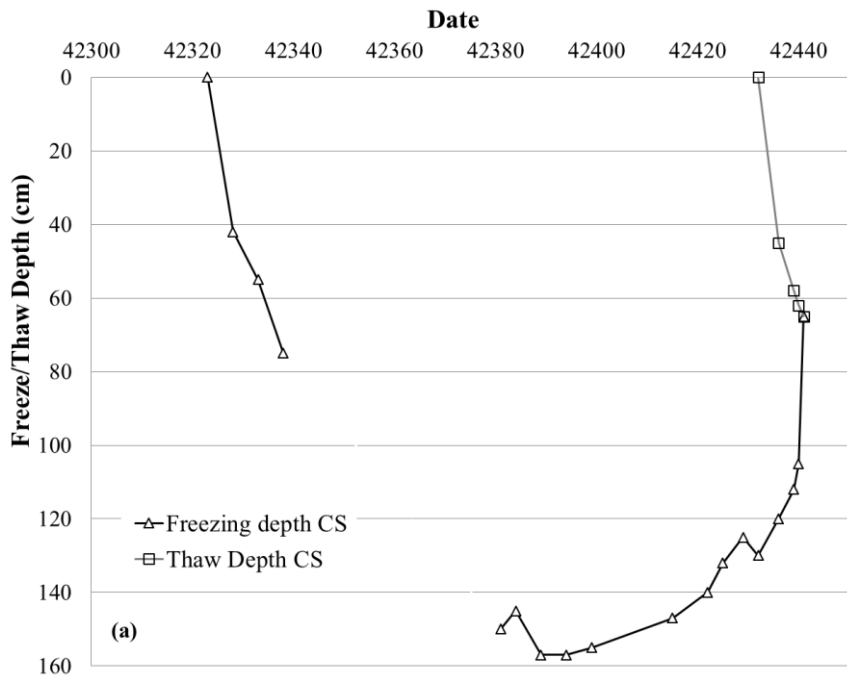


Figure 7-9- Normalized fatigue life of test sections with respect to the control section



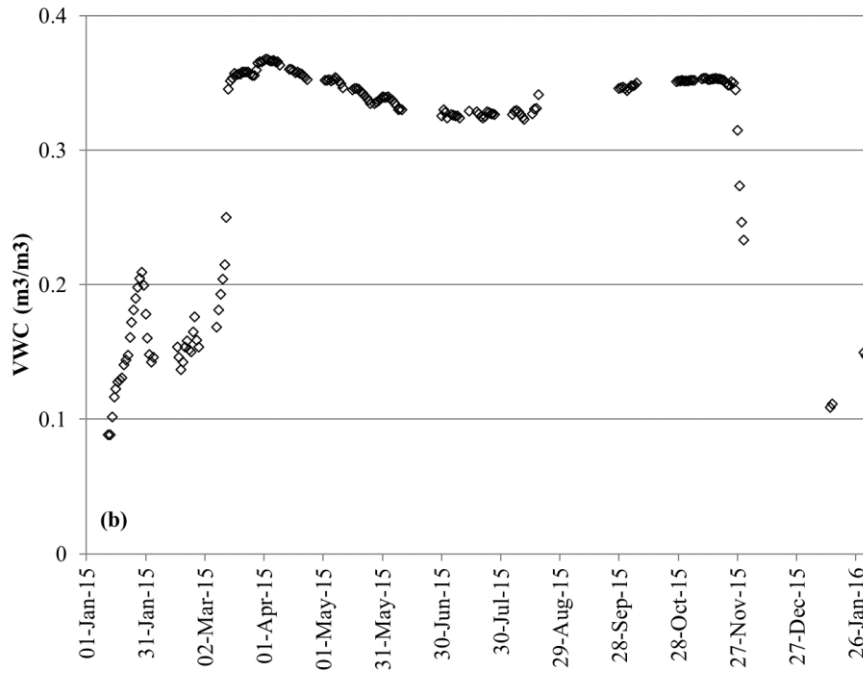


Figure 7-10- (a) Freeze and thaw depths and, (b) volumetric water content on top of the subgrade layer within the control section

Conclusions

This chapter investigated the fatigue life performance of the HMA layer in three different TDA road embankments and compared the results to that of a conventionally built control section comprised of typical pavement layers. To this end, the deflection bowls of eight FWD tests conducted on the IRRF's test road were used. Calculating the BDI parameter for each test, the tensile strain at the bottom of the HMA layer was successfully predicted. The dynamic modulus of the HMA layer was calculated from the developed master curves for the binder and wearing courses based on the FWD loading frequency of 33 Hz and the actual measured pavement temperatures.

- Normalizing the fatigue lives of TDA sections with respect to that of the control section showed their satisfactory fatigue life performance. The average fatigue life of PLTT, OTRT and PLTT-Soil sections was approximately 2, 15 and 27 times more than that of the control section, respectively.

- The PLTT section recorded the highest fatigue life among all four sections. This observation attributes to the fact that the BDI parameter for the PLTT section was the least among all four sections which consequently led to the best fatigue life performance.
- From the deflection bowls of the FWD tests, the performance of the PLTT-soil section was found to be similar to that of the control section. This observation can be pertinent to the fact the PLTT and soil were mixed by 50/50 ratio by volume, therefore the fatigue life performance of this TDA section was more similar to that of the control section.

The results of this study showed the applicability of using waste scrap tire materials as embankment in construction of roads without undergoing the risk of fatigue failure within the HMA layer.

Chapter 8- Conclusions and Recommendations

Conclusions

Based on the established objectives in this research study, the following conclusions were obtained:

- Collected two-year environmental data from the IRRF test road in order to evaluate the performance of SLR prediction models with respect to Edmonton climatic conditions.

Based on this study it was found that:

- The effect of average monthly temperature on the duration of the thawing process was profound.
 - All three methods discussed in the study were very similar in determining the SLR-on date in accordance with the actual thaw condition of the test road.
 - The method proposed by Mahoney et al. (1986) was not able to accurately predict the removal date of SLR since the extra moisture accumulated within the pavement layer did not yet completely drain out of the system.
 - The Manitoba's method (Bradley et al. 2012) accurately estimated the removal date of SLR when most of the excess moisture in the pavement sublayers was out of the system.
 - The regression analysis conducted on the two-year monitored data of CFI and frost depth yielded a linear relationship with high statistics comparable to those of the Manitoba prediction model.
 - Based on the critical contact stress depth of the pavement found via computer simulation, it turned out that the WWP application date found in this study met the recommendations used in Alberta to start WWP.
- Two year weather and HMA temperature data were collected at the IRRF test road. The data were used to develop statistical temperature prediction models. Step-wise

regression analysis was utilized to identify and select the most important variables, which potentially added significant explanatory power to each regression equation.

Based on this study:

- The high R^2 values along with the ANOVA test results indicated the usefulness of models in accurately predicting the measured field data.
- All models were validated by field data and showed satisfactory results.
- The effect of temperature on the stiffness of the HMA was investigated over the course of one year, based on the laboratory developed master curves and shift factors and the measured asphalt temperatures. The stiffness of the HMA layer in July decreased by 73% compared to that of the HMA layer in January.
- The permanent deformation of subgrade soils were studied and modeled in Chapter 5.

Based on this study it was concluded that:

- As the stress ratio (q/p) increased from 0.3 to 1.5, the specimen showed larger permanent deformations. The specimens did not show significant permanent deformation at $q/p = 0.3$ stress ratio. As the stress ratio increased toward $q/p = 1.5$, the amplitude and frequency of the high permanent deformation cases increased.
- Based on the observations obtained from tests results and the high coefficient of determinations in the regression analysis, it was concluded that the ultimate permanent deformation developed in the samples varied linearly with the mean stress (similarly, deviatoric stress).
- For all stress ratios of 0.3, 0.6 and 1.0, the shakedown behavior of the subgrade material was found to be within Range A or plastic shakedown. Only at a stress ratio of 1.5 did the shakedown behavior match Range B or plastic creep. It should be mentioned that the stress levels imposed upon the specimens at this

stress ratio were mostly above the routine traffic loads on top of the subgrade layer at the field condition.

- The effect of bottom ash on enhancing the mechanical properties of subgrade soil was studied in Chapter 6. Based on this study the following outcome were drawn:
 - While adding bottom ash at 15 percent and 35 percent of total dry weight of the mixture led to drastic decreases in M_r at optimum-2 percent, optimum, and optimum+2 percent moisture contents, the 25 percent bottom ash significantly increased M_r with a range of 5 to 23 percent among the 15 test sequences.
 - Two well-referred M_r prediction equations were calibrated for the mixtures.
 - The NCHRP prediction equation showed better statistics compared to the log-log model adopted in MEPDG.
 - The total and matric suctions at different moisture contents in the mixtures were indirectly measured using the filter paper test. The total suction and matric suction of the mixtures showed a descending trend with the increase of bottom ash in the mixtures.
 - Incorporating the total suctions in the two M_r equations led to a higher R^2 and a lower S_e/S_y ratio. Overall, the modified NCHRP model outperformed the other models with the smallest average S_e/S_y of 0.30 and an average R^2 of 0.990 within different soil mixtures.
 - The two models were validated for one sample from each mixture at their respective optimum moisture content, and both showed satisfactory performance.
- Chapter 7 discussed the applicability of TDA material as road embankments and its potential effect on fatigue life performance of the pavement structures. Based on this study it was found that:

- Normalizing the fatigue lives of TDA sections with respect to that of the control section showed their satisfactory fatigue life performance. The average fatigue life of PLTT, OTRT and PLTT-Soil sections was approximately 2, 15 and 27 times more than that of the control section, respectively.
- The PLTT section recorded the highest fatigue life among all four sections. This observation attributes to the fact that the BDI parameter for the PLTT section was the least among all four sections which consequently led to the best fatigue life performance.
- From the deflection bowls of the FWD tests, the performance of the PLTT-soil section was found to be similar to that of the control section. This observation can be pertinent to the fact the PLTT and soil were mixed by 50/50 ratio by volume, therefore the fatigue life performance of this TDA section was more similar to that of the control section.

Recommendations

Even though many research studies have tried to characterize the pavement materials and find solutions to design long lasting pavement structures by using better materials or taking preventive measures to protect pavements from undergoing damages and distresses, there is still need to expand knowledge in pavement engineering. Therefore, in the interest of future research studies, the following recommendations are provided:

- Conduct long-term monitoring of field data in order to develop locally calibrated SLR and WWP models for Edmonton.
- Instrument roads with different HMA thicknesses in order to evaluate the performance of temperature prediction models with respect to different pavement structures.

- Incorporate the effect of moisture content variations in permanent deformation behavior of subgrade soils at different stress ratios and stress states using high number of loading cycles.
- Evaluate the performance of stabilized subgrade soils with fly ash in permanent deformation
- Study the effect of freeze thaw cycles on the performance of subgrade soils including heave, swell, M_r and permanent deformation.
- Construct instrumented test roads incorporating stabilized subgrade soils and study the long-term performance of the road under real traffic and environmental loading.
- Construct test roads on TDA-made embankments with thinner HMA thickness to compare the performance of pavements with different HMA layers.

References

AASHTO. 1961. The AASHTO Road Test, Highway Research Board Special Report 61A. Washington, DC: Highway Research Board, National Academy of Sciences.

AASHTO, Determining the dynamic modulus and flow number for hot mix asphalt (HMA) using the asphalt mixture performance tester (AMPT), 2009, AASHTO TP79-09, American Association of State Highway and Transportation Official, Washington, DC, USA.

AASHTO, Developing dynamic modulus master curves for hot mix asphalt (HMA) using the asphalt mixture performance tester (AMPT), 2009, AASHTO PP61-09, American Association of State Highway and Transportation Official, Washington, DC, USA.

Abbas, A., Fathifazl, G., Fournier, B., Isgor, O.B., Zavadil, R., Razaqpur, A.G. and Foo, S., 2009. Quantification of the residual mortar content in recycled concrete aggregates by image analysis. *Materials characterization*, 60(7), pp.716-728.

Abu-Farsakh, M., Dhakal, S. and Chen, Q., 2014. Performance evaluation of cement treated/stabilized very weak subgrade soils. In *Geo-Congress 2014: Geo-characterization and Modeling for Sustainability* (pp. 1387-1395).

Ahmad, J., Mohamed, K., Rahman, A.S.A., Rosli, M.I.F. and Zulkifli, A.R., 2016. Clay Stabilization Using OPC and Bottom Ash as Additives. In *Regional Conference on Science, Technology and Social Sciences (RCSTSS 2014)* (pp. 27-33).

Alavi, M., Pouranian, M. and Hajj, E., 2014. Prediction of asphalt pavement temperature profile with finite control volume method. *Transportation Research Record: Journal of the Transportation Research Board*, (2456), pp.96-106.

Alberta Transportation 1997. Pavement Design Manual, Edition 1, Alberta Transportation, Edmonton, Alberta, Canada.

Alhassan, M., 2008. Potentials of rice husk ash for soil stabilization. *Assumption university journal of technology*, 11(4), pp.246-250.

Al-Qadi, I.L., Wang, H., Yoo, P.J. and Dessouky, S.H., 2008. Dynamic analysis and in situ validation of perpetual pavement response to vehicular loading. *Transportation research record*, 2087(1), pp.29-39.

ARA Inc. 2004. Guide for Mechanistic-Empirical Design of New and Rehabilitated Pavement Structures. ERES Consultants Division, Final report, NCHRP Project 1-37A. Transportation Research Board of the National Academies, Washington, D.C.

Arulrajah, A., Piratheepan, J., Disfani, M.M. and Bo, M.W., 2012. Geotechnical and geoenvironmental properties of recycled construction and demolition materials in pavement subbase applications. *Journal of Materials in Civil Engineering*, 25(8), pp.1077-1088.

Arulrajah, A., Disfani, M.M., Horpibulsuk, S., Suksiripattanapong, C. and Prongmanee, N., 2014. Physical properties and shear strength responses of recycled construction and demolition materials in unbound pavement base/subbase applications. *Construction and Building Materials*, 58, pp.245-257.

ASTM D2487-11. 2011. Standard Practice for Classification of Soils for Engineering Purposes (Unified Soil Classification System), ASTM International, West Conshohocken, PA.

ASTM D6270-08. 2012 Standard Practice for Use of Scrap Tires in Civil Engineering Applications, ASTM International, West Conshohocken, PA.

ASTM D1557-12e1 Standard Test Methods for Laboratory Compaction Characteristics of Soil Using Modified Effort (56,000 ft-lbf/ft³ (2,700 kN-m/m³)), 2012 ASTM International, West Conshohocken, PA, <https://doi.org/10.1520/D1557-12E01>

Baiz, S., Tighe, S., Haas, C., Mills, B. and Perchanok, M., 2008. Development of frost and thaw depth predictors for decision making about variable load restrictions. *Transportation Research Record: Journal of the Transportation Research Board*, (2053), pp.1-8.

Barber, E.S., 1957. Calculation of maximum pavement temperatures from weather reports. *Highway Research Board Bulletin*, (168).

Barksdale, R.D., 1972, September. Laboratory evaluation of rutting in base course materials. In *Presented at the Third International Conference on the Structural Design of Asphalt Pavements, Grosvenor House, Park Lane, London, England, Sept. 11-15, 1972*. (Vol. 1, No. Proceeding).

Bethanis, S. and Cheeseman, C.R., 2005, February. Manufacture of lightweight aggregate from incinerator bottom ash and pulverised fuel ash. In *Proceedings of the Heleco Conference*.

Bodin, D., Chupin, O. and Denneman, E., 2016. Effect of temperature and traffic speed on the asphalt moduli for fatigue cracking and pavement structural design considerations. In 8th RILEM International Conference on Mechanisms of Cracking and Debonding in Pavements (pp. 397-402). Springer, Dordrecht.

Bosscher, P., Bahia, H., Thomas, S. and Russell, J., 1998. Relationship between pavement temperature and weather data: Wisconsin field study to verify superpave algorithm. *Transportation research record: journal of the transportation research board*, (1609), pp.1-11.

Boulbibane, M. and Collins, I.F., 2015. Development of a pavement rutting model using shakedown theory. *International Journal on Pavement Engineering & Asphalt Technology*, 16(1), pp.55-65.

- Bradley, A.H., Ahammed, M.A., Hilderman, S. and Kass, S., 2012. Responding to climate change with rational approaches for managing seasonal weight programs in Manitoba. In *Cold Regions Engineering 2012: Sustainable Infrastructure Development in a Changing Cold Environment* (pp. 391-401).
- Brooks, R.M., 2009. Soil stabilization with fly ash and rice husk ash. *International Journal of Research and Reviews in Applied Sciences*, 1(3), pp.209-217.
- Bulut, R., Lytton, R.L. and Wray, W.K., 2001. Soil suction measurements by filter paper. In *Expansive clay soils and vegetative influence on shallow foundations* (pp. 243-261).
- Burczyk, J.M., Ksaibati, K., Anderson-Sprecher, R. and Farrar, M.J., 1994. Factors influencing determination of a subgrade resilient modulus value. *Transportation Research Record*, (1462).
- Canadian Strategic Highway Research Program (C-SHRP). 2000. Seasonal load restrictions in Canada and around the world. Canadian Strategic Highway Research Program. <http://www.cshrp.org/products/brief-21.pdf>. [accessed: 25 May 2015].
- Chapin, J., Pernia, J. and Kjartanson, B., 2009. An approach to applying spring thaw load restrictions for low volume roads based on thermal numerical modelling. In *Cold Regions Engineering 2009: Cold Regions Impacts on Research, Design, and Construction* (pp. 496-505).
- Chapin, J., Kjartanson, B.H. and Pernia, J., 2012. Comparison of two methods for applying spring load restrictions on low volume roads. *Canadian Journal of Civil Engineering*, 39(6), pp.599-609.
- Dempsey, B.J. and Thompson, M.R., 1970. A heat transfer model for evaluating frost action and temperature-related effects in multilayered pavement systems. *Highway Research Record*, (342).
- Design, R. (2018). *Rigid versus Flexible Pavement Design* | R.O. Anderson Engineering, Inc - Minden, South Lake Tahoe, Lubbock. [online] R.O. Anderson Engineering, Inc. Available at: <http://www.roanderson.com/2011/12/22/rigid-versus-flexible-pavement-design/> [Accessed 23 Jul. 2018].
- Dickson, T., Dwyer, D. and Humphrey, D., 2001. Prototype tire-shred embankment construction. *Transportation Research Record: Journal of the Transportation Research Board*, (1755), pp.160-167.
- Diefenderfer, B.K., 2002. *Moisture content determination and temperature profile modeling of flexible pavement structures* (Doctoral dissertation, Virginia Tech).
- Doré, G. and Imbs, C., 2002. Development of a new mechanistic index to predict pavement performance during spring thaw. In *Cold Regions Engineering: Cold Regions Impacts on Transportation and Infrastructure* pp. 348-359.

- Dunlap, W.A., 1963. A Mathematical Model Describing the Deformation Characteristics of Granular Materials. *Techn. Report 1, E 51/63, Texas A and M University, 1963.*
- Eldin, N.N. and Senouci, A.B., 1992. Use of scrap tires in road construction. *Journal of Construction Engineering and Management*, 118(3), pp.561-576.
- Elliott, R.P. and Thornton, S.I., 1988. Simplification of subgrade resilient modulus testing. *Transportation Research Record*, 1192, pp.1-7.
- Elliott, R.P., 1988. *Resilient properties of Arkansas subgrades*. Arkansas Highway and Transportation Research Center, University of Arkansas.
- Erlingsson, S. and Rahman, M., 2013. Evaluation of permanent deformation characteristics of unbound granular materials by means of multistage repeated-load triaxial tests. *Transportation Research Record: Journal of the Transportation Research Board*, (2369), pp.11-19.
- Fredlund, D.G., Rahardjo, H. and Rahardjo, H., 1993. *Soil mechanics for unsaturated soils*. John Wiley & Sons.
- George, K. P. 2004. "Prediction of resilient modulus from soil index properties." Rep. No. FHWA/MS-DOT-RD-04-172, Federal Highway Administration, U.S. Department of Transportation, Washington, D.C.
- Gidel, G., Hornyh, P., Breysse, D. and Denis, A., 2001. A new approach for investigating the permanent deformation behaviour of unbound granular material using the repeated loading triaxial apparatus. *Bulletin des laboratoires des Ponts et Chaussées*, (233).
- Güllü, H., 2014. Function finding via genetic expression programming for strength and elastic properties of clay treated with bottom ash. *Engineering Applications of Artificial Intelligence*, 35, pp.143-157.
- Grubbs, F.E., 1969. Procedures for detecting outlying observations in samples. *Technometrics*, 11(1), pp.1-21.
- Haghi, N.T., Nassiri, S., Shafiee, M.H. and Bayat, A., 2014. Using field data to evaluate bottom ash as pavement insulation layer. *Transportation Research Record*, 2433(1), pp.39-47.
- Haghi, N.T., Hashemian, L. and Bayat, A., 2016. Effects of seasonal variation on the load-bearing capacity of pavements composed of insulation layers. *Transportation Research Record: Journal of the Transportation Research Board*, (2579), pp.87-95.
- Han, R., Jin, X. and Glover, C.J., 2011. Modeling pavement temperature for use in binder oxidation models and pavement performance prediction. *Journal of Materials in Civil Engineering*, 23(4), pp.351-359.

Heidrich, C., Feuerborn, H.J. and Weir, A., 2013, April. Coal combustion products: a global perspective. In *World of Coal Ash Conference* (pp. 22-25).

Hornych, P., 1993. Étude des déformations permanentes sous chargements répétés de trois graves non traitées. *Bulletin de liaison des Laboratoires des Ponts et Chaussées*, (184).

2- Huang, Y.H. (1993). Pavement analysis and design. 2nd Edition, Prentice Hall, Inc., Upper Saddle River, NJ, USA.

Huang, Y., Bird, R.N. and Heidrich, O., 2007. A review of the use of recycled solid waste materials in asphalt pavements. *Resources, Conservation and Recycling*, 52(1), pp.58-73.

Humphrey, D.N., 2007, November. Tire derived aggregate as lightweight fill for embankments and retaining walls. In *Proceedings of the International Workshop on Scrap Tire Derived Geomaterials—Opportunities and Challenges, Yokosuka* (pp. 59-81).

Humphrey, D. and Blumenthal, M., 2010. The use of tire-derived aggregate in road construction applications. In *Green Streets and Highways 2010: An Interactive Conference on the State of the Art and How to Achieve Sustainable Outcomes*(pp. 299-313).

Inge Jr, E.H. and Kim, Y.R., 1995. Prediction of effective asphalt layer temperature. *Transportation Research Record*, (1473).

Islam, M.R., Ahsan, S. and Tarefder, R.A., 2015. Modeling temperature profile of hot-mix asphalt in flexible pavement. *International Journal of Pavement Research and Technology*, 8(1), pp.47-52.

Jamshidi, A., Kurumisawa, K., Nawa, T., Jize, M. and White, G., 2017. Performance of pavements incorporating industrial byproducts: A state-of-the-art study. *Journal of Cleaner Production*, 164, pp.367-388.

Janoo, V., 2002. Performance of base/subbase materials under frost action. In *Cold Regions Engineering: Cold Regions Impacts on Transportation and Infrastructure*, pp. 299-310.

Janoo, V. and Cortez, E., 2002. Pavement Evaluation in Cold Regions. In *Cold Regions Engineering: Cold Regions Impacts on Transportation and Infrastructure* pp. 360-371.

Ji, R., Siddiki, N., Nantung, T. and Kim, D., 2014. Evaluation of resilient modulus of subgrade and base materials in Indiana and its implementation in MEPDG. *The Scientific World Journal*, 2014.

Karl, T.R., Melillo, J.M., Peterson, T.C. and Hassol, S.J. eds., 2009. *Global climate change impacts in the United States*. Cambridge University Press.

Kayabal, K. and Buluş, G., 2000. The usability of bottom ash as an engineering material when amended with different matrices. *Engineering geology*, 56(3-4), pp.293-303.

- Khadrawi, A.F., Al-Shyyab, A. and Abo-Qudais, S.A., 2012. Transient Thermal Behavior of Hot-Mix Asphalt Pavement. In *Applied Mechanics and Materials* (Vol. 110, pp. 400-407). Trans Tech Publications.
- Khoury, N. and Zaman, M., 2004. Correlation between resilient modulus, moisture variation, and soil suction for subgrade soils. *Transportation Research Record: Journal of the Transportation Research Board*, (1874), pp.99-107.
- Konrad, J.M. and Morgenstern, N.R., 1980. A mechanistic theory of ice lens formation in fine-grained soils. *Canadian Geotechnical Journal*, 17(4), pp.473-486.
- Leong, E.C., Tripathy, S. and Rahardjo, H., 2003. Total suction measurement of unsaturated soils with a device using the chilled-mirror dew-point technique. *Geotechnique*, 53(2), pp.173-182.
- Li, D. and Selig, E.T., 1994. Resilient modulus for fine-grained subgrade soils. *Journal of geotechnical engineering*, 120(6), pp.939-957.
- Liang, R.Y., Rabab'ah, S. and Khasawneh, M., 2008. Predicting moisture-dependent resilient modulus of cohesive soils using soil suction concept. *Journal of Transportation Engineering*, 134(1), pp.34-40.
- Liu, Q. and Shalaby, A., 2013. Simulation of pavement response to tire pressure and shape of contact area. *Canadian Journal of Civil Engineering*, 40(3), pp.236-242.
- Mahoney, J.P., Rutherford, M.S. and Hicks, R.G., 1987. *Guidelines for spring highway use restrictions* (No. FHWA-TS-87-209) Washington State Department of Transportation, Olympia, WA.
- Meles, D.T., 2014. *Application of Tire Derived Aggregate as Highway Embankment Fill Material* (Doctoral dissertation, University of Alberta).
- Miller, H., Cabral, C., Kestler, M., Berg, R. and Eaton, R., 2012. Calibration of a Freeze-Thaw Prediction Model for Spring Load Restriction Timing in Northern New England. In *Cold Regions Engineering 2012: Sustainable Infrastructure Development in a Changing Cold Environment* (pp. 369-379).
- Miller, H.J., Cabral, C., Kestler, M.A. and Berg, R., 2015. *Aurora SPR-3 (042), Phase 1: Review of Seasonal Weight Restriction Models for Comparison and Demonstration Project*(No. 15-2845).
- Mills, B. and McGinn, J., 2010. Design, construction, and performance of a highway embankment failure repaired with tire-derived aggregate. *Transportation Research Record: Journal of the Transportation Research Board*, (2170), pp.90-99.
- Minhoto, M., Pais, J., Pereira, P. and Picado-Santos, L., 2005. Predicting asphalt pavement temperature with a three-dimensional finite element method. *Transportation Research Record: Journal of the Transportation Research Board*, (1919), pp.96-110.

Minhoto, M., Pais, J. and Pereira, P., 2006. Asphalt pavement temperature prediction. In *Asphalt Rubber 2006 Conference*.

Minnesota Department of Transportation (Mn DOT). 2014. Policy and Process for Seasonal Load Limit Starting and Ending Dates. Minnesota Department of Transportation, Policy, Safety and Strategic Initiatives Division, Technical Memorandum. No. 14-10-MAT-02 October 7

Misra, A., 1998. Stabilization characteristics of clays using class C fly ash. *Transportation Research Record: Journal of the Transportation Research Board*, (1611), pp.46-54.

Modarres, A. and Nosoudy, Y.M., 2015. Clay stabilization using coal waste and lime—Technical and environmental impacts. *Applied clay science*, 116, pp.281-288.

Mohammad, L., Y. Abu-Farsakh, M., Wu, Z. and Abadie, C., 2003. Louisiana experience with foamed recycled asphalt pavement base materials. *Transportation Research Record: Journal of the Transportation Research Board*, (1832), pp.17-24.

Mohammad, L.N., Gaspard, K., Herath, A. and Nazzal, M.D., 2007. *Comparative evaluation of subgrade resilient modulus from non-destructive, in-situ, and laboratory methods* (No. FHWA/LA. 06/417).

A. Mohseni, 1998. LTPP seasonal asphalt concrete (AC) pavement temperature models (No. FHWA-RD-97-103).

Monismith, C.L., Ogawa, N. and Freeme, C.R., 1975. Permanent deformation characteristics of subgrade soils due to repeated loading. *Transportation Research Record*, (537).

Moossazadeh, J. and Witczak, M.W., 1981. Prediction of subgrade moduli for soil that exhibits nonlinear behavior. *Transportation Research Record*, (810).

NCHRP. Laboratory Determination of Resilient Modulus for Flexible Pavement Design. 1997, NCHRP Web Document 14 for Project 1-28. Transportation Research Board, Washington, D.C.

Ningyuan, L., Eng, P., Kazmierowski, T. and Lane, B., 2006. Long-Term Monitoring of Low-Volume Road Performance in Ontario. In *2006 annual conference and exhibition of the transportation association of canada: transportation without boundaries*. <http://www.tac-atc.ca/english/pdf/conf2006/s005/ningyuan.pdf>. [accessed 29 May 2015].

Oman, M. and Hoppe, M., 2013. Use of Tire Derived Products (TDP) in Roadway Construction. *Minnesota Department of Transportation Research Services, St. Paul, MN*, pp.1-49.

- Osinubi, K.J., 2000. Stabilisation of tropical black clay with cement and pulverised coal bottom ash admixture. In *Advances in unsaturated geotechnics* (pp. 289-302).
- Ovik, J. M., Birgisson, B., and Newcomb, D. E. 2000. "Characterizing seasonal variations in pavement material properties for use in a mechanistic-empirical design procedure." MNRoad Final Rep. No. MN/RC-2000-35, Minnesota Department of Transportation, St. Paul, Minn.
- Ovik, J.M., Siekmeier, J.A. and Van Deusen, D.A., 2000. Improved spring load restriction guidelines using mechanistic analysis. Final Report. Office of Material and Road Research, Minnesota Department of Transportation, St. Paul, Minnesota.
- Ozdemir, M.A., 2016. Improvement in Bearing Capacity of a Soft Soil by Addition of Fly Ash. *Procedia engineering*, 143, pp.498-505.
- Özgan, E., Serin, S., Gerengi, H. and Arslan, İ., 2013. Multi-faceted investigation of the effect of de-icer chemicals on the engineering properties of asphalt concrete. *Cold Regions Science and Technology*, 87, pp.59-67.
- Ozgan, E., 2011. Artificial neural network based modelling of the Marshall Stability of asphalt concrete. *Expert Systems with Applications*, 38(5), pp.6025-6030.
- Özgan, E. and Serin, S., 2013. Investigation of certain engineering characteristics of asphalt concrete exposed to freeze–thaw cycles. *Cold Regions Science and Technology*, 85, pp.131-136.
- Park, D.Y., Buch, N. and Chatti, K., 2001. Effective layer temperature prediction model and temperature correction via falling weight deflectometer deflections. *Transportation Research Record: Journal of the Transportation Research Board*, (1764), pp.97-111.
- Park, H. and Kim, Y., 2003. Prediction of remaining life of asphalt pavement with falling-weight deflectometer multiloading-level deflections. *Transportation Research Record: Journal of the Transportation Research Board*, (1860), pp.48-56.
- Park, J.J., Shin, E.C. and Yoon, B.J., 2016. Development of frost penetration depth prediction model using field temperature data of asphalt pavement. *International Journal of Offshore and Polar Engineering*, 26(04), pp.341-347.
- Pirmohammad, S. and Kiani, A., 2016. Effect of temperature variations on fracture resistance of HMA mixtures under different loading modes. *Materials and Structures*, 49(9), pp.3773-3784.
- Priest, A.L. and Timm, D.H., 2006. Methodology and Calibration of Fatigue Transfer Functions for Mechanistic Empirical Flexible Pavement Design (No. NCAT Report 06-03).

- Prusinski, J. and Bhattacharja, S., 1999. Effectiveness of Portland cement and lime in stabilizing clay soils. *Transportation Research Record: Journal of the Transportation Research Board*, (1652), pp.215-227.
- Puppala, A.J., Mohammad, L.N. and Allen, A., 1999. Permanent deformation characterization of subgrade soils from RLT test. *Journal of Materials in Civil Engineering*, 11(4), pp.274-282.
- Puppala, A.J., Saride, S. and Chomtid, S., 2009. Experimental and modeling studies of permanent strains of subgrade soils. *Journal of geotechnical and geoenvironmental engineering*, 135(10), pp.1379-1389.
- Qi, J., Vermeer, P.A. and Cheng, G., 2006. A review of the influence of freeze-thaw cycles on soil geotechnical properties. *Permafrost and periglacial processes*, 17(3), pp.245-252.
- Qin, Y. and Hiller, J.E., 2011. Modeling temperature distribution in rigid pavement slabs: impact of air temperature. *Construction and Building Materials*, 25(9), pp.3753-3761.
- Quigley, J. By the numbers: A hard look at Canada's declining coal industry. CBC News. February 04, 2016. Accessed July 28, 2017. <http://www.cbc.ca/news/business/canadian-coal-by-the-numbers-1.3408568>.
- Rahman, M.T. and Tarefder, R.A., 2015. Assessment of Molding Moisture and Suction on Resilient Modulus of Lime Stabilized Clayey Subgrade Soils. *Geotechnical Testing Journal*, 38(6), pp.840-850.
- Rifa'i, A., Yasufuku, N. and Tsuji, K., 2010. Characterization and effective utilization of coal ash as soil stabilization on road application. In *International Symposium on Ground Improvement Technologies and Case Histories, ISGI'09*.
- Rumney, T.N., Jimenez, R.A. 1971, Pavement temperatures in the southwest, Highway Res. Rec. 361.
- Sawangsurriya, A., Edil, T. and Benson, C., 2009. Effect of suction on resilient modulus of compacted fine-grained subgrade soils. *Transportation Research Record: Journal of the Transportation Research Board*, (2101), pp.82-87.
- Seed, H.B., Chan, C.K. and Lee, C.E., 1962. Resilience characteristics of subgrade soils and their relation to fatigue failures in asphalt pavements. In *International Conference on the Structural Design of Asphalt Pavements. Supplement University of Michigan, Ann Arbor*.
- Senol, A., Edil, T.B., Bin-Shafique, M.S., Acosta, H.A. and Benson, C.H., 2006. Soft subgrades' stabilization by using various fly ashes. *Resources, Conservation and Recycling*, 46(4), pp.365-376.
- Seo, J., Kim, Y., Cho, J. and Jeong, S., 2013. Estimation of in situ dynamic modulus by using MEPDG dynamic modulus and FWD data at different temperatures. *International Journal of Pavement Engineering*, 14(4), pp.343-353.

Sezer, A., İnan, G., Yılmaz, H.R. and Ramyar, K., 2006. Utilization of a very high lime fly ash for improvement of Izmir clay. *Building and environment*, 41(2), pp.150-155.

Siddique, R. and Naik, T.R., 2004. Properties of concrete containing scrap-tire rubber—an overview. *Waste management*, 24(6), pp.563-569.

Shafiee, M.H., Hashemian, L. and Bayat, A., 2015. Seasonal analysis of flexible pavement response to falling weight deflectometer. *International Journal of Pavement Research and Technology*, 8(5), pp.346-352.

Sharp, R.W. and Booker, J.R., 1984. Shakedown of pavements under moving surface loads. *Journal of Transportation Engineering*, 110(1), pp.1-14.

Sharp, R.W., 1985. Pavement design based on shakedown analysis. *Transportation research record*, 1022(99), p.107.

Shenton, M.J., 1974. Deformation of railway ballast under repeated loading triaxial tests. *Soil Mechanics Section, British Railways Research Departement, Derby, England*.

Shukla, P.K. and Das, A., 2008. A re-visit to the development of fatigue and rutting equations used for asphalt pavement design. *International Journal of Pavement Engineering*, 9(5), pp.355-364.

Solanki, P., Zaman, M.M. and Dean, J., 2010. Resilient modulus of clay subgrades stabilized with lime, class C fly ash, and cement kiln dust for pavement design. *Transportation Research Record*, 2186(1), pp.101-110.

Soliman, H., Kass, S. and Fleury, N., 2008. A simplified model to predict frost penetration for Manitoba soils. In *2008 Annual Conference of the Transportation Association of Canada. Transportation Association of Canada, Toronto, Ontario*.

Southgate, H.F., 1968. An evaluation of temperature distribution within asphalt pavements and its relationship to pavement deflection.

Tandon, V., Velazco, D.A., Nazarian, S. and Picornell, M., 2007. Performance monitoring of embankments containing tire chips: case study. *Journal of Performance of constructed Facilities*, 21(3), pp.207-214.

Tao, M., Mohammad, L.N., Nazzal, M.D., Zhang, Z. and Wu, Z., 2010. Application of shakedown theory in characterizing traditional and recycled pavement base materials. *Journal of Transportation Engineering*, 136(3), pp.214-222.

The City of Edmonton Transportation, “Roadway- Design Standard Construction Specifications”, 2012 Edition, https://www.edmonton.ca/city_government/documents/Volume_2_-_Roadways.pdf.

- Thompson, M.R. and Robnett, Q.L., 1976. *Resilient properties of subgrade soils* (No. FHWA-IL-UI-160 Final Rpt.).
- Transportation Officials, 1993. *AASHTO guide for design of pavement structures, 1993* (Vol. 1). AASHTO.
- Tseng, K.H. and Lytton, R.L., 1989. Prediction of permanent deformation in flexible pavement materials. In *Implication of aggregates in the design, construction, and performance of flexible pavements*. ASTM International.
- Tweedie, J.J., Humphrey, D.N. and Sandford, T.C., 1998. Tire shreds as lightweight retaining wall backfill: active conditions. *Journal of geotechnical and geoenvironmental engineering*, 124(11), pp.1061-1070.
- Ullditz, P., 1993. *Mathematical model of pavement performance under moving wheel load* (No. 1384). 94-99.
- Uzan, J., 2004. Permanent deformation in flexible pavements. *Journal of Transportation Engineering*, 130(1), pp.6-13.
- Wang, D.Y., Ma, W., Niu, Y.H., Chang, X.X. and Wen, Z., 2007. Effects of cyclic freezing and thawing on mechanical properties of Qinghai–Tibet clay. *Cold regions science and technology*, 48(1), pp.34-43.
- Wang, R., Zhou, F., Chen, D.H., Zheng, G., Scullion, T. and Walubita, L.F., 2009. Characterization of rutting (permanent strain) development of A-2-4 and A-4 subgrade soils under the HVS loading. *Journal of Performance of Constructed Facilities*, 24(4), pp.382-389.
- Watson, D.K. and Rajapakse, R.K.N.D., 2000. Seasonal variation in material properties of a flexible pavement. *Canadian Journal of Civil Engineering*, 27(1), pp.44-54.
- Werkmeister, S., Dawson, A. and Wellner, F., 2001. Permanent deformation behavior of granular materials and the shakedown concept. *Transportation Research Record: Journal of the Transportation Research Board*, (1757), pp.75-81.
- Werkmeister, S., 2003. Permanent deformation behaviour of unbound granular materials in pavement constructions//Ph. D. thesis, University of Technology, Dresden, Germany.-2003.-189 p.
- Werkmeister, S., Dawson, A.R. and Wellner, F., 2005. Permanent deformation behaviour of granular materials. *Road materials and pavement design*, 6(1), pp.31-51.
- Williams, P.J., 1964. Unfrozen water content of frozen soils and soil moisture suction. *Geotechnique*, 14(3), pp.231-246

Witczak, M.W. and Uzan, J., 1988. The universal airport pavement design system. *Report I of V: granular material characterization, Department of Civil Engineering, University of Maryland, College Park, MD.*

Witteveen, P.J., Ferrari, A. and Laloui, L., 2013. An experimental and constitutive investigation on the chemo-mechanical behaviour of a clay. *Geotechnique-London-*, 63(EPFL-ARTICLE-181824), pp.244-255.

Xue, Y., Hou, H., Zhu, S. and Zha, J., 2009. Utilization of municipal solid waste incineration ash in stone mastic asphalt mixture: pavement performance and environmental impact. *Construction and Building Materials*, 23(2), pp.989-996.

Yang, S.R., Huang, W.H. and Liao, C.C., 2008. Correlation between resilient modulus and plastic deformation for cohesive subgrade soil under repeated loading. *Transportation Research Record: Journal of the Transportation Research Board*, (2053), pp.72-79.